Gas path analysis for the MTT micro turbine

Pieter Bauwens (4238044)
Flight Performance and Propulsion
(043#15#*MT*#*FPP*)

Technische Universiteit Delft

Delft University of Technology

Challenge the future

Gas path analysis for the MTT micro turbine

by

Pieter Bauwens (4238044)
Flight Performance and Propulsion
$(043\#15\#MT\#FPP)$

in partial fulfillment of the requirements for the degree of

Master of Science
in Aerospace Engineering

at the Delft University of Technology

Supervisor:	Dr. ir. W.P.J Visser,	TU Delft/MTT
Head of the department:	Prof. Dr. ir. P. Colonna,	TU Delft
Industrial supervisor:	Ir. I. D. Dountchev,	MTT

This thesis is confidential and cannot be made public until August 13, 2015

Delft University of Technology

PREFACE

This report is the result of my master thesis project prepared at MTT (Micro Turbine Technology), Eindhoven, The Netherlands as part of my Master in Aerospace Engineering at the Delft University of Technology.

I would like to express my gratitude to Mr. W. Visser and Mr. I. Dountchev of MTT for their time and effort to assist me in the completion of this M. Sc. Thesis project. I am grateful that I could learn from their expertise in gas turbine performance modelling, engine testing and maintenance. I would also like to thank the complete MTT-team for their continued interest in the project and the interesting discussion we had.

I dedicate this piece of work to my parents and girlfriend Jessie. Without their love and support I would not be the person I am today. I would like to thank them for giving me these opportunities and being there when needed.

Pieter Bauwens (4238044)
Flight Performance and Propulsion
(043#15#MT#FPP)
Delft, June 2015

"Do not guess, when you can calculate. Do not calculate, when you can measure."

Archimedes

Executive summary

Gas turbine diagnostics is as old as the gas turbine itself. Over the years, performance based diagnostics allowed for a shift from time-based maintenance to more economical condition based maintenance playing a fundamental role in enhancing the availability and reliability of gas turbines. By monitoring the condition of the engine over time, maintenance actions can be taken based on information collected from the field.

MTT (Micro Turbine Technology) is currently developing a low cost 3kWe micro-turbine CHP (Combined Heat and Power)-system by using off-the-shelf technologies. Once the system will be launched on the market an organized, cost-effective maintenance procedure will be required. The objective of this M. Sc. thesis project was to develop and demonstrate a Gas Path Analysis diagnostic concept for the micro-turbine. *Gas Path Analysis* (GPA) is a method to assess the condition of the gas turbine by using performance measurements from the gas path. The feasibility of the diagnostic concept was demonstrated by some case studies using data from the first generation field test units.

After reviewing a number of gas turbine diagnostic techniques, a non-linear model based gas path analysis approach was chosen. For the development of the diagnostic concept, a non-linear model of a healthy reference engine was used to simulate the off-design behaviour of the engine and derive healthy performance parameter baselines. These baselines are used to compare the performance of field engines against. A component based modelling environment called GSP or the *Gas turbine Simulation Program* was used to simulate the effect of ambient conditions and deterioration on performance. The diagnostic concept relies on the principle that deterioration causes corrected measurement parameters to shift from the healthy reference baselines. Measurement performance parameters are first corrected to standard ISA conditions before being compared against the healthy baselines. By modelling specific types of deterioration in GSP, signature parameter shifts could be recorded for each of the deterioration modes. These signature parameter shifts are used to compare shifts in performance parameters against and determine the closest pattern-match which can be used to identify the most probable cause of deterioration.

The proposed concept is capable of performing engine level diagnostics and partially component level diagnostics. Multiple fault diagnostics and quantifying the level of deterioration are more difficult due to the limited number of sensors and the relatively large impact of second-order effects such as heat-loss, auxiliary power take-off, mechanical losses, etc. The performance parameter baselines together with the derived rule-sets can easily be implemented in a maintenance tool making the concept flexible and easy to use.

Keywords: Micro gas turbine, gas turbine simulation, performance modelling, trending, diagnostics.

Contents

List of Figures

LIST OF TABLES

Nomenclature

Abbreviations

AI	Artificial Intelligence
AM	Adaptive Modeling
ANN	Artificial Neural Network
CBM	Condition Based Maintenance
CDPDI	Compressor Discharge Pressure Deterioration Index
CHP	Combined Heat and Power
DGPA	Differential Gas Path Analysis
ERT	Exchange Rate Table
ES	Expert System
FCM	Fault Coefficient Matrix
FI	Fouling Index
GA	Genetic Algorithm
GPA	Gas Path Analysis
GPDI	Grid Power Deterioration Index
GSP	Gas Turbine Simulation Program
ICM	Influence Coefficient Matrix
ISA	International Standard Atmosphere
LGPA	Linear Gas Path Analysis
MTT	Micro Turbine Technology
NLGPA	Non Linear Gas Path Analysis
PC	Power Code
PR	Pressure Ratio

Greek symbols

Δ	Change in parameter
δ	Ratio of pressure to standard sea-level pressure
η	Efficiency
ϵ	Effectiveness
γ	Ratio of specific heats
γ	Slip factor
ϕ	Power input factor
ρ	Density
θ	Ratio of temperature to standard seal level temperature

Latin Symbols

C_p	Specific heat at constant pressure
$\dot{P}$	Input vector
$\dot{V}$	Measurement error vector
$\dot{X}$	Component vector
$\dot{Y}$	Dependent measurement parameter vector
H	Heat
h	Specific enthalpy
N	Shaft rotational speed
P	Pressure
PW	Power
Q	Heat
R	Gas constant
T	Temperature
TIT	Turbine inlet temperature
U	Impeller speed
W	Flow rate

Subscripts

1	Gas turbine inlet
2	Compressor inlet face
3	Compressor exit face
4	Turbine inlet face
5	Turbine exit face
6	Heat exchanger inlet
7	Heat exchanger exit
9	Exhaust face
34	Combustion inlet face
57	Recuperator exit
amb	Ambient operating conditions
c	Compressor component
cab	Cabinet
comb	Combustion chamber
cor	Corrected gas path parameter
det	Deteriorated parameter
f	Fuel
is	Isentropic
meas	Measure value
T	Turbine
th	Thermal
w	Water

1
INTRODUCTION

MTT (Micro Turbine Technology), a small start-up company developing a low cost 3kWe micro CHP (Combined Heat and Power) system by using off-the-shelf technologies is about to launch its product on the market. When the large fleet of CHP systems will be installed in the field, an organized and reliable maintenance procedure will be required to optimize the availability and maintainability of the systems while minimizing the operational costs. Over the years, maintenance has evolved from *Reactive Maintenance*, where problems are tackled after they have arisen, to *Preventive Maintenance*, where maintenance is carried out at regular scheduled intervals with the intention to prevent problems from arising, to *Predictive Maintenance* where maintenance is done based on the actual state of the system [1]. Various diagnostic methods such as visual inspection, vibration analysis, lubrication analysis and performance based gas path analysis are available to evaluate the condition of gas turbines. By combining and sharing information between several of these methods, the condition of the gas turbine can be evaluated more accurately.

This particular thesis assignment focusses on the development of a real-time performance based gas path analysis (GPA) diagnostic concept that will help to evaluate the condition of engines in the field. *Gas path analysis* (GPA) is a method to assess gas turbine performance margins and condition using performance measurements from the gas path. Based on the result form the gas path analysis, *Condition Based Maintenance* (CBM) could be performed which could replace the more conservative *Preventive or Scheduled maintenance*. According to Jardine et al. [2] "CBM is a maintenance program that recommends maintenance actions based on information collected through condition monitoring. CBM attempts to avoid unnecessary maintenance tasks by taking maintenance actions only when there is evidence of abnormal behaviours of a physical asset".

The effect of changing power settings, ambient conditions and deterioration on performance is difficult to investigate because of the interaction of many gas path components. Therefore, software tools such as the *Gas Turbine Simulation Program* (GSP) are used to predict the effect of changing operating conditions and deterioration on the performance. The limited number of sensors available in the gas path together with the small size of the gas turbine will make the development of the performance based gas path analysis concept a challenging endeavour.

1.1. PROBLEM DEFINITION AND RESEARCH OBJECTIVES

The main objective of this thesis is to develop and assess the feasibility and potential of a performance based GPA (Gas Path Analysis) diagnostic concept suitable for integration in the MTT on-line condition monitoring software. For the development of the concept, modern gas turbine simulation tools such as GSP are used to analyse the behaviour of the engine for changing operating conditions and deterioration. The simulation results are used to develop reference performance parameter baselines and analyse the effect of deterioration on performance. The capabilities and limitations of the concept are showcased by a case study on a first generation field test system.

Research question *Is it possible to develop a performance based Gas Path Analysis diagnostic concept for the MTT micro-turbine CHP-system equipped with a limited set of sensors and if so, what are the corresponding limitations and capabilities with respect to detecting, isolating and quantifying gas path faults?*

Novelty, motivation, feasibility of the project: Although many GPA diagnostic concepts have been suggested, most of the methods are applied to *large* gas turbines. This project focusses on the development of a performance based GPA concept for a recuperated micro turbine CHP system having a limited sensor-set. The big influence of secondary effects together with the relatively large heat losses in small gas turbines made the development of the tool a challenging project.

1.2. DOCUMENT STRUCTURE

Chapter 2 starts with a literature review assessing various performance based diagnostic methods that are currently used in the industry. Chapter 3 gives a system description of the micro CHP system and discusses the specifications of the engine. In chapter 4, the non-linear performance modelling environment (GSP) is introduced together with a description of the model. Chapter 5 demonstrates the capabilities of differential gas path analysis through adaptive modelling. The development of the performance based GPA concept is presented in chapter 6. The concept relies extensively on performance parameter trending where the performance of the field engine is compared against reference performance parameter baselines. The chapter gives an overview of various deterioration modes and how they can be simulated in GSP by using map modifiers. The chapter concludes with a case study showing the capabilities and limitations of the concept. Finally, the conclusions and recommendations regarding future work are discussed in chapter 9.

2

LITERATURE REVIEW

The performance of gas turbines deteriorates over time due to various degradation mechanisms such as fouling, erosion, corrosion, increasing tip clearances, foreign object damage, etc. These physical faults have a direct impact on the performance of the individual gas path components causing changes in the component health parameters (efficiencies, pressure-ratios, mass-flows, etc.) which in turn results in a shift in measurement performance parameters (temperatures, pressures, rotational speeds, fuel-flows, etc.). From the start of gas turbine development, many approaches for gas turbine condition monitoring and diagnostics have been proposed such as visual inspection, vibration monitoring, oil debris monitoring, noise monitoring and performance analysis [3]. Among these approaches, performance based gas path analysis is a powerful method to detect, isolate and quantify component faults by establishing relations between measurement and health parameters. Because sensors do not allow for direct measurement of the health parameters, thermodynamic relations between the measurement and health parameters are required to diagnose the gas path components. This chapter starts with short overview of various model based and data driven performance based gas path analysis diagnostic methods. The benefits and shortcoming of the each of methods are discussed in section 2.2. Based on the review, a method capable of diagnosing the condition of field engines equipped with a limited number of gas-path sensors is selected.

2.1. OVERVIEW OF PERFORMANCE BASED GAS PATH ANALYSIS DIAGNOSTIC METHODS

The underlying logic behind GPA is to use measurement parameters such as temperatures and pressures (dependent parameters) to detect shifts in health parameters such as efficiencies, pressure ratios and flow capacities (independent parameters). Because health parameters can usually not be measured directly, thermodynamic relations between the measurement and health parameters should be established. Detailed knowledge of the effect of deterioration on performance is as well required to link shifts in performance to the root cause of deterioration. The main objective is to detect, isolate and quantify deterioration by using an adequate set of measurements. Because the diagnostic method relies on observable performance parameter shifts, faults that do not cause shifts in performance such as crack and fatigue cannot be detected through GPA. In this section, an overview of various model-based and data-driven gas path analysis methods is given. Methods such as linear and non-linear gas path analysis, adaptive modelling, artificial neural networks, genetic algorithms, expert systems and fuzzy logics are discussed.

2.1.1. MODEL BASED GPA METHODS

A thermodynamic model of the engine is at the heart of this approach which means that detailed knowledge of the thermodynamic behaviour of the individual gas-path components is required. The off-design behaviour of gas turbines is simulated by using complex simulation-software tools that require performance characteristics of individual gas-path components. The simulation results are used to establish relationships between dependent measurement parameters (temperatures, pressures, rotational speeds, etc.) and independent health parameters (isentropic efficiencies, flow capacities, etc.). In following paragraphs, linear and non-linear model based gas path analysis are discussed.

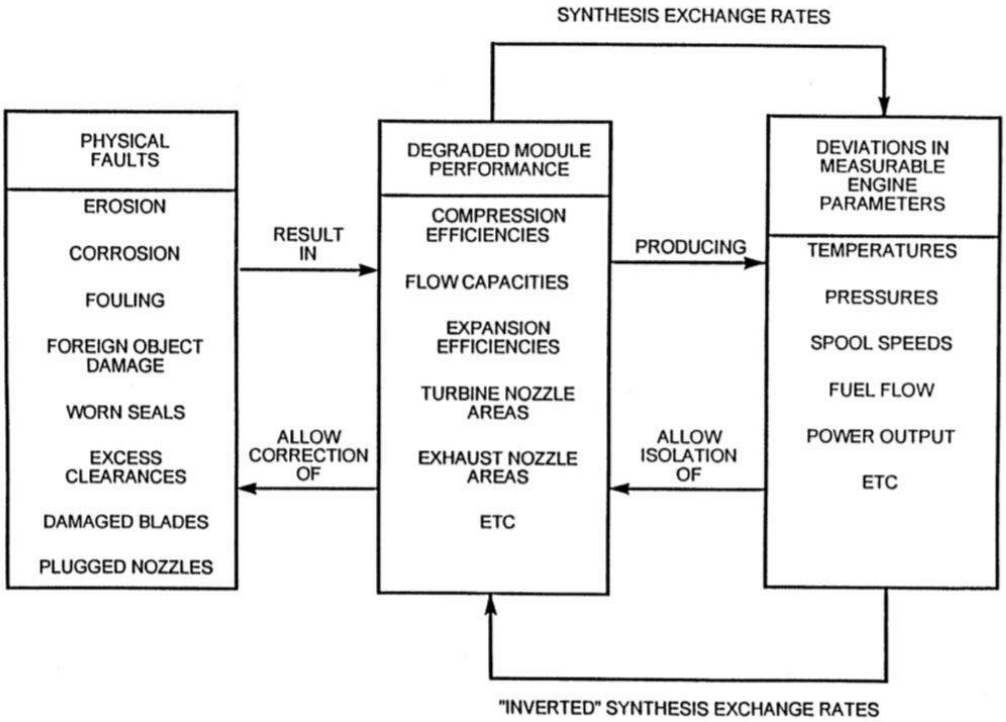

Figure 2.1: Process of fault analysis [4]

Linear gas path analysis Linear model based gas path analysis was first introduced by Urban L.A in 1967 [5, 6]. Urban's conceptual framework is shown in Figure 2.1 and relies on following reasoning: gas path faults cause changes in the component characteristics which in turn cause changes in the dependent measurement parameters along the gas path. Although the relationship between the health parameters and measurement parameters is highly non linear due to the non-linear performance characteristics of the individual gas path components, LGPA tries to simplify this relationship by linearizing the equations around a specific steady-state operating point. Equation 2.1 shows the highly non-linear relationship between the health and measurement parameters for specific ambient conditions and power-settings. The dependent measurement parameter vector, $\bar{Y}$, is a function of the component vector, $\bar{X}$, and input vector $\bar{P}$. $\bar{V}$ is the measurement error vector. The component vector contains the independent health variables such as efficiencies, pressure ratios and capacities whereas the input vector contains the ambient conditions and power-settings of the gas turbine.

$$\bar{Y} = f(\bar{P}, \bar{X}) + \bar{V} \tag{2.1}$$

This non-linear relationship can be linearized around a specific steady-state operating point ($\bar{P}$ =constant) such as maximum power which gives Equation 2.2.

$$\delta\bar{Y} = ICM(\bar{P}) \cdot \delta\bar{X} + \bar{V} \tag{2.2}$$

The ICM (*Influence Coefficient Matrix*) is used to approximate the highly non-linear relationship between the dependent and independent variables. The ICM is obtained by perturbing the independent health variables and ambient conditions one by one and identifying the effect on the dependent measurement variables. As it is not possible to measure changes in health parameters (efficiencies and flow capacities), the effect of deterioration should be determined indirectly by measuring changes in dependent parameters (temperature, pressure, rotational speed, etc.). Inverting the *ICM* gives the *Fault Coefficient Matrix* (FCM) which shows the linear relationship between changes in dependent measurement parameters and independent health parameters for a specific operating condition. This linear relationship is shown in Equation 2.3.

$$\delta\bar{X} = ICM^{-1} \cdot \delta\bar{Y} = FCM \cdot \delta\bar{Y} \tag{2.3}$$

For low levels of deterioration and a fixed operating point, the linearisation errors are not too great (about a few percent) which makes LGPA a simple and quick solution to perform gas turbine performance diagnostics. However, for higher levels of deterioration the method shows instability and large inaccuracies [7].

Non-linear model based gas path analysis (NLGPA) was introduced to cope with the non-linear behaviour of gas turbines. The method is based on accurate modelling of the non-linear steady state gas turbine performance. Mathematically, the model consists of a system of non-linear algebraic equations representing the compatibility of mass, energy, heat and rotational speed between individual gas-path components. The non-linear relationship is shown in Equation 2.1. Simulation programs using numerical methods are used to calculate the off-design engine performance by determining the operating point of each gas-path component as it is matched to the others. Matching the operating points of the individual components while satisfying the conservation laws is usually a highly iterative process which requires successive guesses of the operating points of individual gas path components. The iteration is usually achieved through serial nested loops or via a matrix solution [1]. The *Gas Turbine Simulation Program (GSP)* available relies on a Newton-Raphson technique to solve the set of algebraic equation. Although the NLGPA is more complex compared to LGPA, NLGPA allows for a more accurate prediction of the engine performance especially for operation far away from the design point [8].

Differential gas path analysis (DGPA) through *adaptive modelling (AM)* is a subset of non-linear gas path analysis. In adaptive modelling, a healthy baseline engine model is adapted iteratively by adjusting the component characteristics in such a way that the model performance becomes equivalent to the measured engine performance. Modification factors or map modifiers are used to adapt component maps to account for the degree of deterioration present in the engine. By analysing shifts in component health parameters, gas path faults can be detected, isolated and quantified accurately. Mathematically, a non-linear gas-path model can be converted into an adaptive model by adding a number of equations equal to the number of measurements to correct for [8]. In chapter 5, the capabilities and numerical methods of adaptive modelling in GSP are discussed more in detail. Differential GPA can only be applied if the number of measurement performance parameters is greater than or equal to the number of health parameters to be estimated. Which means that the method can only be applied if a large number of measurements is available. This problem, however, can be overcome by introducing Discrete Operating Conditions Gas Path Analysis which uses a predefined set of map modifiers for fault isolation [9].

Genetic algorithm model based diagnostics is a model based non-linear GPA method using a *genetic algorithm* (GA) as optimization tool to make the predicted and measured performance variables become identical. A genetic algorithm is an optimization technique which mimics the process of natural selection to minimize a cost function which is in our case the difference between the measured and predicted performance parameters. A population of candidate solutions evolves towards a better solution by following a selection-procedure. First, a population of random individuals (health-parameter vector) is generated and evaluated by the cost function. Secondly, the individuals for the next generation are chosen according to the "survival of the fittest" criterion (lowest value for the cost-function). Next, a crossover operation tries to obtain fitter individuals by allowing information exchange between parts of the parameter vectors. Finally, a mutation operation introduces random changes to randomly chosen vector components. This procedure is repeated till the objective function becomes minimal [10].

This method has some advantages compared to the typical calculus-based optimization methods because no derivatives are needed during the optimization process which means that any non-smooth function can be optimized. Due to the global search, the optimization will not get stuck in a local minimum which could be the case in a Newton Raphson optimization [3]. As for Differential GPA, the method is best suitable for engines with a relatively large measurements-set.

2.1.2. DATA-DRIVEN METHODS

For data-driven GPA methods, the cause-effect relationship between measurement and health parameters is established based on pattern recognition theory using experimental engine data. The data-driven methods discussed in this section rely on *Artificial Intelligence (AI)* which is defined as "the study and design of intelligent agents" [11]. An intelligent agent is a system that takes actions that maximize the chance of success based on the perception of the environment. In the case of gas turbine diagnostics, the intelligent agent will take actions to predict the health state of the system as accurate as possible based on measurement data. This approach has become more and more popular because of its capability of reasoning and revealing cause-effect relationships between observable and non-observable health parameters without the need of functional relationship between both.

Artificial neural networks (ANN) are inspired by nervous systems using many simple processing elements that work in parallel so that high computation rates can be obtained. ANN are trained in such a way that the input and output parameters are mapped each other without the need of any physical relation between both. One of the most common used ANN in gas turbine diagnostics are Feed-Forward Back-Propagation Networks consisting of 3 layers of neurons (input, hidden and output) interconnected by synapses. The way the network works is shown in Figure 2.2. First, the input layer receives input neurons in the form of gas path measurements. Next, the input neurons are multiplied by the synoptic weights (W) before being sent to the hidden layer where they are summed. The output of the hidden layer is given by Formula 2.4. Finally, the output signals of the hidden layer are again multiplied by weights before being transferred to the output layer. The output of the network are the component health parameters. The network is trained by the back-propagation method which requires a substantial amount of training data in the form of inputs and desired outputs to determine the synaptic weights of the network so that the error between the calculated outputs and real outputs becomes minimal. ANN have the advantage that no physical engine model is required. Next, they can also deal with noisy data, system faults and adapt to different circumstances. The main disadvantages are that the method requires a substantial set of training data and that the results are invalid outside the training scope [12].

$$z_i = \sum_{i=1}^{n} W_i \cdot X_i \tag{2.4}$$

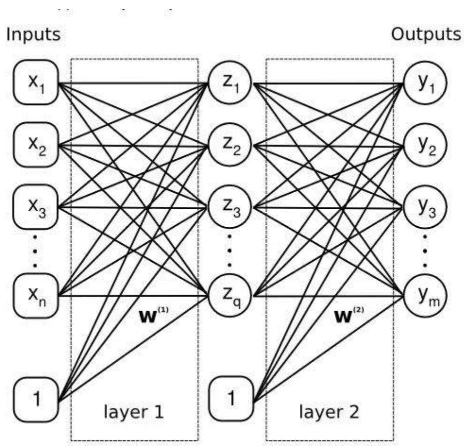

Figure 2.2: Feed-forward Back-Propagation network with 1 hidden layer

Expert System diagnostics *Expert Systems* try to solve complex problems by reasoning about knowledge just like a human expert. The most popular Expert Systems used in gas turbine diagnostics are knowledge and rule based expert systems using a set of if-then rules to identify the most probable cause for possible engine damage. The system consists of two subsystems: a knowledge base and an interference engine. The knowledge base contains facts and rules about the gas turbine, whereas the interference engine applies the rules to the facts so that new facts can be deduced. The interference engine tries to link the deterioration modes and symptoms in such a way that accurate diagnostics with the highest probability can be prevailed. Faults are usually detected by comparing the engine component deviations to predefined thresholds [13]. Because of its capability to interpret deteriorated data by applying rules and pattern recognition methods, ES are often combined with other diagnostic tools which generate the required symptoms that are analysed by the ES.

Fuzzy logic based methods are based on the human capability of imprecise reasoning. The method deals with approximate reasoning instead of fixed or exact reasoning. Truth values do not only take true or false values, but can take values between 0 and 1 [14]. The method tries to map an input space with an output space by using a list of if-then statements called rules. The rules are evaluated in parallel without taking into consideration the order[15]. The method can be used in combination with neural networks, expert systems or other techniques. Applebaum [16] suggested a rule-based fuzzy expert system for gas turbine fault classification. The proposed diagnostic concept is shown in Figure 2.3 and consists of two steps: residual generation and residual evaluation. In the first step, the recorded measurement data is validated, corrected and compared against a baseline so that a residual vector of measurement deltas showing the differences between the baseline data and the actual engine data is generated. Next, the residual vector containing measurement deltas is transformed into qualitative diagnostic knowledge by using a fuzzy filter. For example, if the residual vector shows a 3 percent decrease in compressor discharge pressure together with 8 percent reduction in output power, the fuzzy filter may interpret this information and come to the conclusion that the compressor shows a high degree of fouling. Faults are classified based on the accumulated knowledge and experience of human diagnostic expertise and likelihood of occurrence. Fuzzy logics have the advantage of being capable of easily modelling non-linear functions with a good trade-off between significance and precision.

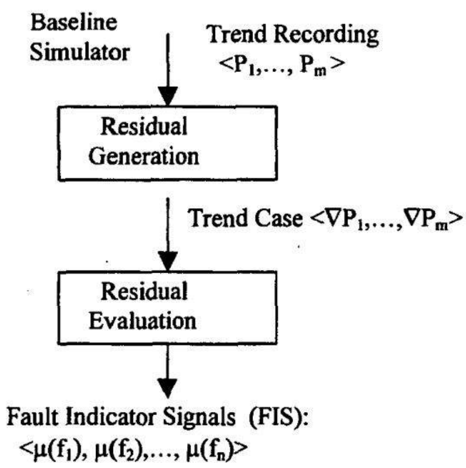

Figure 2.3: Proposed fuzzy logic-based diagnostic process [16]

2.2. DISCUSSION AND CONCLUSION

From the review it becomes clear that the choice of a specific diagnostic approach depends highly on the engine configuration, the accuracy and number of available sensors and the level of diagnostic-accuracy required. Model based approaches have the advantage that they rely on clear physical relationships between the dependent and independent parameters. Data driven methods on the other hand rely on experimental engine data and experience. The results generated by data driven methods approach are also only valid within the training envelope meaning that unrealistic results might be generated for input data outside the training scope. The fact that no physical engine model is required can be considered as an advantage if no detailed knowledge about the individual gas path components is available. Data driven methods such as ANN have the advantage that they can deal with noisy data and system faults. The choice of the approach depends also on the available sensor-set. Non-linear differential gas path analysis through adaptive modelling for example has the ability to detect, isolate and quantify deterioration accurately over a large operating range. However, the method requires a large number of sensors. Linear gas path analysis on the other hand becomes inaccurate outside the validation envelope due to its linearisation assumption meaning that only small shifts in performance can be predicted accurately.

As for the MTT micro turbine engine, data driven methods will not be possible because no large pool of experimental data is available to train the model. Linear gas path analysis will as well not be applied due to its restriction in application due to the linearisation assumption. Differential gas path analysis requiring a large number of sensors will also be difficult because of the limited number of available measurements. Therefore, a more traditional method relying on performance parameter trending is used to diagnose the condition of the engine. A non-linear engine model built in GSP (Gas Turbine Simulation Program) is used to derive reference performance parameter baselines of a healthy engine which are used to compare the performance of field engines against. Once the reference performance baselines are determined, the effect of deterioration on performance is investigated by simulating different types of deterioration in GSP. Next, the simulation results are interpreted and rule-sets to detect specific types of deterioration are established. The approach is explained more in detail in Chapter 6.

3

MTT's Micro-CHP system description and specifications

Before the development of the diagnostic concept can start, it is important to understand how the micro-turbine CHP system of MTT works and why it defers from bigger gas turbines. In this chapter, the working principles of the CHP system will be explained together with some specific performance characteristics of micro-turbines. Next, the available sensor-set together with the control logic of the engine are discussed. The chapter concludes with a simplified power balance of the Enertwin giving an overview of the various losses in the system and their magnitude.

3.1. General system description

In May 2008, MTT started the development of the Enertwin, a heat demand driven micro *Combined Heat and Power* (CHP) system by using off-the-shelf automotive turbocharger technology for the turbo-machinery. Now, a first generation field test units is installed to have a better understanding on how the system behaves over a long period of time and changing operating conditions. The engine is a single shaft centrifugal gas turbine running on natural gas and designed to deliver a net electrical output of 3kWe and 15kW of heat at standard ISA conditions (288.15K, 1.01325bar and 60 % humidity). Figure 3.1 shows the design of the micro-turbine assembly.

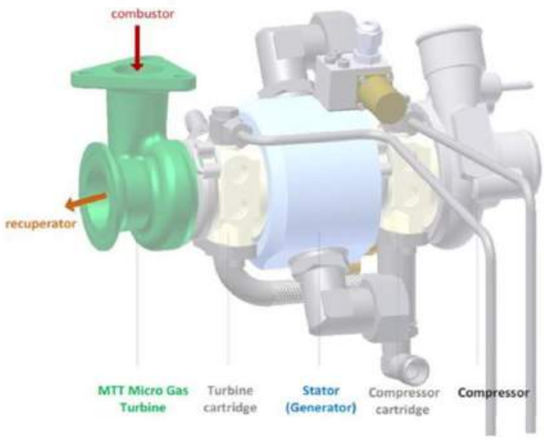

Figure 3.1: Micro-turbine assembly [17]

Combined heat and power generation is an efficient way to generate electricity and useful heat simultaneously. The gas turbine generates both, mechanical power and useful heat. The mechanical energy is converted into electricity by the generator whereas a heat exchanger converts heat from the exhaust gasses

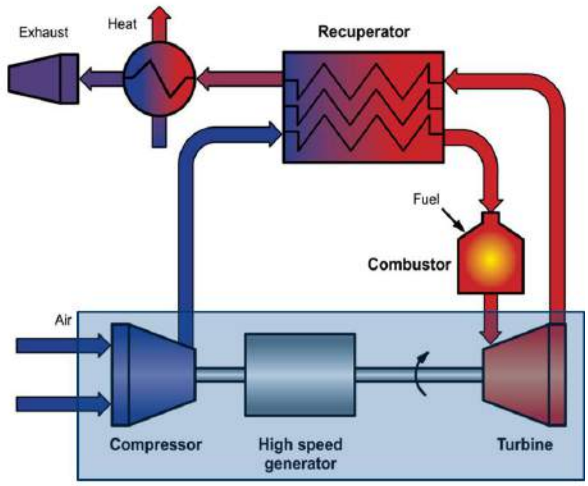

Figure 3.2: Typical CHP system layout

into useful hot water. A typical layout of a CHP-system using a gas turbine as main driver is shown in Figure 3.2. To improve the cycle efficiency, the gas turbine is equipped with a recuperator that recovers heat from the gas turbine exhaust gasses to preheat the compressor discharge air prior to combustion. This results in fuel savings and hence an increase in efficiency. Although the recuperator increases the thermodynamic efficiency of the cycle, the CHP potential decreases due to the lower exhaust temperatures. Other disadvantages of the recuperator are the large size and high cost. Table 3.1 shows the main specifications of the system.

Compressor type	Radial
Number of stages	1
Fuel	Natural Gas
Turbine type	Radial
Number of stages	1
Shaft Speed	240000 RPM
Net electrical ISA power	3 kWe
Net electrical efficiency	12%
Heat output	15 kW

Table 3.1: Main system specifications

3.2. THERMODYNAMIC CYCLE

The ideal recuperated joule-Brayton cycle in the TS-diagram is shown in Figure 3.3. The cycle follows following sequence:

- 2-3: Isentropic compression of air by the centrifugal compressor. Work required by the compressor: $W_c = \dot{m}_{air} \cdot (h_{03} - h_{02}) = \dot{m}_{air} \cdot C_{p,air} \cdot (T_{03} - T_{02})$
- 3-31: Pressurized air goes through the recuperator where heat from the hot exhaust gasses is used to increase the temperature of the air. Heat added by an ideal recuperator [1]: $Q_{rec} = \dot{m_{air}} \cdot C_{p,air}.(T_{031} - T_{03})$
- 31-4: Additional heat is supplied to the pressurized air by burning fuel in the combustion chamber: $Q_{comb} = \dot{m}_{gas} \cdot C_{p,gas}.(T_{04} - T_{031})$

[1] Effectiveness is defined as the ratio of actual heat transfer to the maximum possible heat transfer that can hypothetically be achieved. An ideal recuperator is assumed to have an effectiveness of 1 meaning that there is no temperature difference between the incoming and exiting fluids. Hence, $T_{31} = T_5$ and $T_3 = T_6$ in Figure 3.3

- 4-5: Energy from the hot gas is converted into useful shaft power by isentropic expansion of hot pressurized air. Work done by the turbine: $W_T = \dot{m}_{gas} \cdot C_{p,gas} \cdot (T_{05} - T_{04})$.
- 5-6: Heat from the exhaust gasses is converted in the recuperator to heat the compressor discharge air. $Q_{rec} = \dot{m_{gas}} \cdot C_{p,gas}.(T_{05} - T_{06})$
- 6-2: Heat transfer to the ambient. $Q_{amb} = \dot{m_{gas}} \cdot C_{p,gas}.(T_{06} - T_{02})$

Assumptions made in the ideal cycle calculations

- Working fluid stays the same throughout the cycle and is considered an ideal gas
- Perfect recuperator with effectiveness of 1
- Isentropic compression and expansion in the compressor and turbine
- No pressure loss in the combustion chamber and heat recovery equipment due to mixing and friction

The thermal efficiency of the ideal recuperated cycle is given by:

$$\eta_{th} = \frac{W_T - W_C}{Q_{Comb}} = \frac{C_p \cdot (T_{04} - T_{05}) - C_p \cdot (T_{03} - T_{02})}{C_p \cdot (T_{03} - T_{05})} = 1 - \frac{T_{02}}{T_{04}} \cdot PR^{\frac{k-1}{k}} \tag{3.1}$$

Equation 3.1 shows that the thermal efficiency of the ideal recuperated cycle depends on maximum cycle temperature and pressure ratio. Efficiency of the cycle increases with increasing turbine inlet temperature and decreasing PR. One should keep in mind that this equation is only valid as long as T_{03} lower than T_{05}, otherwise there is no recuperation any-more. Specific work on the other hand is maximum if the pressure ratio is such that the exhaust temperature of the turbine and compressor are the same.

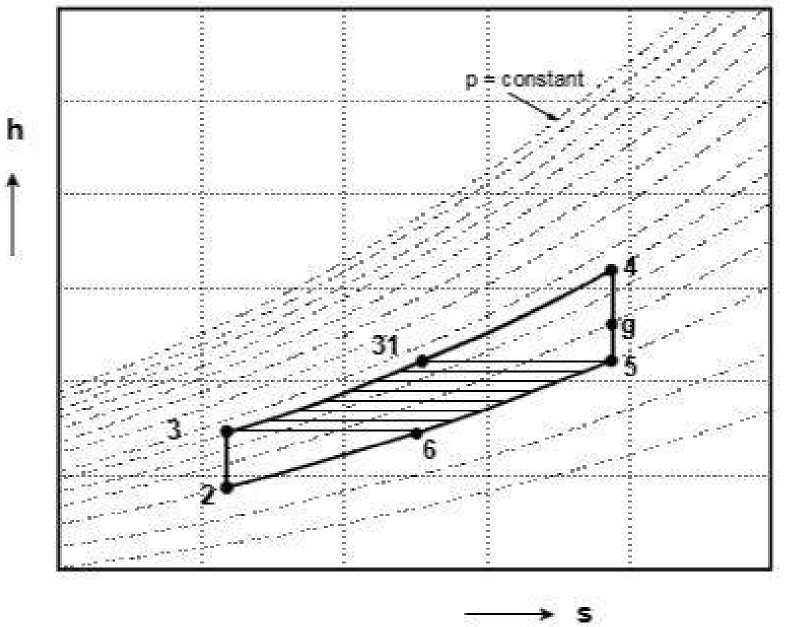

Figure 3.3: Ideal recuperated Bryton cycle in the TS-diagram [18]

3.3. SMALL-SCALE EFFECTS

Apart from the difference in size and rotational speed, micro turbines and large industrial gas turbines behave quite different. In this section, the main differences in performance due to scaling-effects are discussed. The reason for the difference in performance can be summarized by following 3 factors:

Manufacturing and geometrical constraints: When downscaling, relative manufacturing tolerances cannot be maintained resulting in higher relative tip-clearances of the turbo machinery components which has a large impact on component performance [1]. Next, due to the small scale and manufacturing constraints, relative engine-to-engine variations are bigger for micro turbines [19].

Lower Reynolds numbers: As Reynolds number is the ratio of inertia forces over viscous forces [1], a decrease in Reynolds number will result in higher friction losses and hence reduce the thermodynamic efficiency. Reynolds number can be expressed by:

$$Re = \frac{c \cdot R \cdot \rho}{\mu} or \frac{\omega \cdot R^2 \cdot \rho}{\mu} \tag{3.2}$$

whereas tip Mach-number can be written as:

$$M = \frac{\omega \cdot R}{\sqrt{k \cdot R \cdot T}}. \tag{3.3}$$

Where:
c = speed of the flow [$\frac{m}{s}$]
ρ = density of the fluid [$\frac{kg}{m^3}$]
R = diameter impeller [m]
μ = dynamic viscosity [$\frac{Ns}{m^2}$]
ω = impeller rotational speed [$\frac{rad}{s}$]
R = gas constant [$\frac{J \cdot kg}{K}$]
k = isentropic coefficient [/]

When downscaling, tip Mach number remains similar which results in a linear decrease of Reynolds number with decreasing radius. Due to the higher viscous losses, a large fraction of the torque will be used to overcome casing drag exerted by the casing wall viscous layer [20].

Larger heat transfer due to larger surface-to-volume ratios: Heat transfer is the product of heat-flux times surface area whereas the thermal storage is proportional to the volume [21]. When downscaling, the surface area (m^2) of the components becomes relatively larger compared to the volume (m^3) which results in larger heat losses. Because of the heat loss, compression and expansion in the turbo-machinery cannot be considered adiabatic any more. At the entry of the turbine, where the boundary layer is thin and temperature difference between the gas and walls is highest, heat loss is expected to be large which results in a performance reduction. Due to the heat losses, more fuel will required for the same power which results in a lower thermodynamic efficiency.

Relatively high auxiliary system losses and mechanical losses due to low power output levels: When downscaling, the relative power consumption of the auxiliaries (fuel-compressor, oil/water pump, fan, etc.) becomes larger which has an impact on the net electrical output of the system. This is mainly because the efficiencies of the auxiliary system decreases when downscaling.

3.4. Sensor set

A sensor will only be installed if its overall benefit outweighs the added costs [1]. In case of the Enertwin the sensor-set is just sufficient to safely control the engine and do some health monitoring. As performance based condition monitoring capabilities rely heavily on the availability and accuracy of the measurements, the writer expects that the available sensor set will be insufficient for advanced diagnostics. The lay-out of the phase one field-test units together with the available sensor-set as installed in the field is depicted in Figure 3.6. From the lay-out of the system it becomes clear that the sensors can be subdivided into three categories based on their location: gas-path, oil-path or water-path. Although this thesis assignment focusses on the behaviour of components in the gas-path, measurements from the other paths could be used to obtain more information about the gas-path. The cabinet temperature for instance is a useful parameter to detect leakage in the gas-path. Table 3.2 gives an overview of the available gas-path measurements and their accuracy. One additional gas-path measurement has been added to the list which is the compressor inlet pressure. The compressor inlet pressure is measured by the compressor discharge pressure sensor (p_3) when the system is not running and is assumed to stay constant over the run. If one assumes that no heat is exchanged between the temperature sensors and the surroundings, the temperature measured by the sensors placed in the flow-field is the total temperature given by: $T_0 = T_s + \frac{c^2}{2 \cdot C_p}$ [22]. Pressure sensors measure static pressures.

Parameter	Description	Sensor Type	Accuracy
T_0_2	Inlet temperature	NTC	+-3% by 25 deg. Celcius
p_0	Compressor inlet pressure	Absolute Pressure sensor	+- 0.5%
p_3	Compressor discharge pressure	Absolute Pressure sensor	+- 0.5%
T_t34	Inlet temperature combustor	Thermocouple	+- 2.2K
T_t5	Turbine exit temperature	Thermocouple	+- 2.2K
T_exh	Exhaust temperature after mixng with fan-flow	NTC	+-3% by 25 deg. Celcius
N_1	Turbine rotational speed	Hall Sensor	/
p_f	Fuel pressure	Relative Pressure sensor	+- 0.5%

Table 3.2: Available gas-path measurements in the field-units

3.5. CONTROL LOGIC

Although the Enertwin has the capability to operate at various speeds, its design-operational speed is 240000 rpm. The engine is controlled by keeping two parameters constant namely the shaft rotational speed (N_1) and turbine exit temperature (TT5). TT5 is controlled by setting the speed of the reciprocating fuel compressor which determines the fuel flow. For a constant TT5, shaft rotational speed is controlled by controlling the torque required by the synchronous machine. If for instance the rotational speed falls below 240 krpm, the torque absorbed by the synchronous machine will decrease so that the machine can again speed-up to 240 krpm. The control logic of the engine is summarized in Figure 3.4. Different power-codes are used to determine the set-point of the system. A power-code of 100 corresponds to a rotational speed of 240000rpm and a turbine exit temperature of 1060K which is the maximum power-setting of the system. Power-code 20 corresponds to idle power which is the recommended minimal steady-state power setting. Table 3.3 gives an overview of the expected net electrical power output for various power-settings.

PC= Power Code	N [rpm]	PW_el [kWe]
20 %	180000	0.8
60%	200000	1.5
100%	240000	3

Table 3.3: Electrical power output for various power-settings

Another control parameter used during start-up is the combustion entry temperature or TT34. TT34 is used to determine the rate at which the system can accelerate from standstill to 200krpm. For a cold start and hence cold recuperator, the rate at which the engine can accelerate to maximum speed is lower compared to the case where the recuperator is hot. Once TT34 reaches a temperature of 960K, the machine can accelerate to 240krpm. Acceleration of the gas turbine is limited because the fuel-compressor can only deliver a maximum amount of fuel due to its limited power-capacity. Moreover, it would be inefficient to operate at high power codes if the recuperator is still cold as it takes time to heat the recuperator.

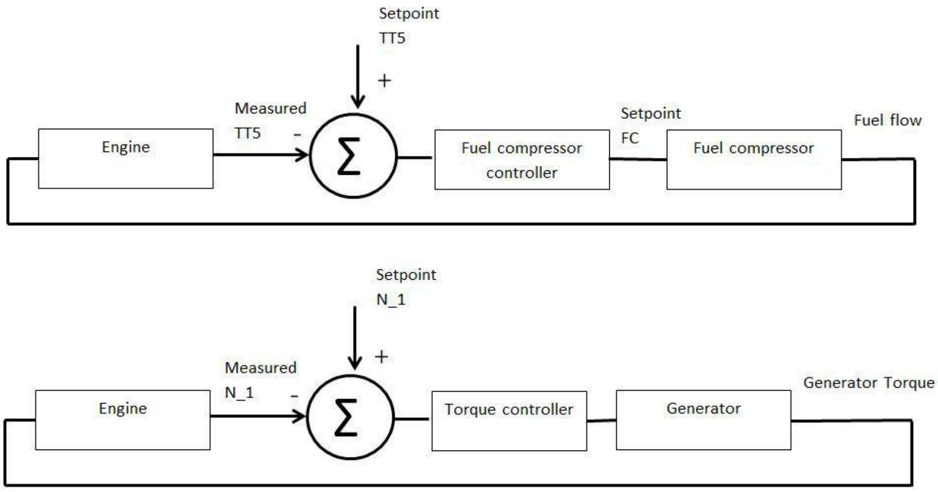

Figure 3.4: Control logic of the engine

3.5.1. FLAT RATING

On cold days, the engine produces more power for the same rotational speed which in some cases might exceed the maximum generator current. To prevent the engine from overloading, the generator power-output is flat-rated for low ambient temperatures by reducing the shaft rotational speed. In Chapter 6, the effect of ambient conditions on performance is discussed more in detail.

3.6. POWER BALANCE

The purpose of the CHP-system is to convert chemical energy coming from the fuel into useful heat and electric power. If the system is treated as a black-box where fuel is inputted and heat and electric power outputted, the system could be approximated as shown in Figure 3.5. A Sankey diagram is used to show how the fuel power is distributed over the system. The power balance for standard ambient conditions and maximum power settings is shown in Figure 3.7. The diagram shows that due to the poor efficiency of the compressor a large portion (about 63 percent) of the turbine shaft power is needed to compress air. Mechanical and generator losses are also relatively large compared to large power plants.

Figure 3.5: Black-box of the CHP system

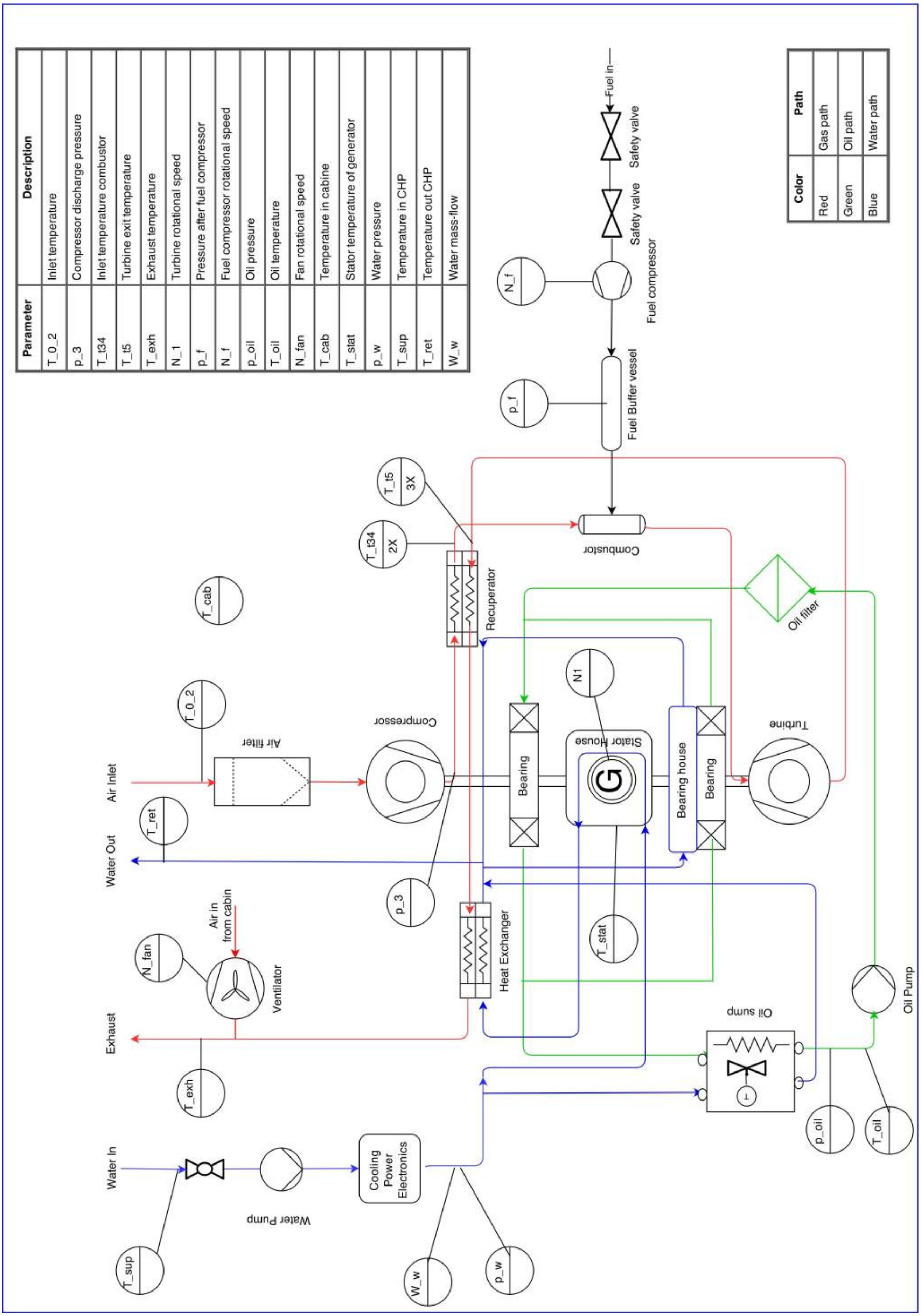

Figure 3.6: Available sensor set

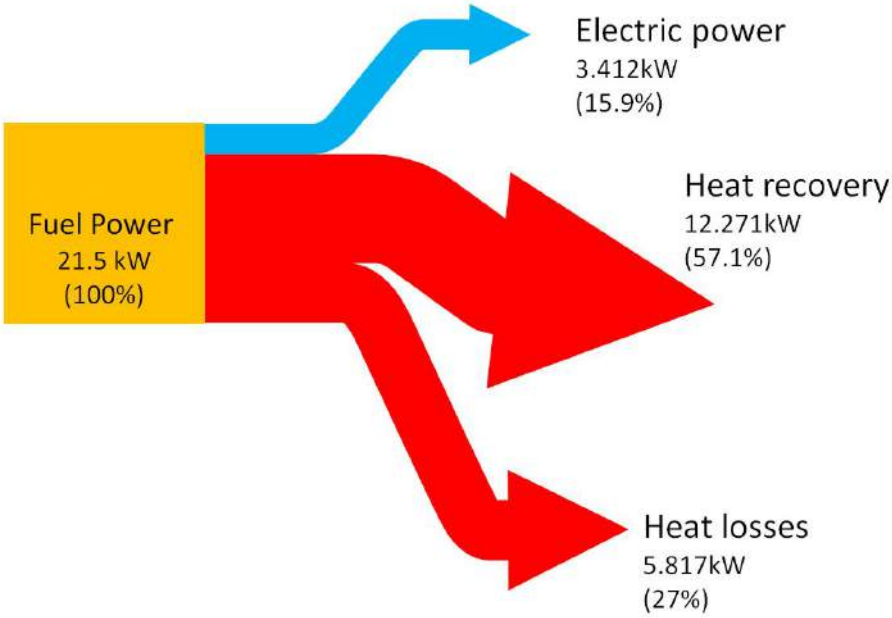

(a) Power balance for standard ambient conditions and maximum power settings

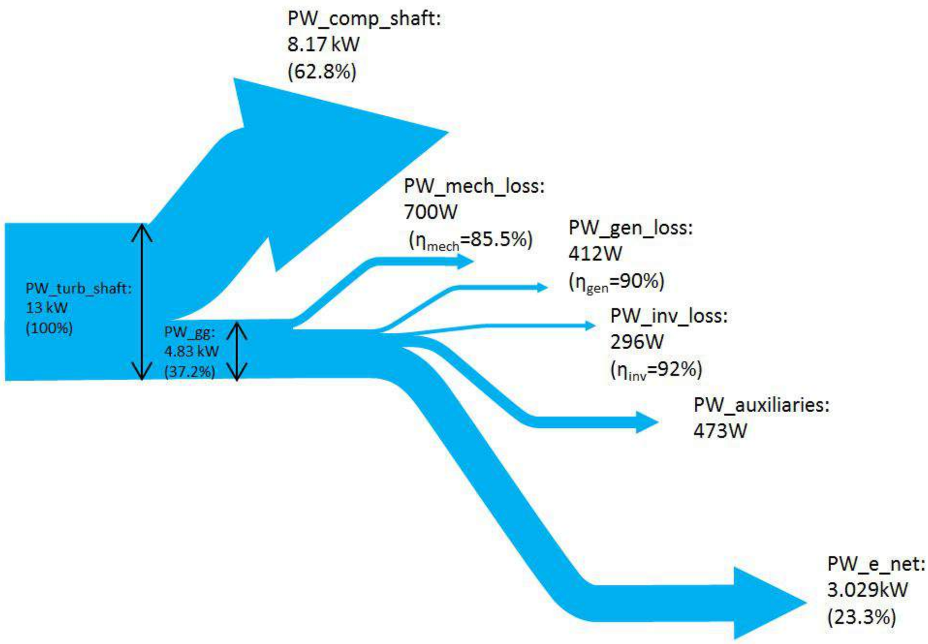

(b) Sankey diagram for standard ambient conditions and maximum power settings

Figure 3.7: Sankey diagram for the micro turbine CHP system

4

ENGINE PERFORMANCE MODELLING IN GSP

In this chapter, the non-linear performance modelling environment of the Gas Turbine Simulation Program is introduced. This is followed by a description of the non-linear reference engine model built in GSP which forms the bases to develop the performance based diagnostic concept. Next, the component performance characteristics, model accuracy and model assumptions are discussed. In section 4.5, a sensitivity analysis is conducted which is used to identify performance parameters that can best detect changes in health parameters. The chapter concludes with some effect studies to investigate the effect changing of operating conditions on performance.

4.1. EXPERIMENTAL SET-UP

The off-design steady-state behaviour of the engine for changing ambient conditions and changing component performance is modelled in the Gas Turbine Simulation Program or GSP. GSP is a zero-dimensional object oriented gas turbine simulation program that allows the user to create a modular non-linear gas turbine model by selecting generic components from libraries. The zero-dimensional gas-turbine model is composed of several component models that together form the complete engine model. By thermodynamically and mechanically coupling of the different components, a solution at discrete points (inlet and exit of each component) is found. Once the model is validated, it allows the user to predict changes in engine performance for various off-design conditions without having to do experimental tests on the system.

The 0-D model does not take the actual geometry of the components into account which means that multi-dimensional and second-order effects such as temperature and pressure variations in the flow path cross-area and Reynolds-number effects are neglected in the calculations. Each component in the model is considered as a black-box of which only the average fluid characteristics at input and exit of the component are calculated [23].

The model will first be used to establish performance parameter baselines of a healthy reference engine. Next, the effect of deterioration on performance will be investigated by simulating various types of deterioration in GSP. Map modifiers are used to simulate deterioration in the model which is further elaborated in Chapter 7.

4.2. DESCRIPTION OF GSP-MODEL

The micro turbine engine model as implemented in GSP is depicted in Figure 4.1. The primary components of the model consist of an inlet, radial compressor, recuperator, combustion chamber, radial turbine, heat-exchanger and exhaust. Ducts can be used to simulate pressure losses and bleed flows whereas heat sink components are used to simulate heat losses to other components and the environment. Each of the components have their own component characteristics which are stored in the form of individual values or tables. Compressor and turbine maps for instance are stored in tables. The off-design behaviour of the engine is obtained by matching the performance characteristics of the individual components while satisfying the conservation laws. This procedure is described more in detail in Appendix F. The design point performance characteristics of the important gas path components for base-load operation and standard ambient conditions are summarized in Table 4.1. The compressor map is shown in Figure 4.2. The red line on the map indicates the compressor surge line. Operation near to the surge line should be avoided as blade-surge might lead to a sudden drop in delivery pressure. The compressor operating point is indicated by a black dot. The relative location of the operating point in the compressor map is determined by the *corrected speed* and a *beta value* [23]. This beta value is introduced to avoid numerical convergence problems.[1]

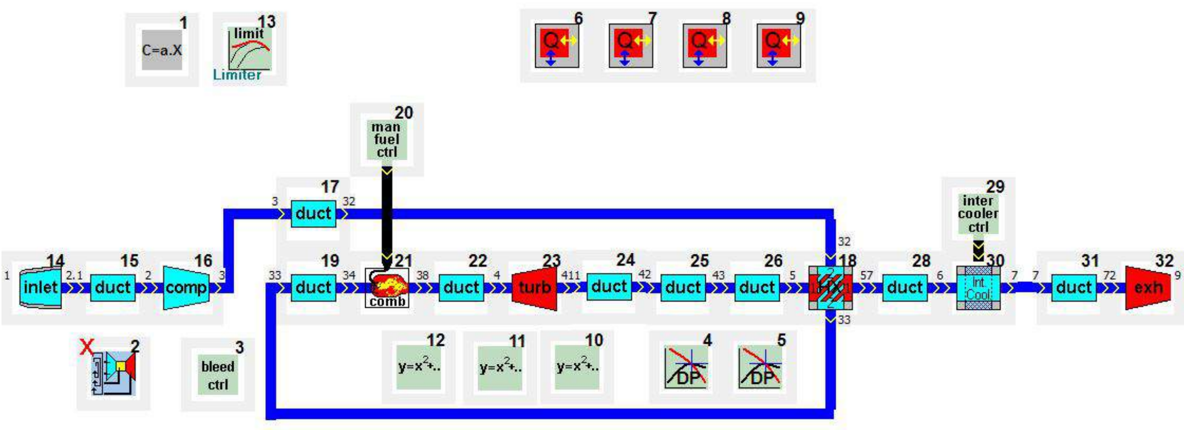

Figure 4.1: Model of the Micro-Turbine engine in GSP

Component	**Performance characteristic**	**Value**
Inlet	Pressure ratio	0.995
Compressor	Pressure ratio	3.1
	Corrected mass flow	54.3
	Corrected rotational speed	2400000
	Isentropic efficiency	0.73
Combustion Chamber	Pressure ratio	0.985
Turbine	Corrected mass flow	40.88
	Isentropic efficiency	0.67
Recuperator	Efectiveness	0.89
	Pressure ratio	0.98

Table 4.1: Design point component performance characteristics for a healthy engine

[1] If a combination of corrected speed and corrected mass-flow would be used to determine the operating point in the compressor map, the operating point would not be uniquely defined once the turbine is chocked.

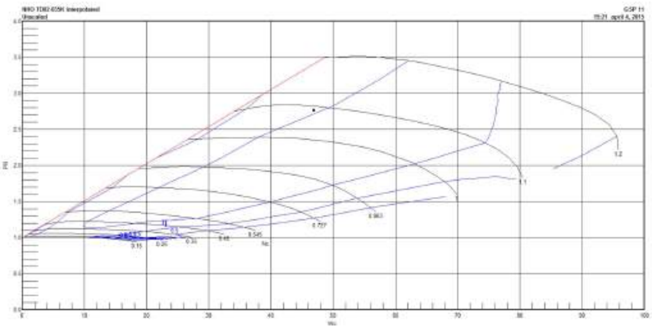

Figure 4.2: Compressor map of the centrifugal compressor

Validation of the model The model developed by previous students and MTT employees is validated by comparing the performance results from tests against simulation results for similar inlet conditions [24]. Table 4.2 shows the difference between real and simulated performance parameters for three pass-off tests. The percentage errors between the measured and simulated values are shown in Figure 4.3. The accuracy of the model can be improved by using the embedded *Adaptive Modelling* capability of GSP which allows the component characteristics to be adapted so that measured and calculated performance parameter match [25]. However, due to component-to-component variations and installation losses, large variations in performance between different systems are possible [2]. Because of these reasons the reference engine model is considered to be sufficiently accurate to use for effect studies which are required to develop the performance based diagnostic concept.

Engine	**T_amb**	**p_amb**	**p_2**	**ps3**	**TT3**	**TT34**	**w_fuel**	**w_air**
757_2	296.95	1.027	0.990	2.900	445.40	987.69	0.566	55.03
GSP	296.95	1.027	0.985	2.898	444.17	997.88	0.563	53.59
828_2	298.27	1.013	0.987	2.862	446.56	978.60	0.565	53.87
GSP	298.27	1.013	0.983	2.879	445.20	997.94	0.558	53.48
842_5	297.24	1.015	0.983	2.925	448.00	972.40	0.571	55.92
GSP	297.24	1.015	0.985	2.895	444.40	997.90	0.562	53.56

Table 4.2: Test results from pass-off test used to validate model at design-point operation

[2]Due to manufacturing constraints, the relative difference in performance between various parts becomes larger for small part which affects the overall system performance.

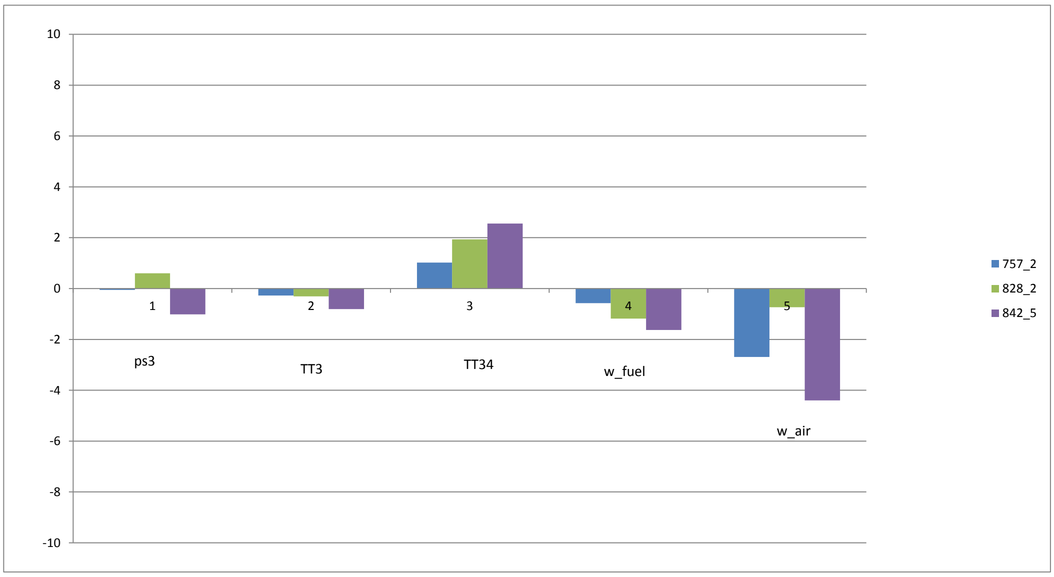

Figure 4.3: Errors between measured and simulated values.

4.3. ASSUMPTIONS

Following assumptions were used for the model and hence apply for the derived performance parameter baselines in next chapter.

- Recuperator effectiveness is assumed constant over the operating range.
- Installation losses are assumed constant. In reality pressure loss depends on the installed ducting, filter and damper.
- Reynolds number effects are neglected
- Multi-dimensional effects are neglected
- Inverter, generator and bearing losses are assumed constant in the simulations. In practice, generator and inverter losses depend on the power generated whereas bearing losses dependent on the health state of the bearings, the oil-characteristics such as viscosity and rotational speed.

4.4. SIMULATING DETERIORATION IN GSP

Practically, component deterioration is simulated in GSP by using *map modifiers*. Map modifier alter the operating point in the component map with respect to the operating point of the healthy engine. For instance, a reduction in compressor isentropic efficiency ($\Delta\eta_c$) results in a deteriorated compressor isentropic efficiency that can be calculated as follows:

$$\eta_{c_{det}} = \eta_c \cdot (1 - \frac{\Delta\eta_c}{100}) \tag{4.1}$$

Figure 4.4 shows the effect of a reduction in pressure ratio (ΔPR) and corrected compressor mass-flow (ΔW_c) on the operating point in the compressor map. Both, the values on the x-axis and the y-axis are shifted according to the pre-defined map modifiers.

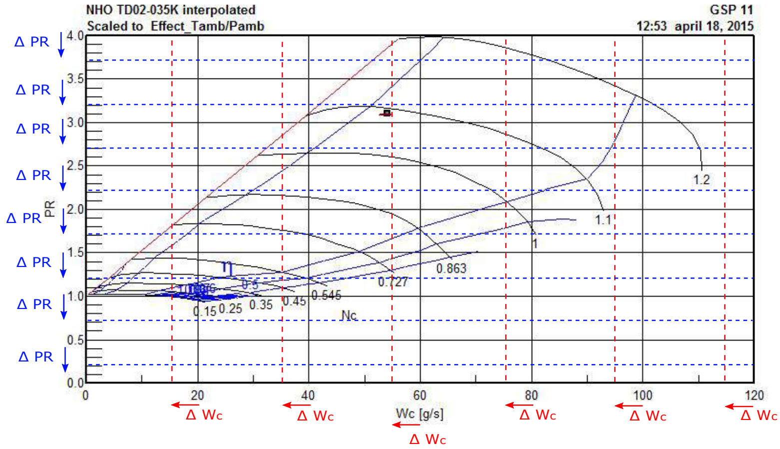

Figure 4.4: Effect of map modifiers for corrected compressor mass-flow and pressure ratio in the compressor map.

4.5. SENSITIVITY ANALYSIS

The accuracy and reliability of the diagnostic concept is highly dependent on the availability and accuracy of the measurements. A non optimal sensor-set might lead to non-detection of engine faults which in turn might reduce the engine availability and increases the costs of ownership. This section discusses a method to determine performance parameters that are most sensitive to shifts in certain health parameters. The results help to determine the optimal sensor-set to detect, isolate and assess specific shifts in health parameters.

4.5.1. EXCHANGE RATE TABLE

By investigating shifts in performance parameters (pressures, temperatures, etc.) for changing health parameters (efficiencies, mass-flow, pressure ratio's, etc.), sensors that are most sensitive to a certain changes in performance can be identified. In GSP, map modifiers are used to change the values of the health parameters. The relations between both parameters can be summarized in the *Exchange Rate Table (ERT)* which is a table showing the percentage change in performance parameter values for a change in health parameters for one specific operating point. The values in the table show the *linear* thermodynamic relation between the performance and health variables. Due to the linearisation assumption, the relation between both variables is only valid for small changes in health parameters and operating conditions. The Exchange Rate Table for the Enertwin is shown in Figure 4.6. The Table is subdivided in following 3 parts:

- Component exchange rates, showing the effect of changing health parameters on performance.
- Environment exchange rates, showing the effect of ambient conditions and installation effects on performance.
- Bias, showing the effect of sensor bias [3] of TT5 on performance.

The performance parameter values of the healthy reference engine for standard operating conditions are summarized in Table 4.3. By using this table together with the ERT absolute shifts in performance due to changes in health parameters can be calculated. From the ERT one can for example say that a three percent decrease in compressor isentropic efficiency causes a 1.05 percent increase in compressor exit temperature (TT3) and a decrease in net electric power of 7.016 percent. The table can be used to select performance parameters that are most sensible to shifts in health parameters which is helpful to select the appropriate measurement-set to detect specific types of deterioration. Figure 4.5 gives an overview of the performance parameters that are most sensitive to shifts in health parameters and how they behave.

[3] A bias of 5K for TT5 means that sensor TT5 under-estimates the actual turbine exit temperature by 5K, which means that the actual turbine exit temperature is 5K higher than measured.

$\Delta\ \eta_c$ (-3%)	$\Delta\ w_c$(-3%)	ΔPR (-3%)	$\Delta\ \eta_t$ (-3%)	$\Delta\ \varepsilon_{rec}$ (+1%)	$\Delta\ TT5$(+5K)
• ΔTT3: +1.05% ↑ • ΔPW_e: -7.02% ↓	• ΔTT3 : -0.53% ↓ • ΔPW_e: +2% ↑	• ΔPT3: -1.82% ↓ • ΔPW_e: -4.74% ↓	• ΔPW_e: -12.1% ↓ • No change in compressor performance	• ΔTT6: -1.18% ↓ • ΔTT34 :+0.49% ↑	• ΔTT34: +0.45% ↑ • ΔTT6: +0.21% ↑ • ΔPW_e: +1.11% ↑

Figure 4.5: Selection of performance parameters to detect shifts in health parameters.

HEALTHY ENGINE AT ISA CONDITIONS		
TT2	[K]	288.1
PT2	[bar]	1.00815
TT3	[K]	437.7
PS3	[bar]	3.06348
TT34	[K]	997.5
PT34	[bar]	3.058426
TT4	[K]	1323.4
PT4	[bar]	3.012285
TT5	[K]	1060
PT5	[bar]	1.0447470
TT6	[K]	531.5
PT6	[bar]	1.02374
TT7	[K]	314.7
PT7	[bar]	1.02374
TT9	[K]	314.7
PT9	[bar]	1.023748
I_rms	[I]	11.96
WF	[g/s]	0.63241
PW_e_net	[kW]	3.0285
W1	[g/s]	54.06
PWshaft	[kW]	4.820
Heat rate (Fuel input power/ Shaft power)	[/]	5.455

Table 4.3: Reference performance values for a healthy engine at standard ISA conditions and standard operating conditions (TT5=1060K and N=240000rpm) in GSP

	COMPONENT EXCHANGE RATES						ENVIRONMENT EXCHANGE RATES				BIAS	
	COMPRESSOR ETA (-3%)	COMPRESSOR CAPACITY (-3%)	COMPRESSOR PRESSURE RATIO (-3%)	TURBINE ETA (-3%)	TURBINE CAPACITY (+3%)	RECUPERATOR EFFECTIVENESS (+1%)	AMB. TEMP. (+10K)	AMP. PRESSURE (-10mBAR)	PRESSURE RECOVERY (3%)	BACKPRESSURE (3%)	TT5 BIAS (5K)	TT34 (1K)
TT2	0	0	0	0	0	0	3.47	0	0	0	0	0
PT2	0	0	0	0	0	0	0	-0.987	-3.015	0	0	0
TT3	1.05	-0.527	-0.368	-0.054	-0.492	-0.009	1.687	0.012	-0.003	-0.037	0.044	0
PT3	-0.019	-0.375	-1.816	-0.047	-0.466	-0.008	-3.544	-0.983	-3.037	-0.032	0.038	0
TT34	0.039	-0.021	-0.022	-0.002	-0.007	0.489	0.051	-0.004	-0.015	-0.001	0.453	-1
PT34	-0.019	-0.376	-1.817	-0.047	-0.472	-0.003	-3.545	-0.984	-3.038	-0.032	0.037	0
TT4	-0.01	-0.027	-0.149	-0.545	-0.192	-0.055	-0.364	0.043	-0.26	-0.373	0.47	0
PT4	-0.02	-0.376	-1.819	-0.057	-0.565	-0.013	-3.552	-0.983	-3.042	-0.039	0.038	0
TT5	0	0	0	0	0	0	0	0	0	0	0	0
PT5	0	-0.021	-0.102	0.014	0.151	0	-0.195	-0.988	-0.169	2.834	-0.002	0
TT6	0.704	-0.355	-0.254	-0.113	-0.374	-1.177	1.139	0.021	-0.015	-0.077	0.208	0
PT6	0	-0.007	-0.036	0.005	0.052	-0.001	-0.067	-0.987	-0.059	2.943	-0.004	0
TT7	0.061	-0.031	-0.022	-0.01	-0.033	-0.103	0.099	0.002	-0.001	-0.007	0.018	0
PT7	0	-0.007	-0.036	0.005	0.052	-0.001	-0.067	-0.987	-0.059	2.943	-0.004	0
TT9	0.061	-0.031	-0.022	-0.01	-0.033	-0.103	0.099	0.002	-0.001	-0.007	0.018	0
PT9	0	-0.007	-0.036	0.005	0.052	-0.001	-0.067	-0.987	-0.059	2.943	-0.004	0
I_rms	-6.243	1.725	-4.483	-10.941	3.629	-0.192	-9.877	-1.128	-11.077	-7.482	1.025	0
w_f	-0.169	-0.407	-2.276	-2.077	1.715	-1.648	-4.957	-0.801	-3.898	-1.421	0.455	0
P_e_net	-7.016	2.001	-4.743	-12.131	3.955	-0.065	-10.496	-1.142	-11.964	-8.295	1.11	0
m_air	-0.012	-0.361	-1.733	0.269	2.534	0.045	-3.341	-1.008	-2.893	0.184	-0.218	0
P_shaft	-5.337	1.474	-3.832	-9.352	3.102	-0.164	-8.443	-0.964	-9.468	-6.395	0.876	0

Figure 4.6: Exchange rate table of the Enertwin for standard operating conditions.

Observations from the ERT

- The Exchange Rate Table shows that a decrease in compressor capacity of 3 percent results in a power increase. This is because for standard operating conditions, the compressor is not operating at its most efficient operating point. Because the compressor is over-sized for the turbine, the velocity-triangles at the compressor inlet are not optimal for the given rotational speed. A decrease in compressor capacity causes a shift to the left of the corrected speed lines resulting in an efficiency increase. Figure 4.7 shows how the compressor isentropic efficiency increases with decreasing compressor capacity.
- A change in turbine performance has almost no effect on the performance of the compressor.
- Effect of inlet pressure loss is bigger than the effect of backpressure.
- Change in compressor pressure ratio has a large effect on fuel flow. This is mainly because a change in PR affects the air mass-flow of the gas-turbine.

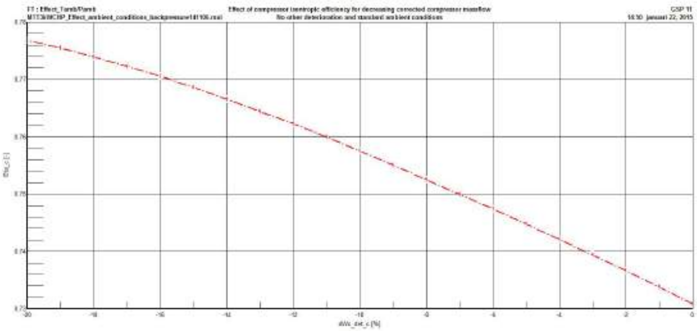

Figure 4.7: Effect of decreasing compressor capacity on compressor isentropic efficiency for standard ambient conditions.

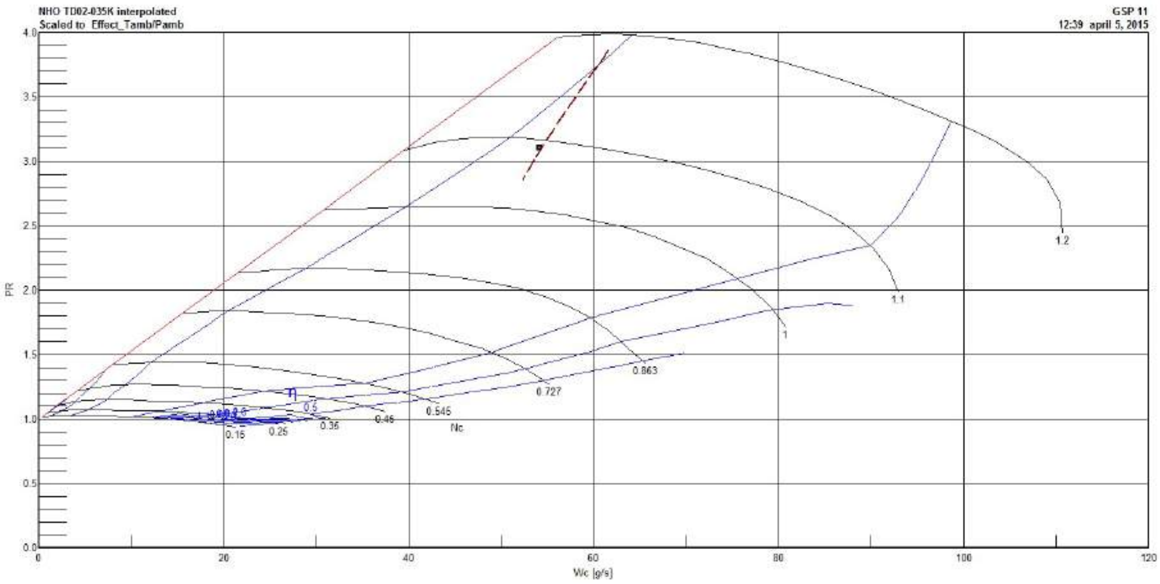

Figure 4.8: Running line in the compressor-map for changing ambient temperatures.

4.6. EFFECT STUDIES

In this section, the effect of changing ambient conditions and installation losses on engine performance are discussed. Only the effect of ambient temperature and pressure is considered as studies have shown that the effect of humidity on performance can be neglected [3]. To investigate the effect of ambient conditions on performance, steady-state series are simulated in GSP for varying ambient pressures from 0.8 bar to 1.1 bar and ambient temperatures from 243K to 313K. The effect of installation loss on performance is simulated by varying the inlet pressure-ratio and backpressure in the inlet-component and backpressure-component respectively.

4.6.1. EFFECT OF AMBIENT TEMPERATURE

For increasing ambient temperature, the density of air drops what results in a reduction in air mass flow rate, shaft power and fuel flow. Next, the corrected rotational speed of the compressor reduces for increasing ambient temperature resulting in a reduction in compressor pressure ratio. Net electric efficiency decreases too because more power is required to compress air of a higher temperature. Thermal and total efficiency on the other hand increase with increasing ambient temperature. This is because the temperature difference between the exhaust gasses and the ambient becomes smaller for increasing ambient temperatures meaning that less heat is transferred form the exhaust gasses to the environment. Turbine inlet temperature decreases for increasing ambient temperature which has a positive effect on the turbine's creep life. TIT decreases because the expansion ratio over the turbine decreases for increasing ambient temperatures resulting in a lower TIT as shown by equation 4.2

$$T_{04} = \left(1 - \eta_t \left[1 - \frac{p_{04}}{p_{05}}^{\frac{\gamma-1}{\gamma}}\right]\right) \cdot T_{05} \tag{4.2}$$

Figure 4.8 shows the effect of ambient temperature on compressor performance in the compressor map. The running line shows that pressure ratio and corrected mass-flow decrease for increasing compressor inlet temperature. Figures A.1 and A.2 in the appendix show the effect of ambient temperature on engine performance for constant standard ambient pressure and base-load operation. Following definitions for efficiency where used:

- $\eta_{e,net} = \frac{PW_{e,net}}{PW_{fuel}}$
- $\eta_{th} = \frac{PW_{heat}}{PW_{fuel}}$
- $\eta_{tot} = \frac{PW_{e,net}+PW_{heat}}{PW_{fuel}}$

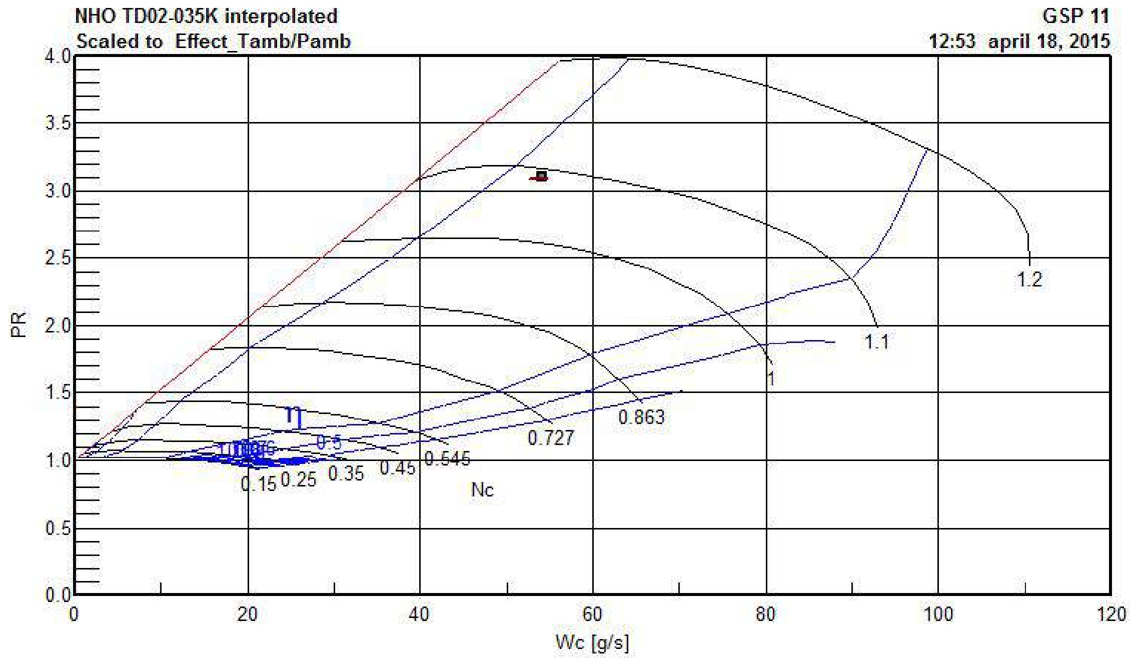

Figure 4.9: Compressor running line for varying ambient pressure from 0.4 to 1.1 bar

Flat rating At low ambient temperatures, more power and a higher current is generated resulting in more copper losses and hence higher stator temperatures which could be harmful for the stator. To prevent overheating in the generator and the power-electronics, flat-rating should be applied when operating at low ambient temperatures. Flat rating is introduced by reducing the rotational speed while keeping the current to a maximum value of 12 Amperes. Simulations for the reference model show that flat-rating should be applied for ambient temperatures below 282 K which corresponds to a TIT of 1326K. The effect of flat-rating on engine performance is shown in Figures A.3 in the appendix.

4.6.2. EFFECT OF AMBIENT PRESSURE

Ambient pressure drops with increasing altitude resulting in a decrease in density, air mass-flow, fuel flow and shaft power. Because the corrected speed lines in the compressor map are almost horizontal within the operating range, PR is almost independent of ambient pressure. The compressor running line for changing ambient pressure from 0.4 bar to 1.1 bar while keeping ambient temperature 288.15K is shown in Figure 4.9. The effect of ambient pressure on engine performance is shown in Figures A.5 and A.6. One should notice that the turbine inlet temperature increases with both; decreasing ambient temperature and pressure meaning that operation at high altitudes could be harmful for the turbine if the TIT would not be limited.

4.6.3. INSTALLATION EFFECTS

Installation losses consist of inlet pressure loss and backpressure. Inlet pressure loss is the result of air passing around obstacles such as filters, ducts, bends and silencers. Exhaust pressure loss is a pressure drop caused by exhaust ducts, silencers and heat recovery equipment creating a backpressure on the turbine. Backpressure reduces the pressure-ratio across the turbine, and, therefore the power output of the turbine. Inlet pressure loss has a slightly bigger effect on the performance compared to the backpressure because it reduces the inlet air density and increases the relative backpressure [26]. Pressure loss is linearly proportional to the dynamic head of the flow as shown in Formula 4.3. The value of the pressure loss coefficient depends on the obstacles in the flow. The effect of inlet and exhaust pressure loss was investigated by varying the inlet pressure ratio and exhaust pressure in the inlet-component and the backpressure component respectively. The effect of installation losses on engine performance are summarized in Table 4.4. The simulation results show that pressure loss has a significant impact on net electric power and efficiency. In practice, the effect of installation losses on performance will not be significant simply because the dynamic head of the flow in the inlet and exhaust ducting is low resulting in relatively small pressure losses. Table 4.5 gives an overview of the flow properties and estimated pressure losses at the different sections obtained by using Moody's diagram. The dimensions of the inlet ducting are shown in Figure 4.10

$$p_{loss} = C_f \cdot \frac{\rho c^2}{2} \tag{4.3}$$

Where:
C_f = Pressure loss coefficient
ρ = Density of the fluid [$\frac{kg}{m^3}$]
c = Air velocity [$\frac{m}{s}$]

	PW_e_net	**Eta_e_net**	**TIT**
Inlet pressure loss	-118 W per 10mBar	-0.36 % per 10mBar	-1.1K per 10mBar
Exhaust pressure loss	-93 W per 10mBar	-0.31 % per 10mBar	-1.6K per 10mBar

Table 4.4: Effect of installation loss on engine performance

Inlet air mass flow of 55g/s				
Duct diameter (m)	Mean Airspeed (m/s)	Dynamic Head (pa)	Reynolds number	Pressure loss (pa) per m pipe
0.10	5.72	20.04	39141.73	5.41
0.08	8.94	48.92	48927.16	15.90
0.033	52.52	1689.52	118611.30	1279.94

Table 4.5: Flow properties and pressure loss at different section for friction factor of 0.03 (drawn pipe) mass-flow rate of 55 g/s

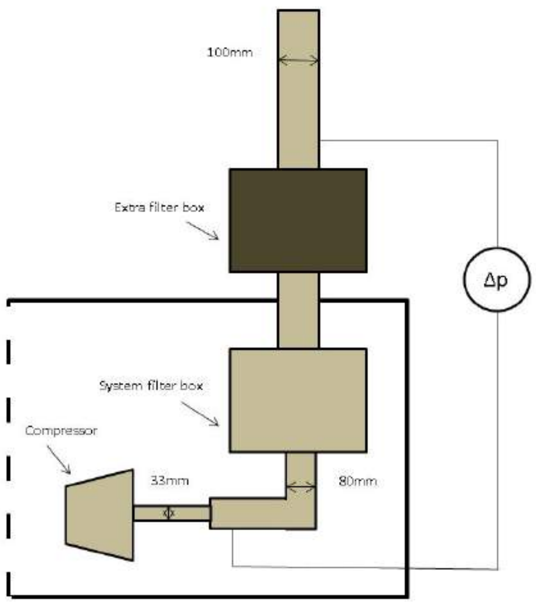

Figure 4.10: Set-up of the experiment to determine the effect of inlet pressure loss on performance

Effect of cabinet fan on system performance Field units are equipped with a fan which has two functions. Firstly, the fan creates an under-pressure to prevent natural gas form being spread in the room when a leakage would occur. Secondly, the fan controls the temperature inside the cabinet. The cabinet fan sucks air from the inlet through the filter into the cabinet back to the exhaust. Due to the fan, the air mass-flow through the inlet and exhaust becomes larger which has an effect on the installation losses and hence the system performance. To determine the effect of the cabinet fan speed on the system performance, a test was performed. The set-up of the experiment is shown in Figure 4.10. During the test, the fan-speed was varied from zero to maximum speed while measuring the generator power and inlet pressure loss. The experiment showed that the effect of fan speed on system performance is small. The maximum variation in generator power due to the change in inlet pressure loss was 20W.

4.6.4. EFFECT OF SUBSYSTEM LOSSES ON MEASURED GRID POWER

This section discusses the effect of heat losses, bearing losses and generator losses on measured grid power. The main objective is to get an insight in possible factors, other than gas-path related factors, that might be responsible for deviations in measured grid power.

POWER MEASUREMENT

Shaft power cannot be measured directly. The only indication for shaft power in the field is *grid power* measured at the exit of the grid inverter before the auxiliaries. Figure 4.11 shows where grid power is measured. Due to the small size of the system, changes in heat losses, generator losses and bearing losses could possibly have a large effect on the measured grid power. In following subsections the effect of subsystem power losses on measured grid power is discussed more in detail.

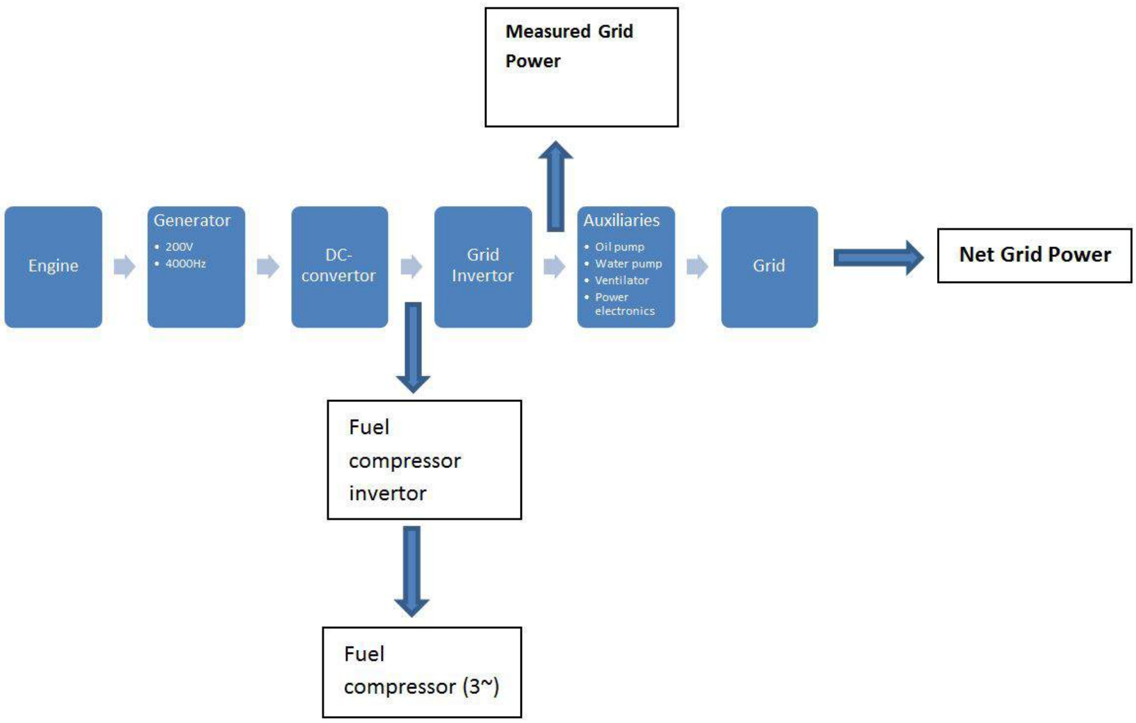

Figure 4.11: Location of the Grid Power Measurement

EFFECT OF WATER TEMPERATURE ON PERFORMANCE

Due to the large heat transfer from the hot parts (turbine and combustor) to the cooler parts, the bearing house on turbine side is cooled by the return water [4]. A decrease in return water temperature and hence increase in temperature difference between the hot parts and the cooling water results in an increasing heat transfer from the hot parts to the water. Due to the larger heat loss from the turbine to the water, more fuel will be required to keep the TT5 at a constant value of 1060K. The turbine inlet temperature increases as well for decreasing return water temperature which might affect the turbine's creep life. Besides cooling the turbine bearing house, the water is also used to cool the stator-house and the oil in the oil-sump which has an effect on the oil temperature and hence oil viscosity. The stator-house should be cooled to prevent the stator-windings from over-heating when large power-levels are generated. Because the resistance of copper is temperature-dependent (see section 4.6.4), copper losses will also be function of the cooling water.

MECHANICAL LOSSES ($\approx 700W$)

Mechanical losses due to friction in the bearing house exit the machine through heat which is passed to the oil, cooling water and ambient. Bearings can be lubricated by either mineral or more expensive synthetic oil which has a higher self-ignition temperature. Due to the high temperatures in gas turbines, synthetic oil is used for lubrication. Besides lubrication, the oil also provides cooling and damping of vibrations in the shaft. The shaft of the MTT micro-turbine is supported by floating ring bearings which require a continuous supply of pressurized oil for proper functioning. In axial direction, the movement is restricted by a thrust bearing. The power dissipation by the floating ring bearings depends on the bearing geometry, oil viscosity, rotational speed and oil film thickness [27]. Equation 4.4 also known as Petroff's equation can be used to estimate the radial bearing loss in journal bearings where μ is the dynamic viscosity of the oil, ω is the rotational speed, L is the length of the bearing and h is the oil film thickness. The modified Petroff equation shown in equation 4.5 can be used to predict the frictional loss in double sided thrust bearings where r_o and r_i are the outer and inner radius respectively and ϵ_{th} is the axial clearance. Petroff's equation shows that friction loss is highly dependent on the geometry of the bearings: the larger the contact surface is, the larger the power loss will be.

$$P_{radial} = \frac{\pi}{4}\frac{\mu\omega^2 LD^3}{h} \tag{4.4}$$

$$P_{radial} = \frac{\pi\mu\omega^2(r_o^4 - r_i^4)}{\epsilon_{th}} \tag{4.5}$$

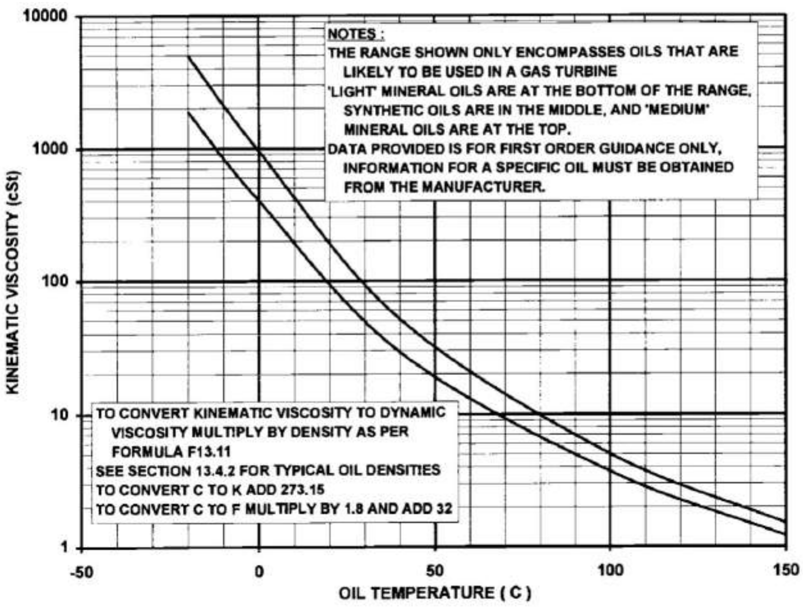

Figure 4.12: Kinematic viscosity in function of temperature for oil [1]

[4]Return water = cold water flowing into the system

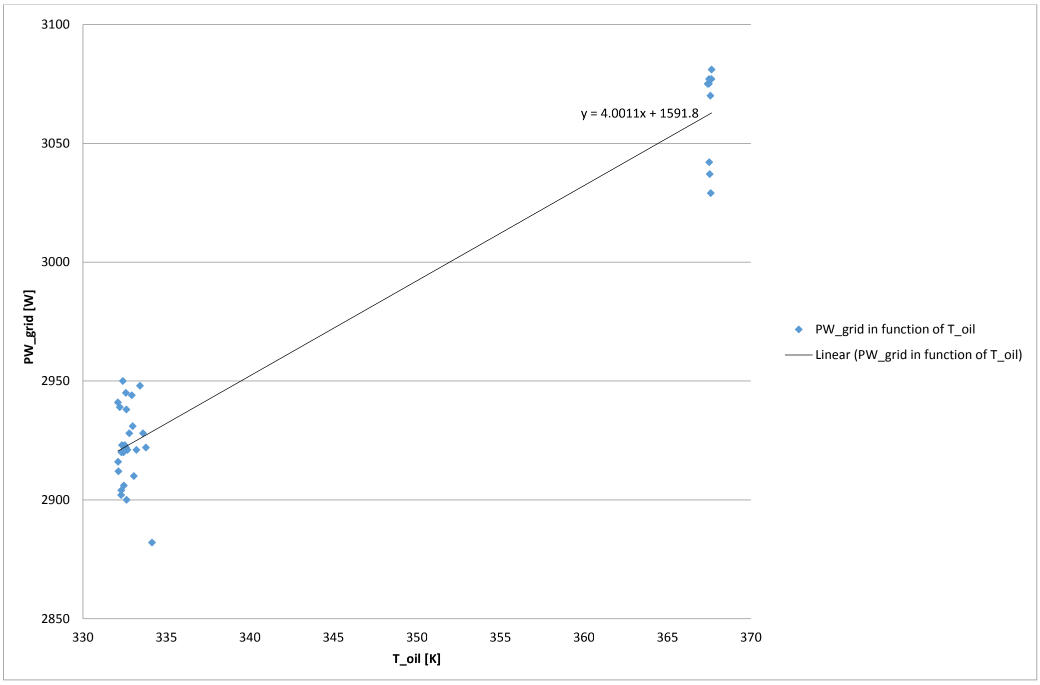

Figure 4.13: Effect of oil temperature on grid power

Effect of oil temperature on mechanical losses Figure 4.12 shows the relation between oil viscosity and oil temperature for various types of oil. The graph shows that the viscosity decreases logarithmically for increasing oil temperatures which causes a reduction in bearing losses and damping. If the viscosity of the oil decreases, the damping-effect of the oil decreases as well which might cause excessive vibrations in the shaft which in turn might cause rubbing of rotating parts against the static parts. From experience, oil temperature varies between 60 °C and 90 °C whereas the oil pressure varies between 2 bar and 3.5 bar overpressure.

Tests were performed to investigate the effect of oil temperature on performance. During the tests, oil temperature was varied while keeping the other performance parameters constant. The oil-temperature was varied from 330K to 370K by changing the cooling water-flow through the oil-sump. The effect of changing oil temperature on grid power is shown in Figure 4.13. If the relation between oil temperature and grid power is assumed linear within this temperature-range, grid power is expected to increases at a rate of **4 Watt per degree Kelvin** increase in oil temperature.

GENERATOR LOSSES ($\approx 400W$)

Generator losses can be subdivided into following 3 groups: [28]:

- Iron loss due to eddy currents and hysteresis loss.
- Copper losses due to the resistance of the winding coils.
- Windage loss due to friction between the rotor and the air.

Iron losses are losses induced by changes in flux that can be subdivided into hysteresis losses and eddy current losses. The losses are function of internal voltage, frequency, type of iron and thickness of the laminated plates in the core. Equation 4.6 shows how Iron loss (PW_{iron}) can be calculated [28].

$$PW_{iron} = B^2 \left\{ \sigma_H \left\{ \frac{f}{100} \right\} + \sigma_E d^2 \left\{ \frac{f}{100} \right\}^2 \right\} (W/kg) \tag{4.6}$$

Where:
B = Flux density

σ_H = Hysteresis loss coefficient

σ_E = Eddy current loss coefficient

f = Frequency

d = Thickness of the core steel plate

Equation 4.7 shows the relation between internal voltage E and flux [28].

$$E = 4.44 \cdot f \cdot k_w \cdot N \cdot \phi \tag{4.7}$$

Where:
E = Internal Voltage

f = Frequency

k_w = Winding factor which is function of winding distribution over the stator [28]

N = Number of turns

ϕ = Flux

From Equations 4.6 and 4.7, one could say that iron losses will remain constant if the generator operates at a constant rotational speed and voltage. Iron losses will remain constant for maximum power settings because in that case the machine operates at a constant speed and nearly constant voltage.

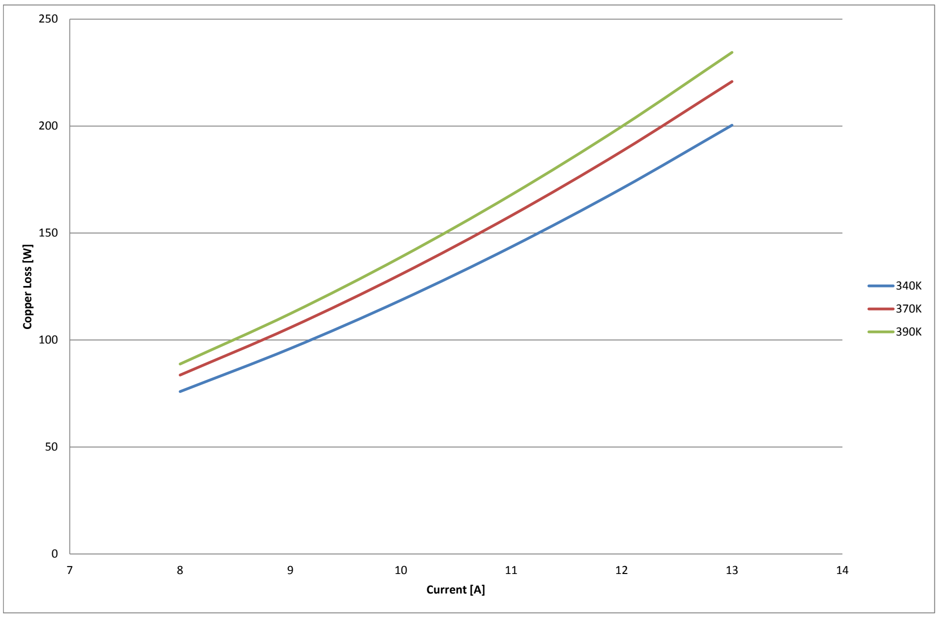

Figure 4.14: Copper loss for changing stator temperature and output current

Copper losses are losses due to the resistance of the of the windings. Copper losses can be calculated from the winding resistance and current flowing through the windings. Equation 4.8 shows how copper losses can be estimated.

$$P_{Cu} = 3 \cdot R(f) \cdot (1 + \alpha \Delta T) \cdot I^2 \tag{4.8}$$

Where:
P_{Cu} = Copper loss

$R(f)$ = Winding resistance at room temperature (293K) and frequency f: R(4000Hz) =0.3322 Ω

α = Temperature coefficient of copper (0.004041 $\frac{\Omega}{K}$)

ΔT = Copper temperature [K] - 293 K

I = rms value of the current

From Equation 4.8 one should notice that copper losses increase quadratically with increasing current and linearly with increasing copper temperature. Practically, copper losses can be estimated from the stator temperature measurement and grid current measurement. Figure 4.14 shows how copper losses vary with changing output current for various stator temperatures.

Windage loss is friction loss due to friction between the rotor and the surrounding air. Equation 4.9 shows that windage loss ($PW_{windage}$) increases quadratically with increasing rotational speed [28]. For maximum power settings and hence constant rotational speed (240000rpm) windage losses remain constant.

$$PW_{windage} = K_W \cdot \omega_m^2 \tag{4.9}$$

Where:
K_W = Friction factor

ω_m = Rotational speed

4.6.5. EFFECT OF SENSOR BIAS IN TT5

The impact of bias in turbine exit temperature measurement (TT5) is investigated because an error in TT5 measurement causes the engine to operate in a different operating point which has an impact on the engine performance. Next, turbine inlet temperature increases with increasing TT5 which has a large impact on the creep-life of the blades and the backplate of the turbine. An increase in hot section temperature of 10-20K can cause a two-fold reduction in blade life [29].

CAUSES FOR BIAS IN TT5 MEASUREMENT

TT5 is measured by three redundant thermocouples located in one single tip. Ideally, the measurement value should be equal to the average cross-sectional turbine exit temperature. However, in practise the measured and true average temperature will deviate due to sensor errors. Measurement bias of sensor TT5 is defined as the difference between the true average turbine exit temperature and the measured temperature. Errors in TT5 measurement might be the result of:

- A change in cross-sectional flow field at the turbine exit could result in a different total temperature distribution across the section which in turn results in a change in TT5 measurement.
- Radiative heat exchange between the hot junction and the surroundings.
- As thermocouples basically measure a temperature difference between a hot and cold junction, the temperature of one of the junctions should be known to calculate the absolute temperature. In case of TT5 measurement, the temperature of the cold junction is the reference temperature. An error in this measurement will automatically result in an error in the measurement of TT5.

In large industrial gas turbines, a better estimation of the average turbine exit temperature is obtained by sensing the turbine exit temperature at different circumferential locations. Next, the measurements are averaged and cold junction compensated. Measurements showing unrealistic values are rejected from the calculations.

EFFECT ON PERFORMANCE

The effect of TT5 on performance can be deduced from the Exchange Rate. From the ERT, following changes in performance are expected if TT5 is measured 5K too low:

- One percent increase in net electric power.
- Increase in measurement TT34 by 0.453 percent or 4.4K.
- 0.455 percent increase in fuel flow.
- 6.2K increase in turbine inlet temperature.

From the simulation results one can conclude that a bias in TT5 can best be detected by looking at measurements for TT34, power output and fuel compressor speed.

5

Demonstration of differential gas path analysis through adaptive modelling (AM) in GSP

Due to the limited number of measurement parameters available from the field, differential gas path analysis through adaptive modelling is currently not possible for the field test units. In this chapter, the capabilities of adaptive modelling in GSP are demonstrated by using data from a fouled and clean engine.

5.1. Numerical methods

In Adaptive Modelling (AM), the performance of the reference model is compared to the performance of the deteriorated engine. The model is adapted iteratively by changing the performance maps of the turbomachinery components till the performance of the deteriorated engine model matches the performance of the field engine. Numerically, the GSP model can be extended to an adaptive model by adding a number of equations equal to the number of measurements to adapt for. Next, an equal number of unknowns representing shifts in component conditions should be chosen to obtain a 'square' equation set which has one specific solution. Figure 5.1 shows the complete set of equations used for adaptive modelling. The upper left square matrix represents the conservation laws showing the reference engine numerically. s_1 through s_n are the unknown states whereas ϵ is the relative equation tolerance used for convergence which is usually really small (typically 0.0001). To transform the model to an adaptive model, m additional equations (f_{m1} to f_{mm}) are added to the set. These equations require that the specified model performance parameters become equal to the measurement values. s_{c1} through s_{cm} are the measurement performance parameters to be solved for whereas ϵ_{mi} are the measurement tolerances. In practice, the constraints for adaptive modelling can be represented by: $f_{mi} = |P_{i,mdl} - P_{i,meas}| \le \epsilon_{mi}$ where $P_{i,mdl}$ and $P_{i,meas}$ are the modelled and measured performance parameters (P_i) respectively.

$$
\begin{array}{ccc|ccccc}
f_1(s_1)+ & \cdots & f_1(s_n)+ & f_1(s_{c1})+ & \cdots & f_1(s_{cm}) & = & \varepsilon \\
\vdots & & \vdots & \vdots & & \vdots & & \\
f_n(s_1)+ & \cdots & f_n(s_n)+ & f_n(s_{c1})+ & \cdots & f_n(s_{cm}) & = & \varepsilon \\
\hline
f_{m1}(s_1)+ & \cdots & f_{m1}(s_n)+ & f_{m1}(s_{c1})+ & \cdots & f_{m1}(s_{cm}) & = & \varepsilon_{m1} \\
\vdots & & \vdots & \vdots & & \vdots & & \\
f_{mm}(s_1)+ & \cdots & f_{mm}(s_n)+ & f_{mm}(s_{c1})+ & \cdots & f_{mm}(s_{cm}) & = & \varepsilon_{mm}
\end{array}
$$

Figure 5.1: Full set of Adaptive Modelling equations [8, 30]

5.2. AM IN GSP

The GSP model could easily be turned into an adaptive model by adding the adaptive model control component as shown in Figure 5.2 . The AM calculations consist of two consecutive steps. First, the model is calibrated by matching the performance of the model to the measured performance of the healthy reference engine by using so-called calibration factors (f_c). This is required to prevent the reference engine model errors to interfere with the adaptive modelling numerical solution. Equation 5.1 shows how the calibration factors are obtained. The next step is to adapt the baseline reference model to the measured performance parameters of the deteriorated engine by using map modifiers. Finally, the calculated performance parameters from step two are transformed as shown in Equation 5.2 where $P_{i,mdl,raw}$ is the calculated performance parameter and $P_{i,mdl}$ is the calibrated performance parameter. The adaptive modelling simulation process is highly dependent on how accurate the reference model matches with the reference engine performance data [8]. Previous studies have shown that the proposed calibration method has a significant impact on the stability and results when the calibration factor deviates more form unity [8, 30]. It was shown that a deviation of 1 percent form unity already has a significant impact on the results. Due to the large system-to-system variations of the micro CHP-system, the performance of the reference model and the healthy engine might deviate by more than 1 percent (see Table 4.2) which will affect the validity of the AM results.

$$f_{ci} = \frac{P_{i,meas,raw}}{P_{i,mdl,des}} \tag{5.1}$$

$$P_{i,mdl} = f_{ci} \cdot P_{i,mdl,raw} \tag{5.2}$$

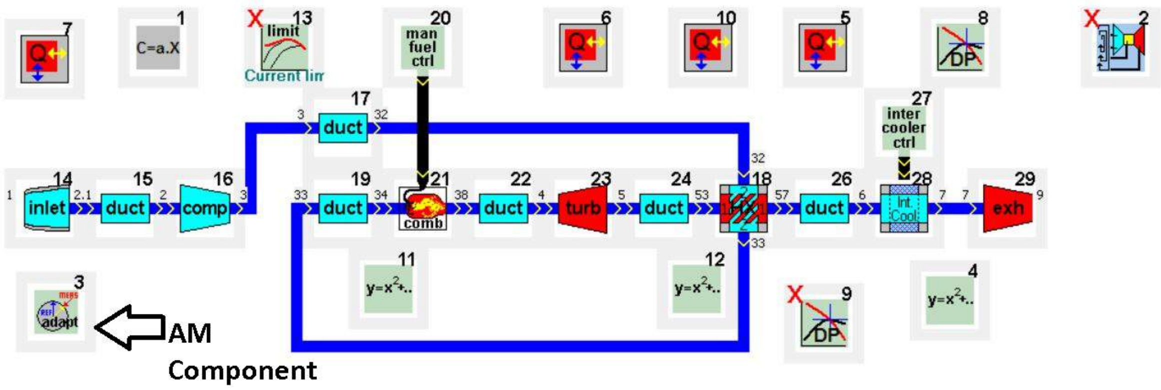

Figure 5.2: Adaptive modelling component in GSP

5.3. TEST CASE

To demonstrate the capabilities of differential gas path analysis test data obtained from a fouled and clean engine were used. The performance values for both engines are summarized in Table 5.1. The clean engine was used to calibrate the model whereas the fouled engine was used to demonstrate the concept. The model was corrected such that the electric power and compressor discharge pressure of the model and the real engine match. Experiments described in Chapter 7 have shown that fouling has a big impact on compressor efficiency and pressure ratio. The model was therefore adapted by changing PR and η_c. The diagnostic results for the fouled engine are summarized in Figure 5.3. The AM results show that the compressor isentropic efficiency in the model decreased significantly (about 11 percent) whereas the compressor pressure ratio did almost not change when matching the electric power and the compressor discharge pressure. The obtained results are not illustrative for fouling because due to fouling the PR should as well decrease and not only the efficiency. Besides the shift in health parameters, the figure also shows the tolerances and deltas used for the performance parameters.

	Health parameters			Performance parameters				
	ETAC	**PRC**	**Wc2**	**Tt2**	**p_amb**	**ps3**	**TT3**	**PW_e_net**
Clean	73.34	2.99	55.54	296.18	0.99	2.805	445.45	3.010
Fouled	66.00	2.83	52.46	295.61	1.00	2.677	450.30	2.210
Deviation in performance [%]	-10 %	-5.3 %	-5.5 %					-26.6 [%]

Table 5.1: Performance and health parameters for the same clean and fouled engine

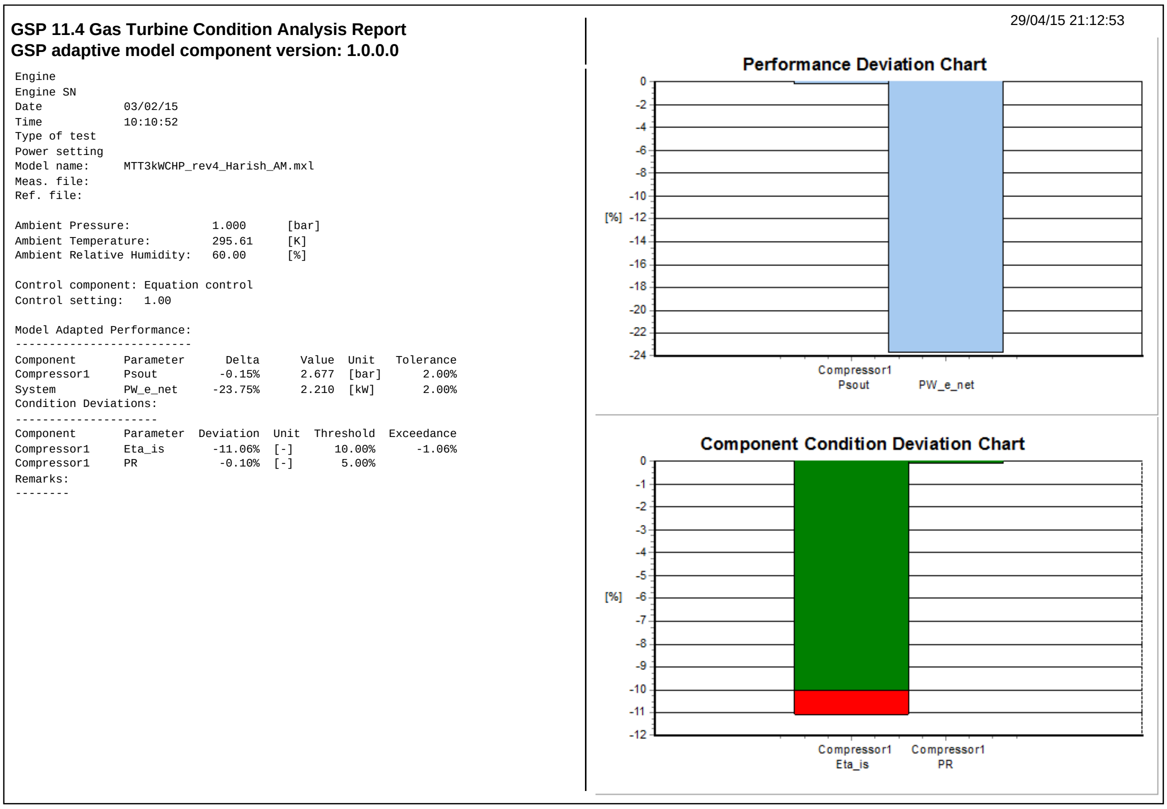

Figure 5.3: Report generated from GSP summarizing the results from AM calculations.

Discussion From the demonstration, one can conclude that AM can currently not be used to diagnose the condition of field units. This is because of the large system-to-system variations and the small number of gas-path measurements available from the field. Due to the limited number of available measurements from the gas path, only a limited number of health parameters can be adapted for making it difficult to use AM as diagnostic tool. One should notice that due to the simple configuration of the engine (single shaft), the compressor health-parameters (PR, η_c) could almost directly be calculated if the compressor discharge temperature would also be measured in the field.

6

GPA BASED DIAGNOSTIC CONCEPT

The developed GPA based diagnostic concept relies extensively on performance parameter trending. Trending is the practice of recording and plotting performance parameters against time. Performance parameters are first corrected for ambient conditions before being compared to reference performance baselines. The healthy reference engine model discussed in Chapter 4 is used to derive the performance baselines. Deviations in baseline and measured performance are analysed and used to diagnose the condition of the engine. As deterioration causes changes in health parameters which in turn induces changes in measurement parameters, relations between both can be used to identify the root cause of the performance degradation.

In this chapter, the procedure to develop reference performance parameter baselines from the healthy reference model is discussed. Section 6.2 shows how the derived baselines can be implemented into the remote condition monitoring software by means of lookup tables. In section 6.3, various causes for deviations from the reference performance parameter baselines are discussed.

6.1. BASELINE TRENDS FOR CONDITION MONITORING

As discussed in previous sections, ambient conditions have a big influence on the performance of gas turbines. To make measured performance parameters comparable, corrections to standard ambient conditions are required which can be achieved by using non-dimensional parameter groups. Once we know how to correct performance parameters to standard conditions, reference performance parameter baselines can be established. These off-design performance curves will form the bases for the diagnostic concept and help to determine the condition of the actual gas turbine. Deviations in expected baseline performance and the actual performance are trended, and patterns in the deviations are used to detect and isolate various gas path faults. An approach based on Mach-number similitude is used to establish corrected performance parameter baselines for the healthy reference engine.

6.1.1. DIMENSIONLESS GROUPS [1, 31]

The performance of gas turbines depends on a large number of variables such as ambient conditions, dimensions, power settings, working fluid and the physical state of the engine. For instance, the steady state mass-flow of an engine with fixed geometry is function of following eight parameters: T_{amb}, p_{amb}, M, N, D, R, γ and μ. Variations of all these quantities independently would require a large number of charts to express the performance of the gas turbine. However, the large number of variables can be reduced by introducing non-dimensional groups. By applying the *Buckingham PI theorem* the function of 8 variables can be reduced to a function of $8-3=5$ non-dimensional groups. This reduction from 8 to 5 variables is due to the presence of three fundamental units (**M**(kilogram), **L**(meter) and **T** (seconds)). Appendix C describes the *Buckingham Pi* theorem more in detail and shows how the large number of variables of a compressor can be reduced by introducing non-dimensional groups. In case of a gas turbine, following non-dimensional groups are obtained after applying the theorem: $\frac{p_{03}}{p_{02}}$, η_{is}, $\frac{m\cdot\sqrt{RT_{02}}}{D^2\cdot p_{02}}$, $\frac{ND}{\sqrt{RT_{02}}}$ and *Re*. For a machine of fixed geometry and working fluid, R and D can be omitted from the groups. Next, Reynolds number (non-dimensional group for viscosity) does not vary much once the flow is highly turbulent and can therefore also be excluded. This leaves us with following non-dimensional groups: $\frac{p_{03}}{p_{02}}$, η_{is}, $\frac{m\cdot\sqrt{T_{02}}}{p_{02}}$ and $\frac{N}{\sqrt{T_{02}}}$. Figures using the non-dimensional parameters as axis will be used to represent the off-design steady-state performance of the engine in a simple way.

6.1.2. MACH NUMBER SIMILARITY

The approach used to correct the performance parameters to standard conditions relies on Mach number similarity. Measured performance parameters are referred to standard day conditions (15°C, 1.01325bar and 60 % relative humidity) by keeping the velocity triangles the same as tested. Since compressibility effects, incidence losses and work dependent on Mach number and flow angles, keeping Mach numbers constant results in a similar gas turbine performance [32]. $\frac{N}{\sqrt{T}}$ is a measure for the rotational Mach-number whereas $\frac{\dot{m}\cdot\sqrt{T}}{p}$ is a measure for the axial Mach number. Similar pairs of $\frac{\dot{m}\sqrt{T}}{p}$ and $\frac{N}{\sqrt{T}}$ give rise to similar velocity triangles which yields to similar performance in terms of pressure ratio and isentropic efficiency [33]. Formula 6.1 gives a general formulation of how performance parameters can be referred to standard ambient conditions where $\Theta = \frac{T_{amb}}{T_{ISA}}$ and $\delta = \frac{p_{amb}}{p_{ISA}}$. Table 6.1 gives an overview of the most widely used standard performance parameter corrections.

$$X_{ref} = \frac{X}{\Theta^a.\delta^b} \tag{6.1}$$

Performance parameter	Corrected performance parameter
Temperature (T)	$\frac{T}{\theta}$
Pressure (P)	$\frac{p}{\delta}$
Mass flow	$\frac{m\cdot\sqrt{\theta}}{\delta}$
Rotational speed (N)	$\frac{N}{\sqrt{\theta}}$
Fuel flow (w_{fuel})	$\frac{w_{fuel}}{\delta\cdot\sqrt{\theta}}$
Shaft power (PW)	$\frac{PW}{\delta\cdot\sqrt{\theta}}$
Shaft Torque (TRQ)	$\frac{TRQ}{\delta}$

Table 6.1: List of standard performance parameter corrections where $\theta = \frac{T_{amb}}{288.15K}$ and $\delta = \frac{p_{amb}}{1.01325bar}$

Restrictions The corrections obtained by the Mach number similarity method are only strictly valid if following conditions apply:

- Gas properties such as R and γ should be invariant. As Mach number is given by $\frac{C}{\sqrt{\gamma RT}}$, changes in gas properties will influence the magnitude of the Mach number. To account for changing gas properties, $\frac{N}{\sqrt{\gamma RT}}$ should be kept constant. Gas properties change for different temperatures, fuel-to-air ratios and humidity.
- Constant Reynolds number and surface roughness. Reynolds number and surface roughness determine the effect of viscosity on engine performance. Ambient pressure has most impact on the value of the Reynolds number. If the geometry of the engine is kept constant and ambient pressure decreases, Reynolds number will fall.
- Geometry of the gas turbine should not change. Deformation of engine hardware leads to variations in tip clearance and blade-twist which has an impact on the flow field and hence the engine performance.
- No heat-loss or leakage to the surroundings.
- Constant installation losses. Flow distortion due to changing installation losses or flow distortion due to cross winds.

Second-order effects might affect the parameter group relations in such a way that additional corrections might be required which will be discussed in the next section.

6.1.3. ESTABLISHING REFERENCE PERFORMANCE PARAMETER BASELINES

This section discusses how the reference performance baselines were established by using data obtained from steady-state simulations in GSP for varying ambient conditions and base-load operation. Because the engine operates most of the time at base-load (TT5=1060K an N=240krpm), the performance parameter baselines are only established for base-load operation. Table 6.2 shows the range of operating conditions for which the reference baselines are valid. Although TT5 should be constant (1060K) for normal base-load operation, TT5 was varied slightly in the simulations to account for the effect of measurement errors in the turbine exit temperature.

Parameter	Operating Range	Units
Ambient temperature	243-313	K
Ambient pressure	0.8-1.1	bar
Relative humidity	60	%
Relative inlet pressure loss	0.5	%
Exhaust pressure loss	0	bar
Shaft rotational speed	240 000	rpm
Turbine exit temperature (TT5)	1040-1070	K

Table 6.2: Operating conditions for which the performance baselines are valid.

Why can standard corrections not be applied? The main reason why the standard corrections from Table 6.1 cannot be applied is because heat-loss cannot be neglected in small gas turbines which is discussed in section 3.3. The effect of heat loss on performance was simulated by adding heat-sink components to the model. Without heat-loss, the performance in terms of corrected performance parameters is independent of ambient pressure. For a constant ambient temperature, the corrected rotational speed ($\frac{N}{\sqrt{TT2}}$) and corrected turbine exit temperature ($\frac{TT5}{TT2}$) are both constant. By keeping these two control parameters constant, all the other corrected parameters remain constant. Figures 6.1a and 6.1b show the corrected air mass-flow and corrected fuel flow in function of corrected rotational speed for an engine without heat-loss. The baselines where obtained by varying the ambient pressure from 0.8 to 1.1 bar and the ambient temperature from 243K to 303K while controlling the engine at base-load. The graphs indeed show that the curves for constant pressure fall on top of each other which indicated that the baselines are independent of ambient pressure if heat-loss would be ignored.

However, if heat-loss cannot be ignored the values for corrected air mass-flow and fuel-flow cannot be derived from one single baseline by only looking at the value for the corrected speed. This is shown in Figures 6.2a and 6.2b. Due to heat-loss from the hot components to the environment, more fuel will be required to keep the turbine exit temperature (TT5) to 1060K which affects the corrected fuel flow. Next, the turbine inlet temperature increases due to the heat-loss which has an effect on the air mass-flow. Once the turbine is chocked, the corrected mass-flow through the turbine remains constant (see Equation 6.2). The increase in TIT due to heat-loss reduces the air mass-flow through the turbine which has an effect on the corrected air mass-flow ($\frac{\dot{m_{air}} \cdot \sqrt{\theta}}{\delta}$). Heat-loss and hence the corrected performance parameters depend on the ambient pressure because:

- Ambient pressure affects the air mass-flow through the turbine which in turn affects the heat transfer to the environment.
- Convection depends on density which in turn is function of pressure.

Due to the heat loss and other second order effects such as changing gas properties for different temperatures, the standard corrections could not be applied. Next section shows how the corrected performance baselines where established so that one single baseline was obtained.

$$\frac{\dot{m}_{04} \cdot \sqrt{TIT}}{p_{04}} = constant \tag{6.2}$$

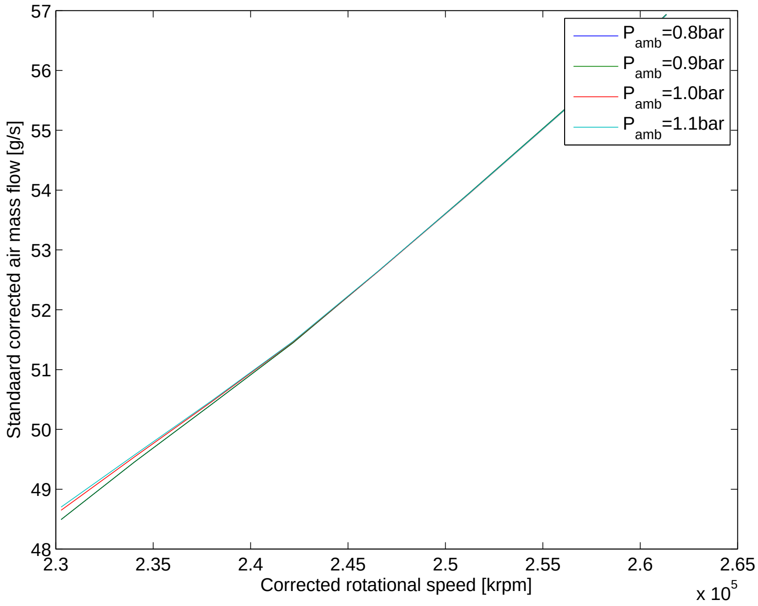

(a) $m_{cor,air}$ in function of N_{cor}

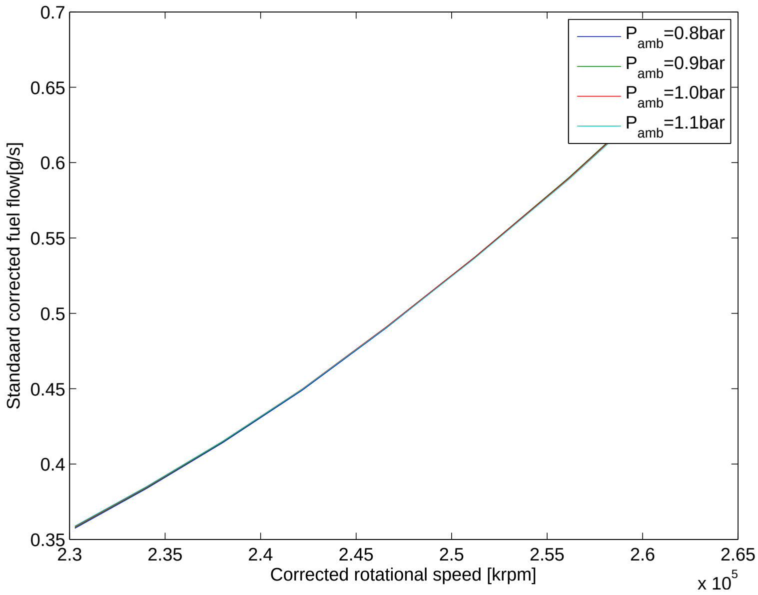

(b) $m_{cor,fuel}$ in function of N_{cor}

Figure 6.1: Corrected performance baselines when heat-loss is ignored. (Note: curves with constant pressure fall on top of each other)

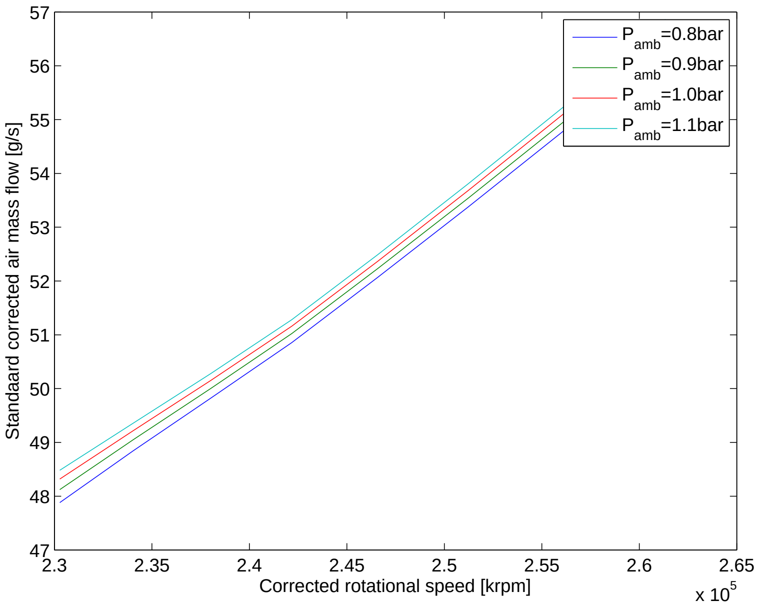

(a) $m_{cor,air}$ in function of N_{cor}

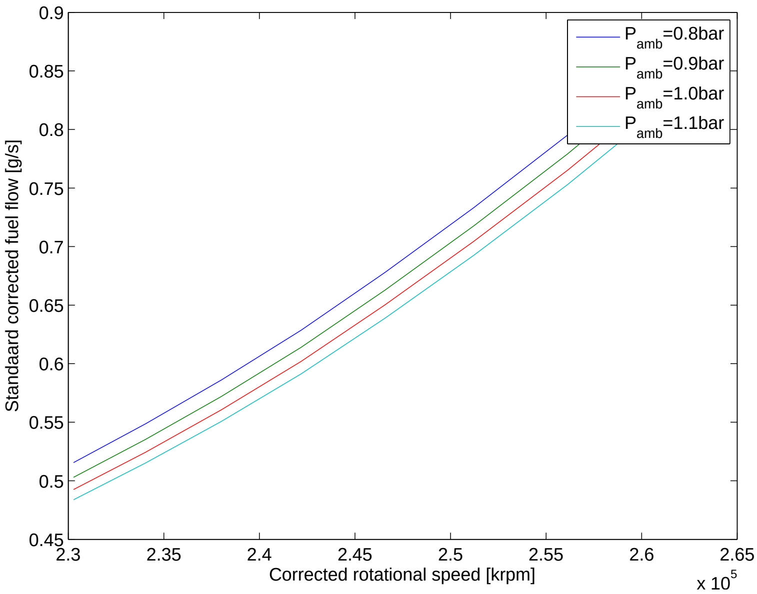

(b) $m_{cor,fuel}$ in function of N_{cor}

Figure 6.2: Corrected performance baselines with heat-loss included. (Note: curves with constant pressure do not fall on top of each other)

Procedure used to derive the performance baselines First, the performance values were corrected using the standard parameter group relations summarized in Table 6.1. Next, temperature (θ) and pressure (δ) exponents are raised to exponents other than 0.5 and 1 so that the curves showing the corrected performance values for various constant ambient pressures become parallel to each-other. Finally, additional linear terms are added so that one single baseline is obtained which is valid over the complete operating range. Figure 6.3 shows how the corrected grid power baseline is obtained using this procedure.

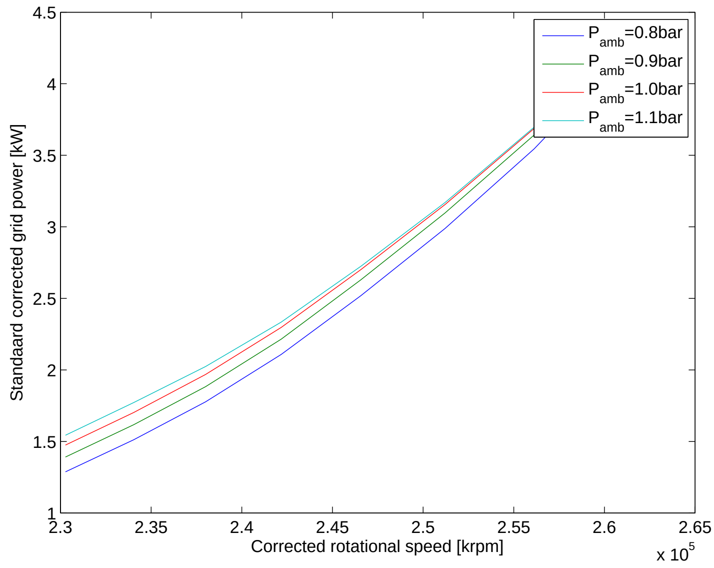

(a) Step 1: Standard correction for grid power ($\frac{PW_{grid}}{\sqrt{\theta}\cdot\delta}$)

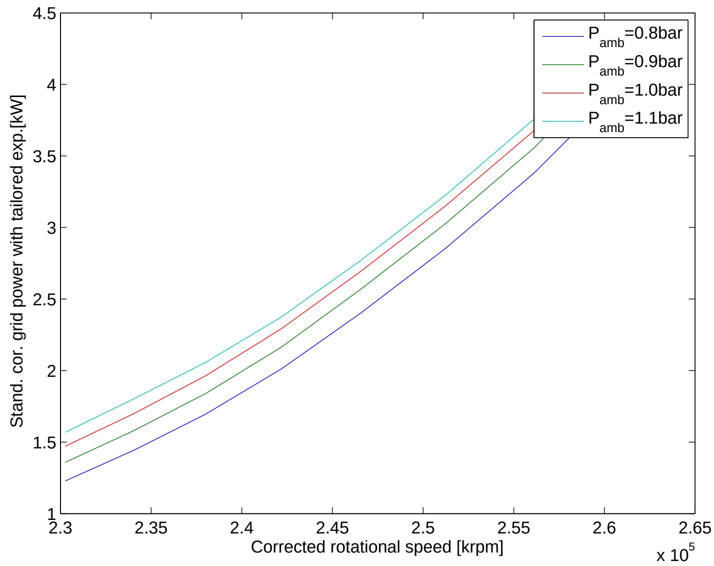

(b) Step 2: Altering the exponents δ and θ so that the performance lines of various ambient pressures become parallel.

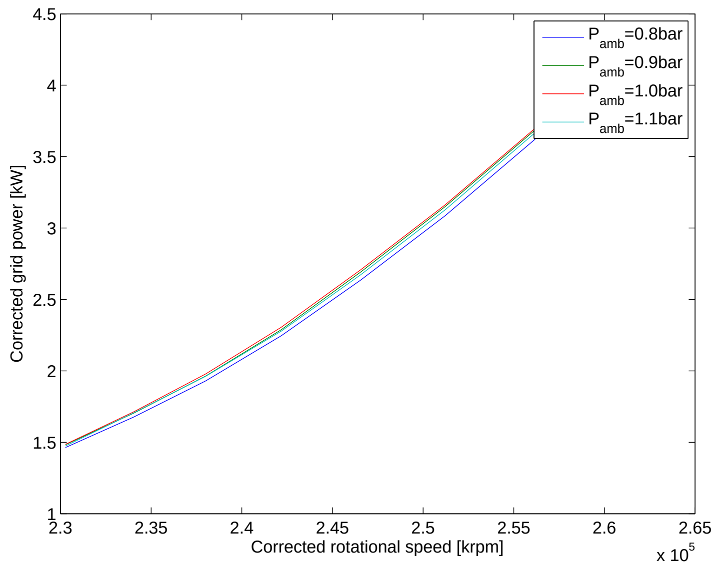

(c) Step 3: Additional linear correction for ambient pressure so that the performance lines fall on top of each-other.

Figure 6.3: Sequence to correct the performance parameter values so that single performance parameter baselines can be established

Standard performance parameter corrections could not be used because of secondary effects such as heat losses. Next, the relatively big power take-off of the auxiliaries and mechanical/electrical losses affect the corrected grid-power too. The corrected performance parameters are all plotted against the corrected rotational speed.

The obtained performance baselines show the expected off-design behaviour of the healthy reference engine for changing ambient conditions while operating at base-load. Table 6.3 shows the expressions found by following this procedure. From these eight expressions, only the corrected compressor discharge pressure and corrected grid power are used for diagnostic purposes because these are the only diagnostic measurements available from the field. The corrected grid power and corrected compressor discharge pressure baselines are shown in Figures 6.4 and 6.5 respectively. The remaining baselines can be found in Appendix B.

Performance parameter	**Referred parameter**
Rotational speed	$\frac{N_1}{\sqrt{\theta}}$
Grid electric power	$\frac{PW_{grid}}{\sqrt{\theta}\cdot\delta^{0.85}} - 1.1\cdot(p_{amb} - 1.01325) - (TT5 - 1060)\cdot 0.0065$
Shaft power	$\frac{PW_{shaft}}{\sqrt{\theta}\cdot\delta}$
Fuel flow	$\frac{w_{fuel}}{\sqrt{\theta}\cdot\delta^{0.9}} + 0.07\cdot(p_{amb} - 1.01325) - (TT5 - 1060)\cdot 0.0005$
Inlet mass flow	$\frac{w_{in}\cdot\sqrt{\theta}}{\delta} - 1.2\cdot(p_{amb} - 1.01325) + (TT5 - 1060)\cdot 0.02$
Compressor isentropic efficiency	$\eta_c - 0.015\cdot(p_{amb} - 1.01325) + (TT5 - 1060)\cdot 0.00015$
Compressor discharge pressure	$\frac{p_3}{\delta}$
Compressor discharge temperature	$\frac{T_3}{\theta} + 5\cdot(p_{amb} - 1.01325) - (TT5 - 1060)\cdot 0.0401$

Table 6.3: Expressions for referred performance parameters

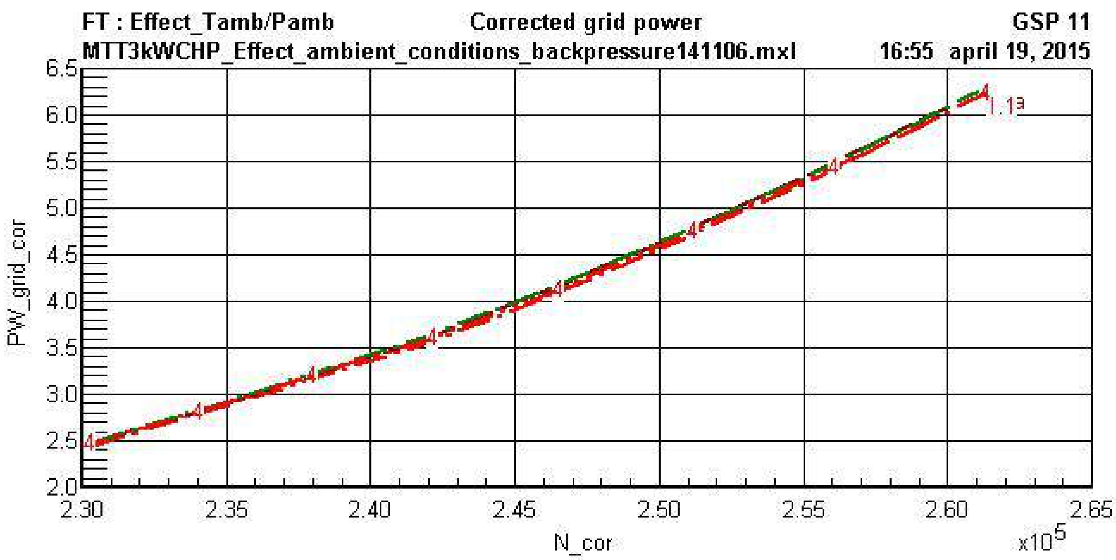

Figure 6.4: Corrected grid power in function of corrected rotational speed

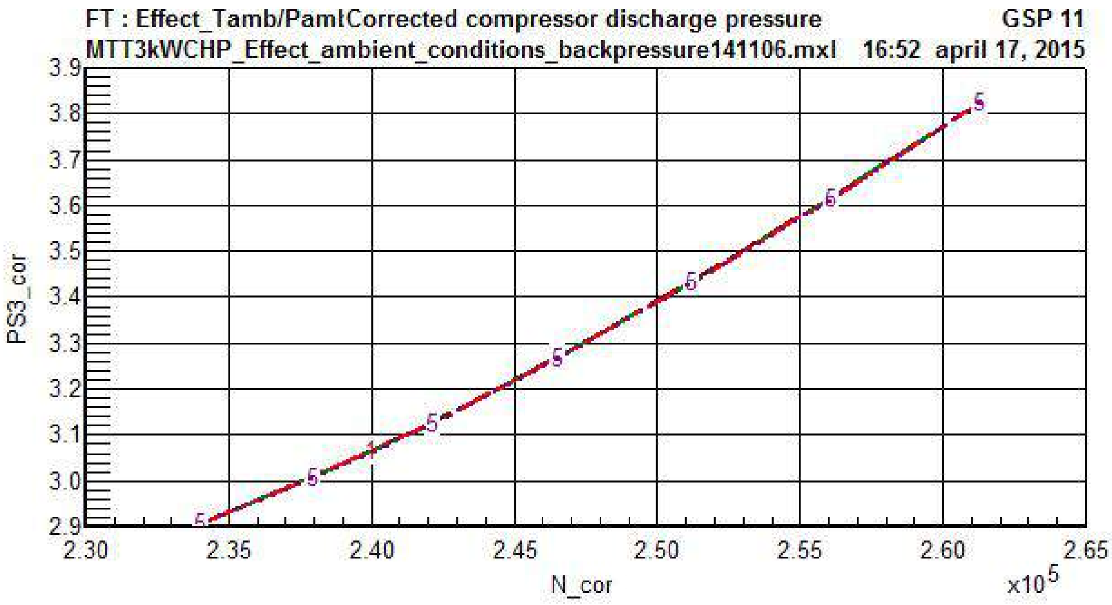

Figure 6.5: Corrected compressor discharge pressure in function of corrected rotational speed

Once the ambient conditions are known, the values for the expected corrected performance parameters of the healthy reference engine can be determined from the baselines. These performance values can then be compares against the corrected performance values of the actual engine. Deviations between reference and actual corrected performance values are used to evaluate the health condition of the engine.

Limitations When using the derived performance parameter baselines for diagnostic purposes, one should keep following limitations in mind:

- The derived baselines are only valid if the system is running at base-load.
- The model used to derive the baselines is only a reference engine. The performance of healthy field engines might deviate from the healthy reference performance baselines because of component-to-component variations, installation effects and other factors.
- Sensor errors are excluded as root cause for performance shifts.

6.2. IMPLEMENTATION IN THE CONDITION MONITORING TOOL

The derived performance parameter baselines can be implemented into a remote condition monitoring software by using a lookup table. Table 6.4 shows the layout of the lookup table that is used to demonstrate the diagnostic concept in Matlab. The one-to-one relations between the corrected rotational speed and the other corrected performance parameters are used to predict the performance of the engine for changing ambient conditions. Linear interpolation is used to calculate corrected performance parameter values that correspond to corrected rotational speeds other that the ones in the table.

N_cor [rpm]	**PS3_cor [bar]**	**T03_cor** [K]	**w_cor** [g/s]	**w_f_cor** [g/s]	**eta_c_cor** [/]	**PW_grid_cor** [kWe]
230275.8	2.817	420.8	52.051	0.538	0.752	2.508
234044.9	2.907	426.9	52.743	0.572	0.745	2.850
238005.4	3.009	433.9	53.570	0.611	0.736	3.234
242173.9	3.126	442.1	54.571	0.656	0.725	3.649
246569.4	3.269	451.1	55.933	0.709	0.717	4.177
251213.3	3.433	460.9	57.509	0.771	0.709	4.791
256129.9	3.617	471.5	59.283	0.841	0.702	5.488
261346.9	3.824	482.9	61.285	0.921	0.696	6.287

Table 6.4: Layout of the lookup table that can be implemented into the condition monitoring software

Use of the lookup table The lookup table is used to predict the performance of the healthy reference engine for specific ambient conditions. Once the reference performance values are known, deviations in performance between the actual and the reference engine can be calculated. The percentage difference between the measured and nominal gas path performance are called *measurement deltas*. The measurement delta of a parameter P is defined as shown by Equation 6.3 where P_{cor} is the corrected measurement parameter value calculated based on the expressions from Table 6.1. $P_{cor,ref}$ is the corrected reference value of the healthy engine derived from the lookup table.

$$\Delta P = 100 \cdot \frac{P_{cor} - P_{cor,ref}}{P_{cor,ref}} \qquad (6.3)$$

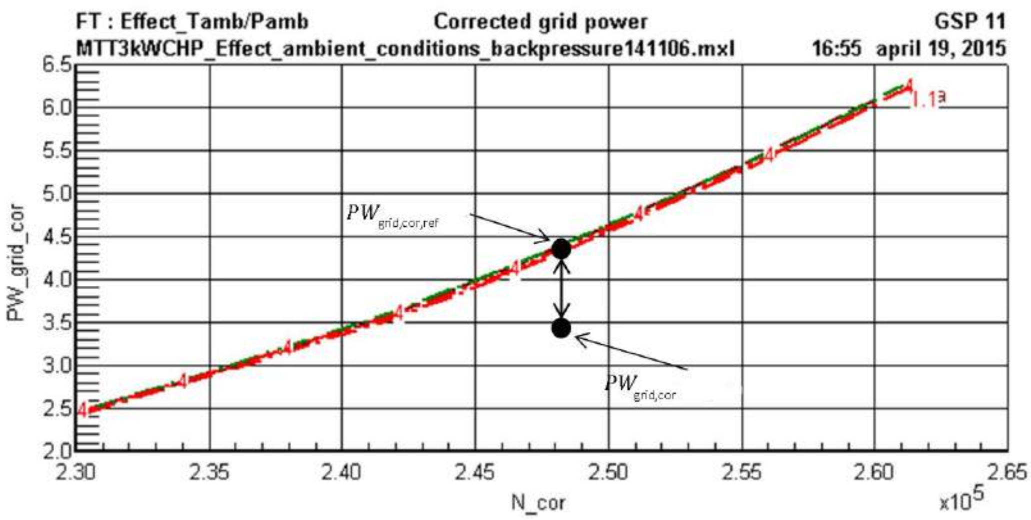

Figure 6.6: Graphical representation of delta grid power where $\delta PW_{grid} = \frac{PW_{grid,cor,meas} - PW_{grid,cor,ref}}{PW_{grid,corref}}$

Figure 6.6 shows hows "delta grid power" can be calculated by using the grid power baseline and the measured corrected grid power. Figure 6.7 shows the corrected performance parameter values of a healthy and deteriorated engine over a range of ambient conditions with respect to the reference baselines. The green dots show the performance of the healthy engine whereas the red dots show the performance of the deteriorated engine. Due to component-to-component variations, installation effects and other secondary effect, the performance of the healthy engine and the reference model might deviate. To account for these effects, the baselines should be reinitialized after each engine replacement by shifting the baselines up or down so that the baseline performance matches the initial healthy engine performance (see dotted lines in Figure 6.7).

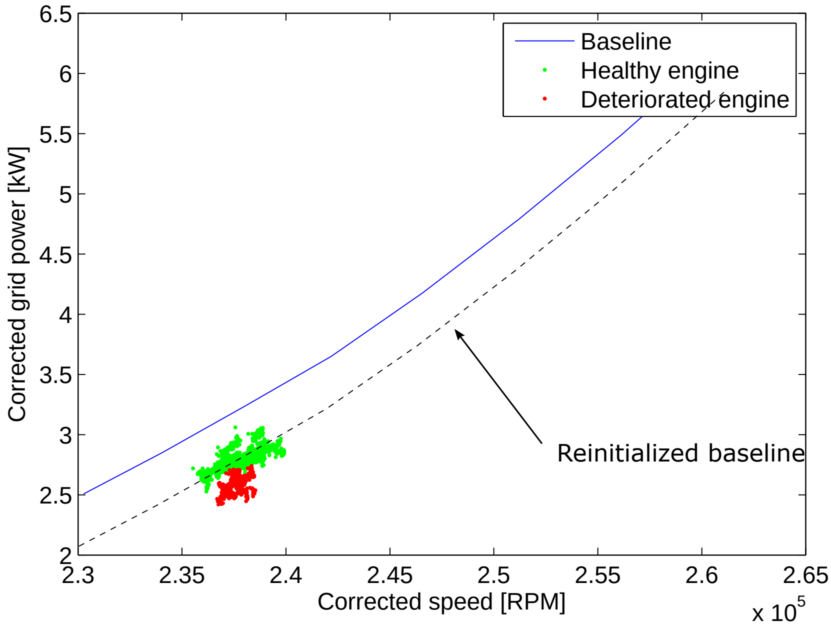

(a) Corrected grid power of a healthy and deteriorated engine wrt the corrected grid power baseline

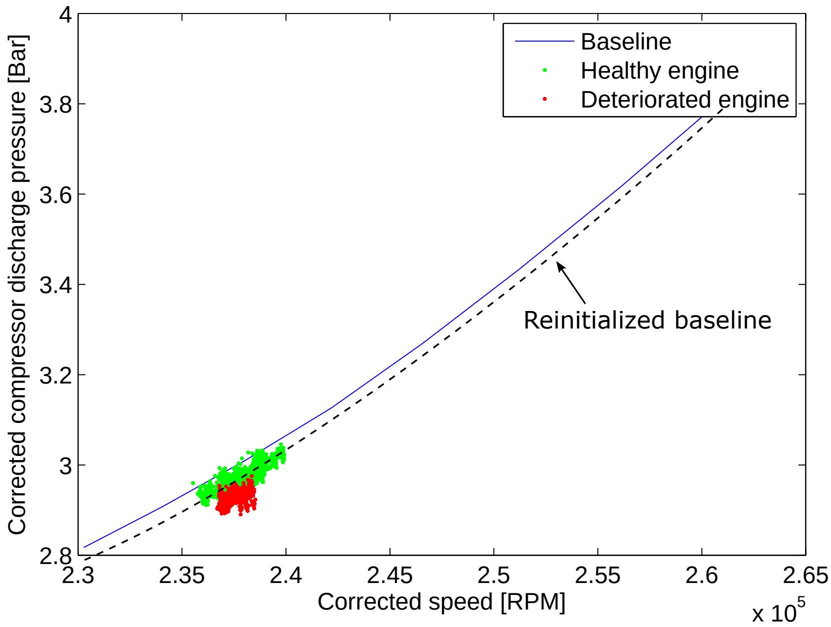

(b) Corrected compressor discharge pressure of a healthy and deteriorated engine wrt the compressor discharge baseline

Figure 6.7: Use of the baselines to determine deltas in performance degradation

Performance parameter trend lines The next step is to plot the measurement deltas against time and use these trends to detect shifts in health parameters. In case of the MTT micro gas turbine, deltas for corrected grid power and corrected compressor discharge pressure are plotted against time.

The performance of a field engine can be compared either against the performance of the healthy reference engine model or against the performance of the field engine at the beginning of its life (healthy engine). In the first case, all field engines are compared against the same reference engine which is useful to compare the performance of different systems to each other. In the second case, the performance of the engine is compared to its initial performance which is more useful to detect deterioration. As mentioned previously, the performance parameter baselines of a newly installed engine are obtained by shifting the baselines of the reference model so that the initial system performance matches the baseline performance as shown in Figure 6.7. The baselines should be reinitialized after each engine replacement to deal with system-to-system variations, installation effects an other possible secondary effects responsible for deviations in performance between the healthy reference engine model and the real, healthy engine. Measurement deltas obtained by comparing the performance of the field engine against the performance of the reference engine model are defined as performance indexes whereas deltas obtained by comparing the field engine performance against the initial, healthy engine are defines as deterioration indexes. For diagnostic purposes only the deterioration index for compressor discharge pressure (CDPDI) and grid power (GPDI) will be considered. Trend-lines in Figure 6.8 show how the deterioration indexes of one specific field engine evolves over time.

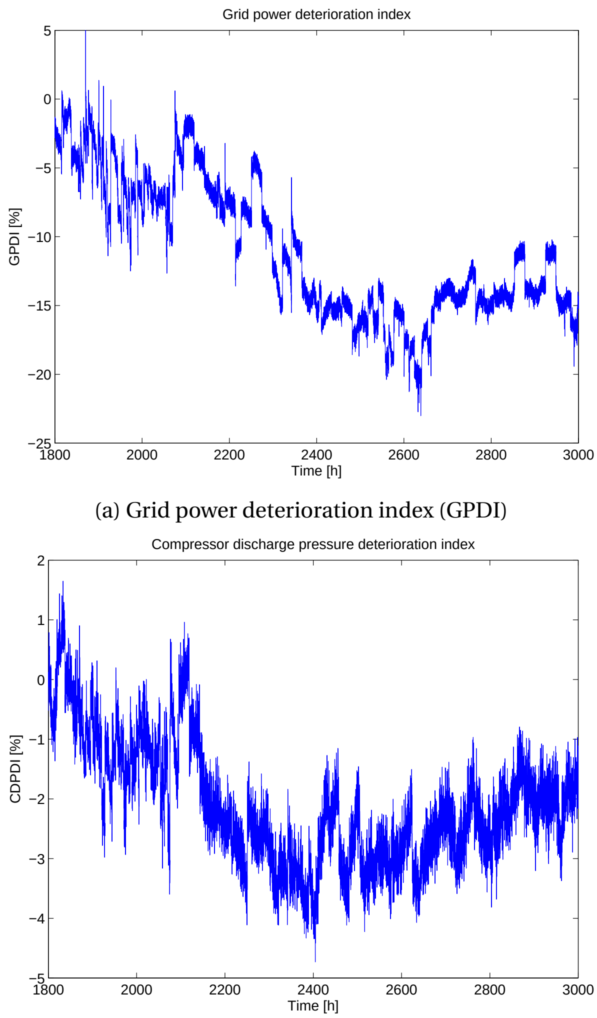

(a) Grid power deterioration index (GPDI)

(b) Compressor Discharge Pressure Deterioration Index (CDPDI)

Figure 6.8: Trending measurement deltas over time

6.3. Causes for differences between predicted and measured corrected performance parameters

Changes in measured and predicted performance might be due to following reasons:

Genuine deterioration Due to degradation the performance of individual gas path components deteriorates which affects the performance of the engine. Gradual changes in performance are trended with the aim to detect various types of deterioration.

Measurement errors in diagnostic-parameters As mentioned in Chapter 3, compressor inlet pressure is only measured once, before the system starts running. This value is used to correct the performance parameters for changing ambient pressure. If ambient pressure varies during the run, the corrected parameters will show some error. Moreover, different values of sensor bias might be generated for different operating points resulting in deviations between modelled and measured performance for different operating conditions.

Measurement errors in control-parameters A bias in measurements TT5 changes the operating point of engine which in turn has an effect on the other performance parameters. A bias in TT5 might be due to a change in flow pattern at the turbine exit. The highly inhomogeneous cross sectional flow field at the turbine exit caused by the swirl in the flow could cause changes in flow pattern.

Inaccurate baselines The established baselines were derived based on an 0-D engine model built in GSP. The performance of this model is used as a reference. Due to engine-to-engine variations and installation effects, the performance of a healthy engine might deviate from the baselines. To account for these effects, the trendlines are re-initialised to zero after a new engine is installed in the system.

7

EFFECT OF COMPONENT DEGRADATION ON ENGINE PERFORMANCE

During operation, the performance of individual components starts deteriorating gradually because of physical faults such as fouling, corrosion, erosion, abrasion, object damage, etc. [34, 35]. A physical fault is defined as a physical process that changes one or more independent health parameters (efficiencies, pressure ratios, flow capacities, etc.). In this chapter, the most common engine faults for the micro turbine and their effect on performance are discussed and quantified. Based on the simulation results and experimental data, rule-sets to detect fouling or increasing compressor tip clearance will be established.

7.1. REMATCHING EFFECTS

Before deterioration is treated it is important to be aware of rematching effects due to engine deterioration. Rematching effects are defined as movements of components working points along their characteristics caused by changes in component performance which might result in unexpected component performance expectations [4]. This phenomena can be explained for a gas turbine with oversized turbine. If the turbine is oversized for a given compressor, the compressor will not operate at its maximum efficiency for base-load operation. A decrease in corrected compressor airflow due to degradation might result in a higher compressor efficiency even though the compressor characteristic has become poorer. This effect is shown in Figure 7.1. The effect of changing health parameters on the other health parameters in GSP is shown in Table 7.1. The values were obtained by modifying each of the health parameters individually by 3 % while running the engine at base-load and standard ambient conditions.

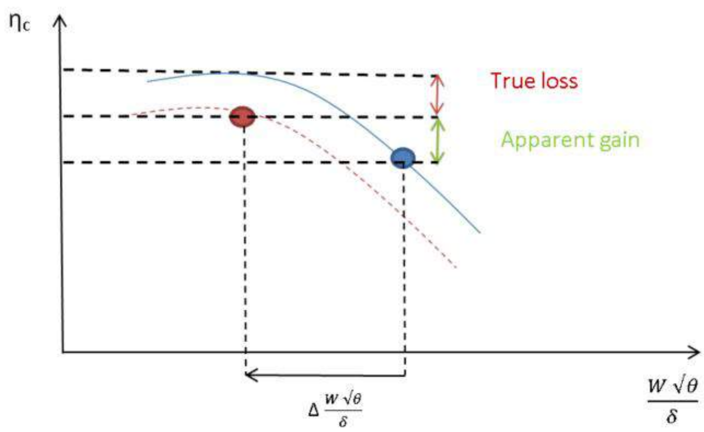

Figure 7.1: Apparent gain in isentropic efficiency due to rematching effects.

	Δ_ETA_c [%]	Δ_CAP_C [%]	Δ_PR_c [%]	Δ_ETA_t [%]	Δ_CAP_t [%]
COMP. ETA -3%	-3.01	-0.01	0.00	0.00	0.00
COMP. CAP -3%	1.17	-0.36	-0.39	0.03	0.00
COMP. PR -3%	-0.82	-1.73	-1.82	0.15	0.01
TURBINE ETA -3%	0.12	0.27	-0.04	-3.06	0.03
TURBINE CAP. +3%	1.10	2.53	-0.36	0.08	3.01

Table 7.1: Effect of changing health parameters on other health parameters

The results show that a decrease in corrected compressor capacity increases the isentropic efficiency which is an indication that the compressor is not operating at its most efficient operating point during base-load operation. Reducing the size of the turbine and hence the mass-flow would increase the isentropic efficiency of the compressor. It should also be noticed that a reduction in compressor isentropic efficiency in GSP has no effect on the PR or mass-flow rate of the compressor which is not realistic for a centrifugal compressor rotating at constant speed. In reality a decrease in isentropic efficiency should result in a decrease in PR as shown by Equation 7.1. This formula can easily be derived by applying the conservation of momentum and using the definition for isentropic efficiency. The formula learns that a decrease in compressor isentropic efficiency should always go together with a decrease in PR when simulated in GSP.

$$\frac{p_{03}}{p_{01}} = (1 + \frac{\eta_c \psi \sigma U^2}{c_p T_{01}})^{\frac{\gamma}{\gamma - 1}} \tag{7.1}$$

Where:
η_c=compressor isentropic efficiency
ψ= power input factor
σ= slip factor
U= impeller tip speed
C_p= specific heat at constant pressure
T_{01}= compressor inlet temperature

7.2. ENGINE DETERIORATION

In following sections, commonly occurring gas path faults and their effect on engine performance are discussed. First, the effect of component degradation on component performance is quantified by relating the physical faults to shifts in health parameters (efficiencies, pressure ratios and flow capacities). Next, the effect of component deterioration on engine performance is simulated by altering the health parameters in the model. Before the effect of deterioration on engine performance is investigated, it is useful to know that deterioration can be subdivided into three types namely [34]:

- **Recoverable** deterioration which compromises all deterioration that can be undone by cleaning the engine parts. Fouling is the major cause of recoverable deterioration.
- **Non-recoverable** deterioration such as corrosion, erosion and increasing tip-clearance which cannot be eliminated through washing, but requires maintenance actions to restore the performance. For instance, performance-loss due to increasing tip-clearances can be restored by applying abradable coating.
- **Permanent** deterioration cannot be recovered despite an overhaul. This is mainly because this type of deterioration is too expensive or too difficult to restore. An example is blade deformation.

7.2.1. FOULING

Fouling is the process of accumulation of deposits coming from the airflow on the surface of turbo-machinery components. Compressor fouling is the most common cause of engine deterioration [36] which caused by two types of particles: hard particles such as dust, dirt, sand, ash and carbon particles and soft particles such as oil, unburned carbons and soot. Fouling causes changes in airfoil shape, inlet angle, airfoil roughness and narrows down the airfoil throat opening [34]. The process is limited by aerodynamic forces that prevent further accumulation on the blade surface [37]. Fouling can be delayed in industrial gas turbines by installing an efficient filtration system which reduces the amount of particles coming into the gas path. Performance deterioration due to fouling can be recovered through periodical on-line or off-line water-washing or cleaning.

Effect of fouling on compressor performance For the MTT micro turbine, the effect of fouling on performance is severe because oil coming from the de-aeration of the oil sump is fed back into the gas path through the compressor inlet. The ingested oil will stick to the compressor impeller and scroll making the surface rough and sticky. The layer of oil deposits will also makes it easier for particles to stick to the surface making the surface even more rough. The difference between a clean and fouled compressor is shown in Figures 7.2 and 7.3 respectively. The effect of oil on fouling becomes more severe if the seal separating the oil-path form the gas-path starts leaking due to deterioration. Once the seal fails, more gas from the gas-path is passed into the oil-circuit which leaves the oil-sump through the de-aeration tube. The gas is dumped into the compressor inlet which aggravates the effect of oil on fouling. The effect of fouling on compressor performance was investigated by analysing data coming from performance tests. First, the performance of a dirty compressor was tested under base-load conditions. Next, the compressor was cleaned and tested under similar conditions without modifying other components. The performance deviations of the compressor due to fouling are shown in Table 7.2. Based on the experimental results, a Fouling Index was established which will be used to simulate fouling in GSP.

Fouling of the MTT micro-turbine For the MTT micro turbine, the effect of fouling on performance is severe because oil coming from the de-aeration of the oil sump is fed back into the gas path trough the compressor inlet. This oil sticks to the compressor impeller and scroll making the surface more rough and sticky. The layer of oil deposits also makes particles stick easier to the surface making the surface even more rough. The difference between a clean and fouled compressor is shown in Figures 7.3 and 7.2 respectively. The effect gets even worse if the seal in the cartridge house separating the oil path form the gas path starts leaking due to deterioration. Once the seal fails, more gas from the gas path is passed into the oil circuit. This gas is removed through the de-aeration which leads to more oil coming into the gas path what causes more fouling of the compressor.

(a) Clean compressor impeller

(b) Clean compressor scroll

Figure 7.2: Clean compressor

(a) Fouled compressor impeller (b) Fouled compressor scroll

Figure 7.3: Fouled compressor due to oil deposits

The effect of fouling on compressor performance was investigated by analysing data coming from performance tests. First, the performance of the compressor was tested under base-load conditions during pass-off. Next, the dirty compressor coming from the field was tested under similar conditions. The performance deviations of the compressor due to fouling are shown in Table 7.2. Based on the experimental results, a *fouling index* could be established that could be used to simulate fouling in GSP.

Engine 12									
	Test	TT2	TT3	(TT3-TT2)	PR	Wc2	Eta_c	PW ISA	Eta_el ISA
pass off	748.00	296.90	446.90	150.00	2.98	56.30	72.20	3500.00	15.90
Inbound	796.00	296.70	450.80	154.10	2.89	55.30	68.00	3180.00	14.80
Delta performance (%)				2.73	-3.02	-1.78	-5.82	-9.14	-6.92

Engine 10									
	Test	TT2	TT3	(TT3-TT2)	PR	Wc2	Eta_c	PW ISA	Eta_el ISA
pass off	608.00	295.70	447.00	151.30	3.07	56.90	73.60	3670.00	16.00
Inbound	749.00	297.10	452.50	155.40	3.00	56.40	70.10	3160.00	14.10
Delta performance (%)				2.71	-2.28	-0.88	-4.76	-13.90	-11.88

Engine 25									
	Test	TT2	TT3	(TT3-TT2)	PR	Wc2	Eta_c	PW ISA	Eta_el ISA
pass off	745.00	297.00	446.50	149.50	3.02	57.30	73.50	3660.00	16.00
Inbound	779.00	296.70	450.40	153.70	2.95	55.60	69.80	3040.00	13.70
Delta performance (%)				2.81	-2.32	-2.97	-5.03	-16.94	-14.38

Engine 17									
	Test	TT2	TT3	(TT3-TT2)	PR	Wc2	Eta_c	PW ISA	Eta_el ISA
pass off	848.00	297.20	446.80	149.60	2.96	56.40	72.00	3620.00	16.30
Inbound	914.00	295.60	450.30	154.70	2.83	52.40	65.91	2710.00	13.00
Cleaned	914.00	296.20	445.40	149.20	2.99	55.60	72.70	3560.00	16.20
Delta Performance (%)				3.41	-4.39	-7.09	-8.46	-25.14	-20.25

Table 7.2: Test results showing the effect of fouling on compressor performance for different engines

The data shows that the effect of fouling on compressor isentropic efficiency is two times bigger than the effect on pressure ratio. Mass-flow rate also reduces due to fouling but not that significantly. The data also shows that cleaning the compressor scroll and impeller restores the performance of the compressor and engine almost completely.

Based on the experimental data and taking into account the results form Table 7.1 fouling could be quantified in GSP by modifying the compressor isentropic efficiency and pressure ratio. Fouling is quantified in GSP by introducing a Fouling Index. A **Fouling Index (FI)** of 1 corresponds to a reduction in compressor isentropic efficiency of 2 percent and a reduction in pressure ratio of 2 percent. Table 7.3 shows the effect of fouling on compressor performance for different fouling indexes while running the model at standard ambient conditions and base-load operation. The simulation results show that the effect of fouling on the isentropic efficiency is about twice as big than the effect on compressor pressure ratio what agrees with the experimental data. The effect of fouling on corrected gas path parameters for various Fouling Indexes and changing ambient conditions is shown in Figures D.1 to D.2 in Appendix D.

Fouling Index	**DELTA ETA_c**	**DELTA PR_c**	***% decrease in*** Eta_c	***% decrease in PR***	***% decrease in*** w_c
FI 1	-2%	-2%	-2.53	-1.21	-1.16
FI 2	-4%	-4%	-5.07	-2.43	-2.33
FI 3	-6%	-6%	-7.60	-3.67	-3.52
FI 4	-8%	-8%	-10.13	-4.93	-4.72
FI 5	-10%	-10%	-12.65	-6.20	-5.95

Table 7.3: Effect of fouling on compressor performance for different FI simulated in GSP for base-load operation and standard ambient conditions.

Specific compressor work as a measure for the degree of fouling? If it is assumed that the air enters the impeller eye in axial direction, the specific work of the centrifugal compressor can be expressed by Equation 7.2. In this formula, the power factor (ψ) is a correction to account for the additional work input required by the compressor to overcome frictional losses between the casing and the air carried round by the vanes. The slip factor (σ) on the other hand is a factor accounting for the difference in speed between the impeller and the air. The slip factor depends on the number of blades of the impeller. The larger the number of blades, the smaller the slip will be [33]. Formula 7.2 shows that the specific compressor work ($C_p \cdot (TT3 - TT2)$) is independent of the compressor isentropic efficiency. For a constant rotational speed, specific compressor work should remain constant if C_p and ψ are assumed constant.

An experiment during which the inlet temperature of the compressor was varied from 297K to 317K while running the machine at a constant rotational speed showed that the specific work of a clean compressor remains almost constant. The results of the experiment are shown in Figure 7.4. The graph shows that specific work decreases slightly for increasing ambient temperatures which can be explained by secondary effects such as increasing C_p with increasing ambient temperatures and heat-loss. However, Table 7.2 shows that the stagnation temperature rise ($TT3 - TT2$) increases with increasing degree of fouling. One possible explanation could be that due to fouling, the surface of the scroll becomes more sticky and rough which increases the disc friction and windage loss. For the same rotational speed, a higher torque will be required to overcome the windage losses resulting in a higher power input factor ψ and hence higher specific compressor work. The specific compressor work could be used as a diagnostic parameter to distinguish fouling from tip-clearance which will be discussed in the following section.

$$T_{03} - T_{02} = \frac{\psi \sigma U^2}{C_p} \tag{7.2}$$

Where:
C_p = specific heat of air for constant pressure
U = impeller tip speed
σ = slip factor
ψ = power input factor

Parameter shifts caused by fouling The effect of fouling on corrected gas path parameters for various Fouling Indexes and changing ambient conditions is shown in Figures D.1 to D.5 in Appendix D. By looking how the values for the corrected gas path parameters shift with respect to the healthy baseline, performance parameters that are most sensitive to fouling can be determined. Based on the simulation results and the experimental data showing the increase in specific compressor power for increasing degree of fouling, following rule-set were determined to detect fouling:

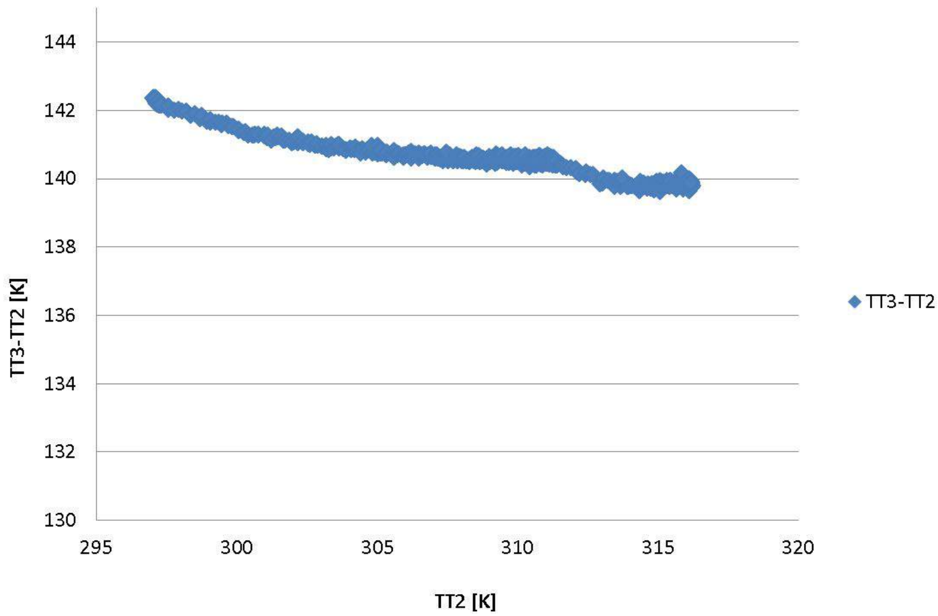

Figure 7.4: Specific compressor work for varying inlet temperatures.

- Increase in $(T_{03} - T_{02})$
- Decrease in corrected grid power
- Decrease in corrected compressor discharge pressure
- Decrease in corrected compressor isentropic efficiency

7.2.2. ABRASION

Abrasion is defined as the rubbing of a rotating surface on a stationary surface causing an increase in tip clearance and hence an increase in flow leakage form the high pressure side to the low pressure side. In this section, the effect of increasing compressor and turbine tip clearance on engine performance is discussed.

EFFECT OF TIP CLEARANCE ON COMPRESSOR PERFORMANCE

An increase in impeller tip clearance results in a decrease in pressure ratio and reduces the isentropic efficiency of the compressor [38]. To quantify the effect of tip clearance on compressor performance a test was performed in which the tip clearance was varied by using shims. In the experiment, the tip-clearance was varied from 0.1 mm to 0.35 mm. The test-results are shown in Table 7.4 . From the experiment one should notice that a small change in tip-clearance (≈ 0.1 mm) has already a large effect on the performance of the compressor. As with fouling an increase in tip-clearance causes a reduction in compressor pressure ratio and isentropic efficiency which makes it difficult to distinguish one from the other just by looking at gas path measurements. However, rubbing of the impeller against the compressor scroll can be considered as an instantaneous event resulting in a sudden drop in system performance. Hence, abrasion could be distinguished from fouling because of its instantaneous character.

Tip clearance[mm]	Test	TT2[K]	TT3[K]	(TT3-TT2)[K]	PR	W_{c2}[g/s]	η_c[%]	PW_{isa}[W]	$\eta_{el,ISA}$[%]
0.35	700	295.9	444.8	148.9	2.88	53.9	70	3050	14.2
0.25	700	295.7	445.1	149.4	2.93	55	71.1	3310	15
0.15	701	295.3	445.6	150.3	3.01	56.9	72.4	3540	15.8
0.1	701	295.6	446.6	151	3.07	57.9	73.8	3820	16.6
Delta in performance between 0.1mm and 0.35mm [%]				-1.39	-6.19	-6.91	-5.15	-20.16	-14.46

Table 7.4: Effect of compressor tip-clearance on performance

Distinguishing fouling from abrasion for compressor with abradable coating In the future, an abradable coating will be applied to reduce the compressor tip-clearance even more which will increase the compressor performance (PR and η_c). The writer expects that the coating will gradually degrade over time causing a gradual increase in compressor tip clearance and hence a gradual reduction in compressor pressure ratio and isentropic efficiency. In that case, the sudden drop in performance due to rubbing of the impeller against the wall cannot be used to distinguish fouling from abrasion. However, the specific compressor power might be a potential diagnostic parameter which could distinguish fouling from increasing tip clearance. As mentioned in the previous section, $(T_{03} - T_{02})$ increases for increasing degree of fouling. The experiments in which the tip clearance was varied show that (T03-T02) decreases slightly for increasing tip-clearance. Hence, this increase in stagnation temperature across the compressor impeller can be used to distinguish both deterioration modes.

Parameter shifts caused by increasing impeller tip-clearance As mentioned before, an increase in impeller tip-clearance and fouling cause similar shifts in engine performance. However, the compressor specific work (T03-T02) might be used as diagnostic parameter to distinguish both. Hence, following performance parameter shifts can be expected for an increase in compressor tip-clearance:

- Slight decrease in (T03-T02)
- Decrease in corrected grid power
- Decrease in corrected compressor discharge pressure
- Decrease in corrected compressor isentropic efficiency

EFFECT OF TIP CLEARANCE ON TURBINE PERFORMANCE

An increase in turbine tip-clearance causes a decrease in turbine isentropic efficiency and a slight increases in turbine mass-flow rate [39]. Both, experimental and theoretical studies show that the overall performance of a radial turbine suffers less from an increase in axial clearance than from the same increase in radial clearance as a percentage of local span [39, 40]. Experimental studies by Futral et al show that the effect of radial clearance is about 10 times bigger than the effect on axial clearance [39]. In the experiments the axial clearance was varied by using shims whereas the radial clearance was changed by machining the tip of the inducer. The dotted line in Figure 7.5a shows the effect of uniform blade-shroud clearance on static isentropic turbine efficiency for a radial inflow turbine. The graph shows that turbine isentropic efficiency decreases by about 1 percent for each percent increase in uniform clearance. The effect of uniform blade-shroud clearance on mass flow rate is shown in Figure 7.5b. From the graph, one can say that mass flow rate does almost not change for increasing turbine tip-clearance. Mass flow rate only increases by about 0.16 percent per percent increase in uniform clearance. The effect of tip clearance on performance is simulated in GSP by changing the turbine isentropic efficiency in the model.

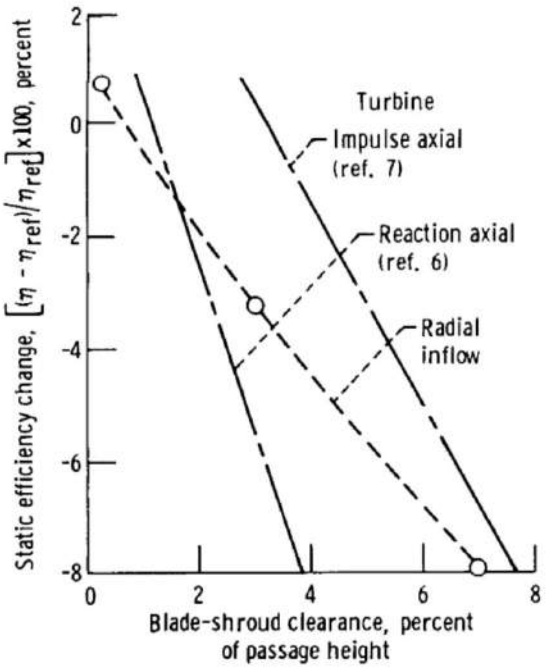

(a) Comparison of effect on static efficiency of clearance variation for three turbines. Uniform percentage clearance at rotor entrance and exit for radial-inflow turbine

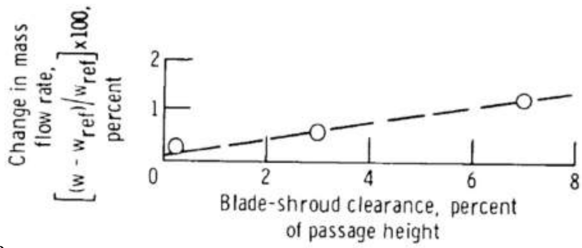

(b) Effect of uniform blade-shroud clearance on mass flow rate at design equivalent speed.

Figure 7.5: Effect of ambient temperature on global engine performance

Parameter shifts caused by an increase in turbine tip-clearance The effect of turbine tip clearance on the corrected performance parameter baselines is shown in figures D.6 to D.10 in Appendix D. From the simulations one should notice that a change in turbine isentropic efficiency has a significant impact on the power output and almost no impact on the compressor performance. As with compressor abrasion, rubbing of the turbine rotor against the casing can be considered as a sudden event and will therefore cause an instantaneous drop in engine performance which might be detected by a sudden drop in output power without any significant changes in compressor performance.

7.2.3. LEAKAGE DUE TO GASKET DETERIORATION

In the first generation field test systems the combustion chamber and turbine scroll are connected by a connection piece. Gaskets are put in between the components to seal the assembly. Figure 7.6a shows the assembly for the first generation field test systems.

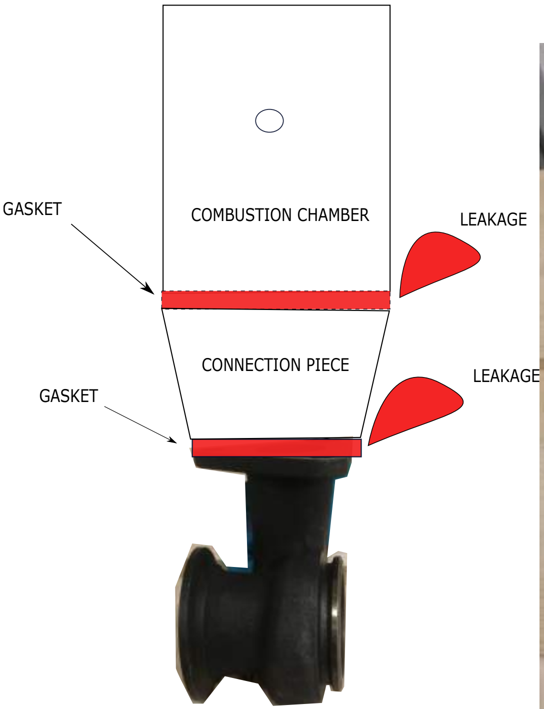

(a) Combustor-turbine assembly for the first generation field test units.

(b) Welded assembly

Figure 7.6: Combustor-turbine assembly

During start-up, the combustion chamber and turbine scroll grow due to thermal expansion which reduces the distance between the contact surfaces of both components. The gaskets will therefore get squeezed between the turbine scroll and the combustion chamber which deforms the gaskets and reduces the sealing capability. Due to the reduced sealing capability, hot gasses will leak from the gas path into the cabinet which affects the performance of the engine. The effect of leakage was simulated in GSP by adding a bleed control component. The fraction of hot gasses leaking from the gas path was varied from 0 percent up to 10 percent of the total mass flow.

Parameter shifts due to leakage between combustion chamber and turbine The effect of leakage between the combustor and the turbine on the corrected performance baselines for various degrees of leakage is shown in Figures D.11 to D.16 in Appendix D. The simulations show following shifts in performance parameter baselines:

- The compressor corrected mass flow increases for increasing leakage. This is because the compressor has to deliver compressed air to the turbine and the cabinet through the leakage-hole. As the turbine is chocked, more air has to be compressed because part of the compressed air will be lost by the leakage.
- The compressor isentropic efficiency decreases for increasing leakage. Due to the increase in mass flow, the inflow velocity triangles of the compressor become less optimal which increases the incidence losses.
- Output power decreases for increasing leakage. This is mainly because the compressor has to compress a larger amount of air at a lower efficiency which increases the power consumed by the compressor. The turbine on the other hand does not generate more power which results in a net decrease in power output.
- Fuel consumption increases for increasing leakage. As the air mass flow increases for increasing leakage, more air should be heated which increases the fuel consumption.
- Decrease in TT34 for increasing leakage. Ratio $\frac{\dot{m_{gas}}}{\dot{m_{air}}}$ decreases for increasing leakage resulting in a decrease in TT34. This can be explained by Equation 7.4

- Increase in cabinet temperature. The hot gasses are dumped into the cabinet which increases the cabinet temperature.

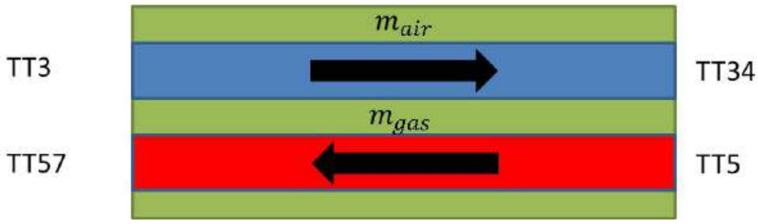

Figure 7.7: Schematics of counter current recuperator

$$\epsilon = \frac{C_{p,air} \cdot \dot{m}_{air} \cdot (TT34 - TT3)}{C_{p,gas} \cdot \dot{m}_{gas} \cdot (TT5 - TT3)} \tag{7.3}$$

$$TT34 = \frac{\epsilon \cdot (C_{p,gas} \cdot \dot{m}_{gas} \cdot (TT5 - TT3))}{C_{p,air} \cdot \dot{m}_{air}} + TT3 \tag{7.4}$$

The problem of leakage was solved by welding the lower part of the connection piece to the scroll and using a metal sealring together with a new type of gasket on the upper connection. This assembly is shown in Figure 7.6b

7.2.4. OTHER POSSIBLE FORMS OF DETERIORATION

In this section, other possible forms of deterioration which are not likely to occur in the MTT micro-turbine are discussed briefly.

Erosion is the abrasive removal of material from flow path components by hard particles such as dirt, dust, sand, ash, etc. in the gas path [34]. Erosion causes an increase in surface roughness, alters the airfoil shape and increases the blade tip and seal clearances. Industrial gas turbines are less prone to erosion compared to aircraft gas turbines because of their effective filtration system [41]. Turbine erosion increases the blade throat opening which causes an increase in turbine flow capacity. Compressor erosion, on the other hand, causes a reduction in compressor flow capacity even though the inlet area has increased. This is because erosion lowers the ability of the compressor to increase total pressure which lowers the mass-flow capacity for the same non-dimensional speed. For both, compressor and turbine, erosion causes a drop in isentropic efficiency. Because field test units are equipped with an inlet filter hard particles are not ingested by the engine. Therefore it is assumed that field engines do not suffer from erosion

Corrosion is defined as the loss of material from gas path components caused by a chemical reaction with contaminants present in the gas path. Both, inlet air contaminants and fuel contaminants cause corrosion. Salts, acids and reactive gases such as chlorine and sulphur oxides in combination with water cause wet corrosion in the compressor and elements as sodium, vanadium, potassium and lead affect the turbine airfoils and scroll by so called high temperature corrosion. Corrosion has a similar effect on performance as erosion. The material loss and an increase in blade surface roughness causes a reduction in compressor flow capacity and reduces the compressor isentropic efficiency. In addition, corrosion reduces the service life of components.

Object damage is a sudden failure which can be sub-divided into 2 types: Foreign Object Damage (FoD) and Domestic Object Damage (DoD). Foreign object damage is the result of external objects striking the flow path components of the gas turbine engine and domestic object damage is the result of pieces of the engine (such as bolts, pieces of the combustion, etc.) breaking off and being carried through the gas path. The damage caused can vary from non-recoverable engine performance deterioration to catastrophic engine failure [34]. The change in component health parameters varies as well depending on the severity and type of damage. For example, loosing blades will result in an increase in flow capacity whereas objects being stuck in the flow path will reduce the flow capacity. Typically, isentropic efficiency is reduced by 5 percent but this number is hardly dependent on the severity of the damage [42].

Thermodynamic distortion normally takes place in the hot regions between the combustor exit and turbine inlet. Thermodynamic distortion is caused by problems such as mall-functioning fuel nozzles or warped combustor components which in turn cause changes in the temperature profile at the combustor exit. Thermodynamic distortion can cause temporary or permanent deformation of downstream components. For example, a distorted temperature profile at the turbine inlet can cause changes in relative thermal growth between the static and rotating members causing abrasion. Next, local high temperatures can cause first stage turbines to untwist and reduce creep life of the blades [43].

Although combustor deterioration can affect the turbine inlet temperature profile, the combustor efficiency will usually stay constant with time which means that combustor deterioration cannot be detected through gas path performance analysis [34]. However, secondary effects such as deformed turbine blades, can be simulated by reducing the turbine isentropic efficiency [43].

7.3. SUMMARY OF GAS PATH FAULT INDICATORS

In previous sections, the effect of most common gas path faults on engine performance was discussed. Table 7.5 gives an overview of the derived gas path fault indicators and maintenance recommendations that can be used to identify the type of deterioration responsible for the shifts in performance. Performance parameters shifts are compared against the rule-sets summarized in this table which will help the maintenance engineer to select the most probable cause of deterioration. In the next chapter, the capabilities of the diagnostic concept are demonstrated.

Deterioration mode	**Effect on performance**	**Gradual or abrupt**	**Maintenance recommendation**
Fouling	-Decrease in $PW_{Grid,cor}$ -Decrease in $p_{s3,cor}$ -Decrease in $\eta_{c,cor}$ -Increase in (TT3-TT2)	Gradual	Cleaning impeller and compressor scroll
Compressor abrasion	-Decrease in $PW_{Grid,cor}$ -Decrease in $p_{s3,cor}$ -Decrease in $\eta_{c,cor}$ -Slight decrease in (TT3-TT2)	-Abrupt: in case of shaft unbalance -Gradual: in case of degradation of abradable coating	Apply abradable coating to the surface of the compressor scroll
Turbine abrasion	-Decrease in $PW_{Grid,cor}$ -No impact on compressor performance	Abrupt	Replace turbine impeller/scroll
Leakage between combustor and turbine	-Decrease in $PW_{Grid,cor}$ -Increase in w_{cor} -Decrease in $\eta_{c,cor}$ -Increase in $w_{f,cor}$ -Slight decrease in TT34 -Increase in T_{cab}	Gradual	Replace gasket
Dirty fuel nozzle	Increase in fuel pressure	Gradual or abrupt	Clean fuel nozzle

Table 7.5: Gas path fault indicators and recommended maintenance actions for most common occurring gas path faults.

8
Demonstration of the concept through case studies

In this section, the condition monitoring capabilities of the developed GPA based diagnostic concept are demonstrated. This is done by trending the diagnostic parameters over time and interpreting shifts in performance parameters by using the rule-sets derived in previous chapter. The main objective is to analyse shifts in performance parameters and link the performance-deviations to specific types of degradation by using the gas path fault indicators derived in previous chapter. Performance parameter values and maintenance logs of Data obtained from field test units are used to demonstrate the concept. Table 8.1 gives an overview of the gas path maintenance actions of the field test system. The maintenance actions are visualised on the plots by vertical red lines and the corresponding index.

Index	**mai_HoursSinceLast**	**Maintenance action gas path**
1	1546	New engine (#17)
2	2496	Replace gasket between lower combustion chamber and turbine scroll.
3	3308	New engine (#7)
4	3677	Clean comp scroll and impeller.

Table 8.1: Maintenance actions for system 1.2 (Note: A new engine is defined as a complete assembly of compressor impeller,compressor scroll and turbine impeller)

8.1. Gas path leakage

Figure 8.1 shows how the corrected performance parameters behave over time for system 1.2. The plots clearly illustrate a gradual decrease in corrected grid power and TT34 after engine 17 was installed in the system. Next, a steep increase in T_{cab} can be observed. The plot also shows an increase in fuel compressor speed over time. The green vertical line indicates when the fuel compressor was replaced. After comparing the corrected parameter shifts to the derived gas path fault indicators (Table 8.2) it turns out that leakage due to gasket deterioration between the combustor and turbine is the most probable cause for the performance deterioration. The problem was solved after replacing the gasket between the lower combustion chamber and the turbine scroll. It can be argued whether the increase in fuel compressor speed is due to the leakage or due to fuel compressor degradation or both.

Decrease in $PW_{grid,cor}$	✓
Increase in w_{cor}	-
Decrease in $\eta_{c,cor}$	-
Increase in $w_{f,cor}$	✓
Slight decrease in TT34	✓
Increase in T_{cab}	✓

Table 8.2: Comparison of the performance trendlines to the rule-sets for leakage.

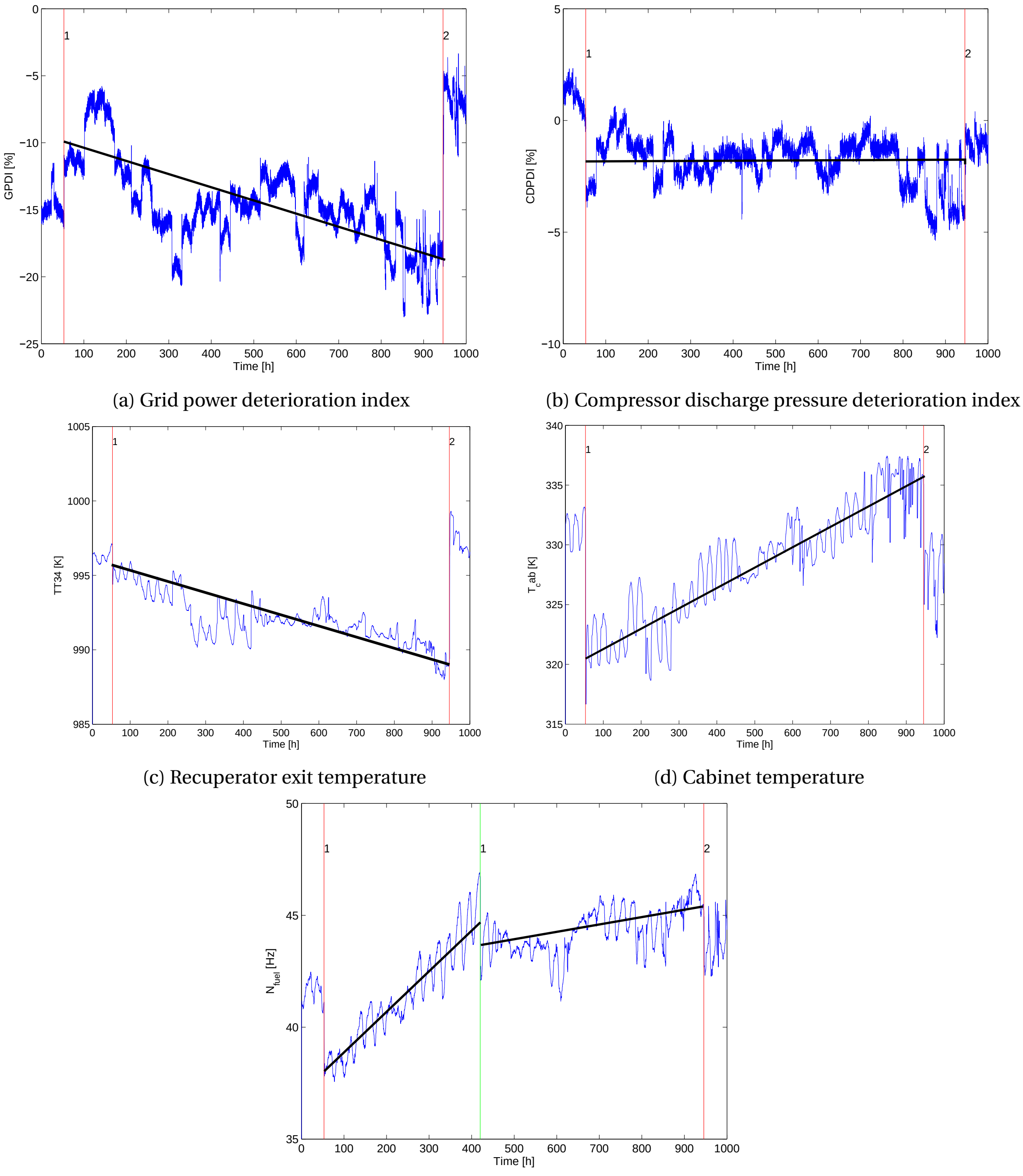

(a) Grid power deterioration index

(b) Compressor discharge pressure deterioration index

(c) Recuperator exit temperature

(d) Cabinet temperature

(e) Fuel compressor speed

Figure 8.1: Corrected performance parameter trendlines for system that has leakage between the lower part of the combustion chamber and the turbine scroll

8.2. FOULING

Figure 8.2 shows how the diagnostic parameters behave over time after engine 7 was installed in the system. The graphs clearly show a gradual decrease in corrected grid power and corrected compressor discharge pressure. Other performance parameters such as cabinet temperature, TT34 and fuel compressor speed remain almost constant over time. According to Table 7.5, a decrease in corrected grid power together with a decrease in corrected compressor discharge pressure could either be caused by fouling or by an increase in compressor tip clearance. However, because the deterioration was gradual and the scroll was not coated with abradable coating, fouling is most plausible which was indeed the root cause for the performance deterioration. The vertical red line with index 4 indicates when the compressor was cleaned. During this maintenance action the compressor impeller was removed and the impeller and scroll were cleaned with a brush. After cleaning, the performance was restored almost completely. Shortly after cleaning the compressor, the performance starts decreasing again which could indicate that the seal separating the oil path from the gas path is deteriorated. Due to the deteriorated seal more oil is fed into the compressor inlet making fouling even worse. This effect is explained more in detail in section 7.2.1. The trendline for the cabinet temperature shows that the problem with the gasket was solved after replacing the gasket.

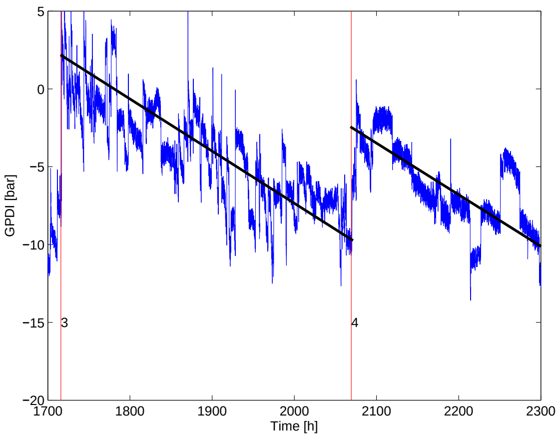

(a) Grid power deterioration index

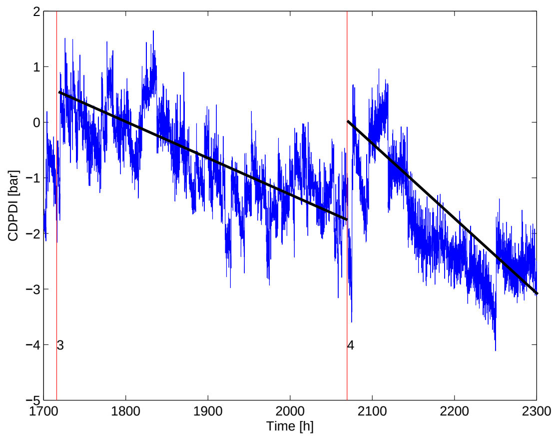

(b) Compressor discharge pressure deterioration index

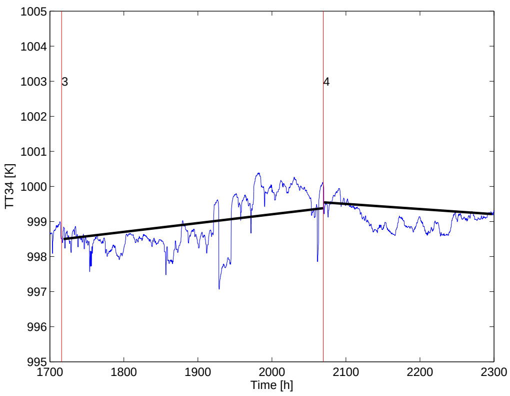

(c) Recuperator exit temperature

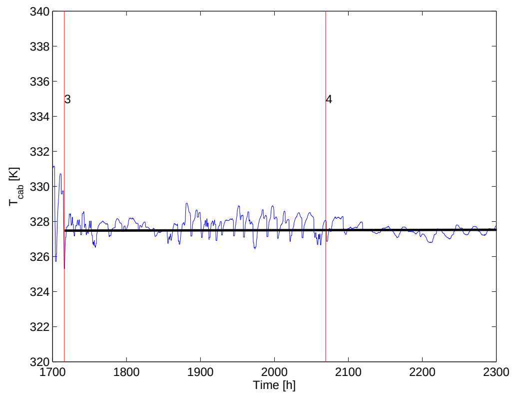

(d) Cabinet temperature

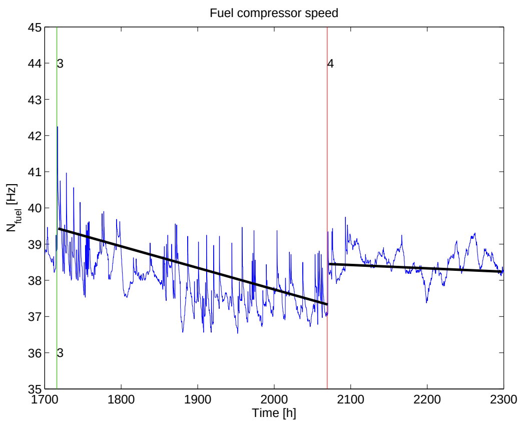

(e) Fuel compressor speed

Figure 8.2: Corrected performance parameter trendlines for system that suffers compressor fouling

8.3. ANOMALIES

After 24 hours the system shuts down to check if the sensors are still working properly. Before and after the shut-down, jumps in grid power where observed. In this section, various hypothesis that could explain this phenomena will be discussed with an attempt to find an explanation for this behaviour. Figure 8.3 shows how grid power behaves for system 1.2 and engine 17. The vertical red lines on the graphs show the shut-down events. Figure 8.3 shows that the corrected power can vary up to 150 Watt after a restart.

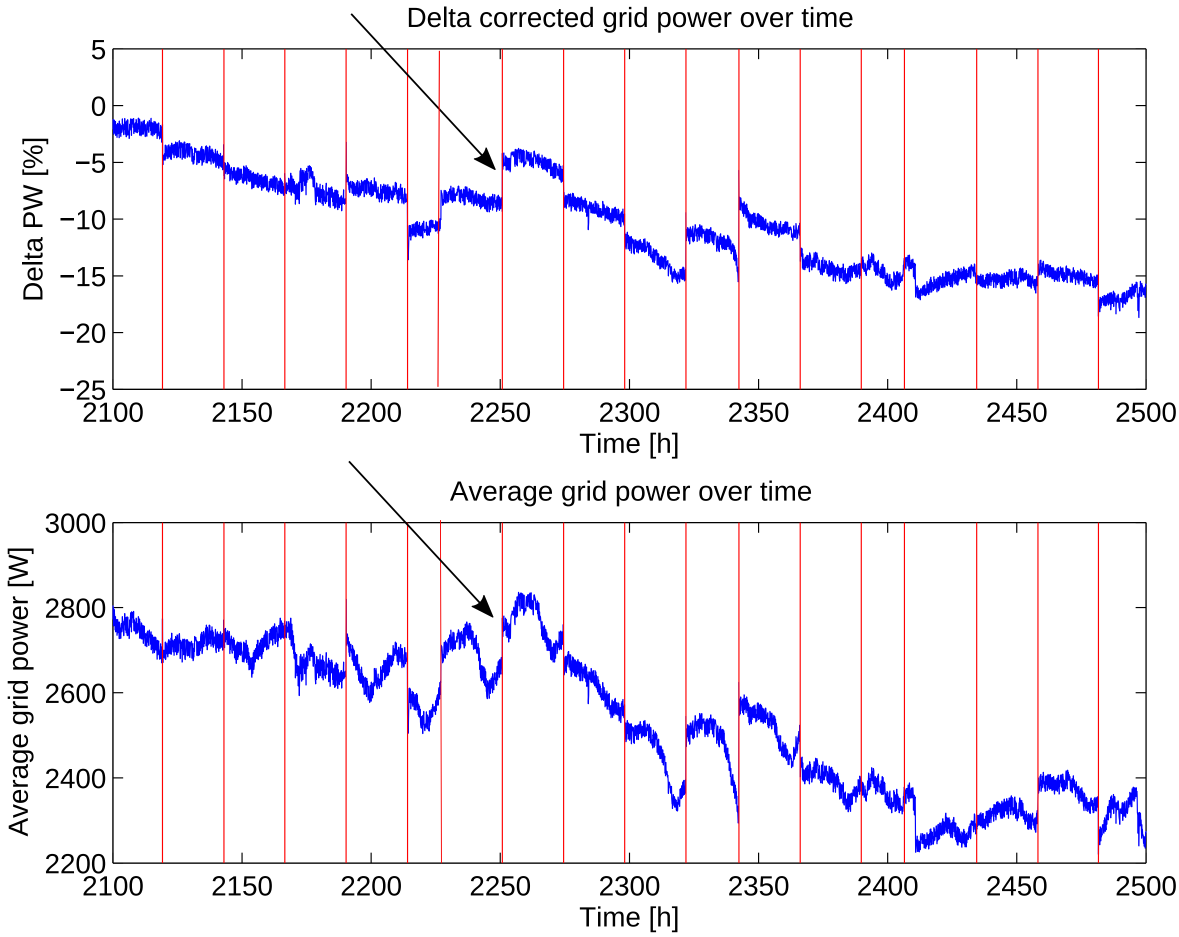

Figure 8.3: Jumps in corrected and non-corrected grid power after start-stop event

Hypothesis 1: Bad corrections for ambient conditions Figure 8.3 shows that both, corrected and measured grid power jump after a stop-start event which is shown by the black arrow. This excludes this hypothesis.

Hypothesis 2: engine operates at different power setting after a restart Bias in TT5 due to thermal distortion caused by a changing flow pattern at the turbine exit might result in a shift in power settings of the gas turbine. Simulations in GSP for standard ambient conditions predict that an increase of 10K in TT5 should result in an increase in grid power of 72W and an increase in TT34 of 8.08K respectively. Next, fuel flow should increase by 0.9%. Figure 8.4 shows that the compressor discharge pressure, TT34 and fuel compressor speed do not show this jumpy behaviour. The jump in TT34 by less than 1 K at time 2370h could be explained by a bias in measurement TT34 or TT5 whereas the gradual increase in fuel compressor speed could be an indication of degradation of the fuel compressor. If one assumes that the engine operates at the same power settings after each restart and that no deterioration of the gas path components applies during this event, the gas generator power should be the same before and after stopping. This implies that either the mechanical or electrical losses change after each restart.

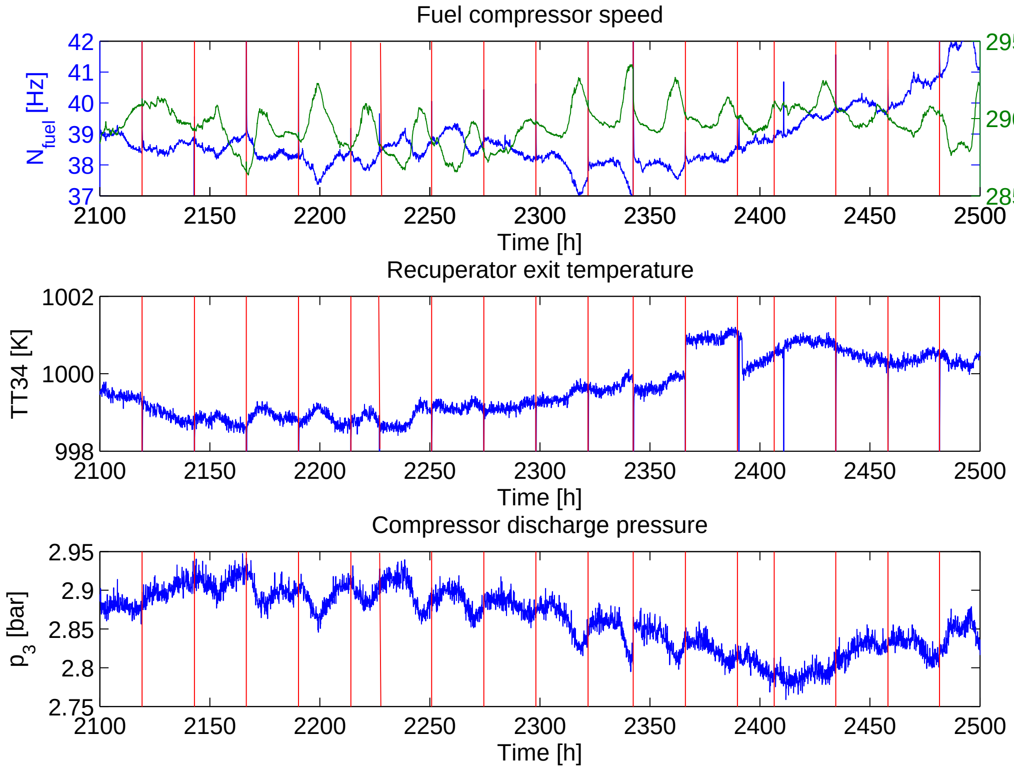

Figure 8.4: Trendlines for p_3, TT34 and N_{fuel}

Hypothesis 3: Change in mechanical losses Gas generator power ($PW_{turb} - PW_{comp}$) is used to overcome mechanical losses and generate electricity to the auxiliaries and the net. The Sankey diagram depicted in Figure 3.7 shows that almost 700 Watt is needed to overcome the mechanical losses. A change in bearing losses should directly result in a change in grid power if one assumes that gas generator power does not change before and after the restart. Changes in bearing losses might be caused by instabilities of the floating ring bearings at high rotational speeds. The floating ring bearings can become unstable with increasing rotational speed what generates self-excited vibrations resulting in higher bearing losses [44]. Mechanical losses are dissipated in heat and could be detected by looking at the oil temperature. Figure 2.3 shows how the oil characteristics change over time. The graph shows that oil temperature and pressure are inversely related to each other. This is because oil viscosity decreases with increasing temperature making it easier for the oil pump to circulate the oil resulting in a lower oil pressure. The graph also shows some correlation between the jumps in power and changes in oil characteristics. For a lower grid power, oil temperature is slightly higher which might be an indication of increasing mechanical losses. Because the oil temperature is measured in the oil sump which acts as a thermal buffer the changes in oil temperature are not big. In the future, this hypothesis might be tested by monitoring the oil characteristics at the entry and exit of the bearing house. It is also recommended to monitor the vibration level which could be used to detect possible changes in vibration modes before and after a restart. One approach to measure the bearing losses is by measuring the frictional heat dissipation to the oil. Equation 8.1 shows how the mechanical friction losses can be estimated from the heat dissipation to the oil. This formula can only be applied if one assumes that the bearing losses are fully dissipated in the oil flow. In the formula, ΔT_{oil} is the difference between outlet and inlet oil temperature in the bearing house.

$$Q_{oil} = PW_{bearing} = \dot{m}_{oil} \cdot C_{p,oil} \cdot \Delta T_{oil} \tag{8.1}$$

Conclusion Although some of the hypothesis could be ruled out by analysing the performance data, it has not been confirmed that the fluctuations in power are due to changes in mechanical losses. More experiments and more in depth research will be required to confirm hypothesis 3.

9

CONCLUSIONS AND RECOMMENDATIONS

9.1. CONCLUSIONS

Following conclusions could be derived from the project:

- The proposed concept is capable of performing engine level diagnostics and partially component level diagnostics. Because different degradation modes can lead to similar shifts in measurement parameters, complete component level diagnostics is not possible. The method can only give a qualitative idea of the degree of degradation.
- The user should not use the derived rule-sets for the various deterioration modes blindly. The concept has some limitations of which the user should be aware of which are listed below:

  The derived baselines are only valid for base load operation.

  Only rule-sets for single faults were derived

  Combustion deterioration is not considered because it does not occur commonly. Combustion deterioration could be detected through emission testing.
- Due to second order effects such as heat loss and relatively large power take-off of the auxiliary systems and bearing/generator losses, standard parameter corrections from the literature could not be used to establish the performance parameter baselines of the micro-turbine.
- The relatively large secondary power losses such as bearing losses, generator losses and auxiliary power take-off have a significant effect on the performance of the micro gas turbine and the measured grid-power. For instance, fluctuations in mechanical losses could affect the measured grid power significantly.

9.2. RECOMMENDATIONS

Following recommendations could improve the capabilities and quality of the diagnostic concept for the MTT micro-turbine CHP system.

- The quality of the diagnostic concept could be improved by adding sensors to the gas path. An additional measurement for the compressor discharge temperature would allow for a better estimation of the compressor isentropic efficiency. Especially during testing it is recommended to extract as much information as possible from the gas path so that system improvements and degradation can be monitored over time during the test phase.
- Filtering methods and data averaging methods could reduce data scattering and measurement noise.
- The derived baselines depend highly on the non-linear GSP model which relies extensively on the component maps put into the model. By increasing the accuracy of the maps, the accuracy of the baselines will as well improve.
- The root cause for the jumps in power should be investigated more in depth by doing more experiments. Especially hypothesis 3 could be investigated more in detail by monitoring the difference in oil temperature before and after the bearing house.
- The derived rule-sets from the non-linear model based diagnostic approach could be used as *if-then rules* rules for an expert system which could be used to automate the decision making. For instance, the slope of the trendlines monitored could be used to decide when compressor cleaning should be scheduled. Based on threshold values for the deltas and the current slope of the trend-lines, maintenance actions could be predicted.

Appendices

A

Effect of ambient conditions on engine performance

A.1. EFFECT OF AMBIENT TEMPERATURE

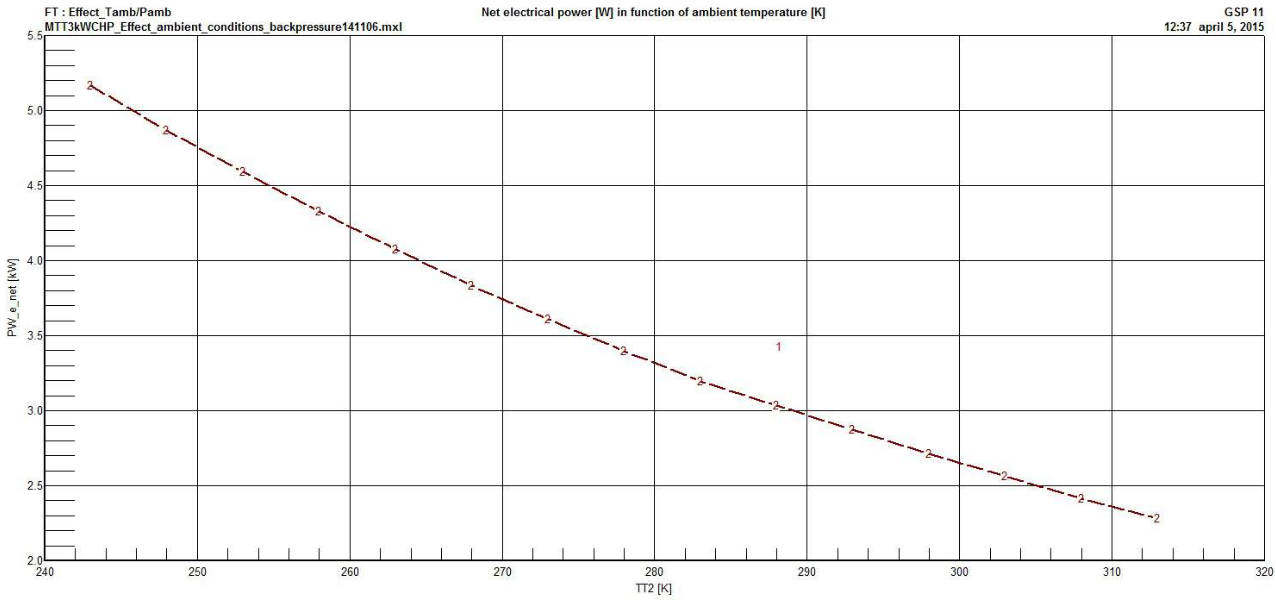

(a) Effect of ambient temperature on net electric power

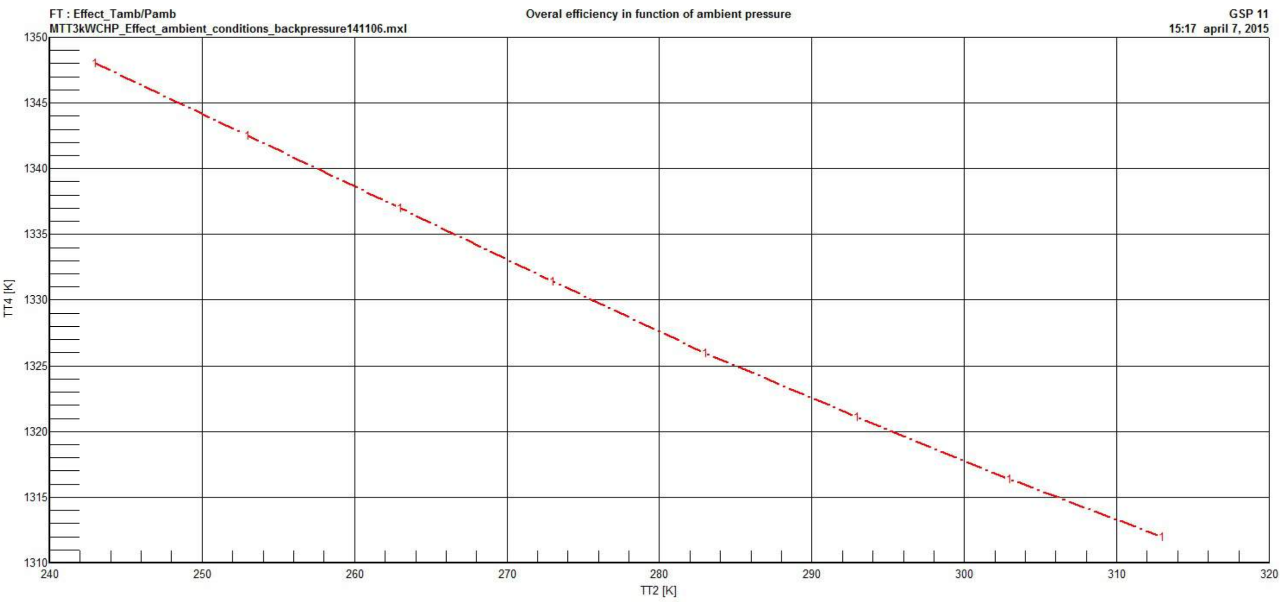

(b) Effect of ambient temperature on turbine inlet temperature

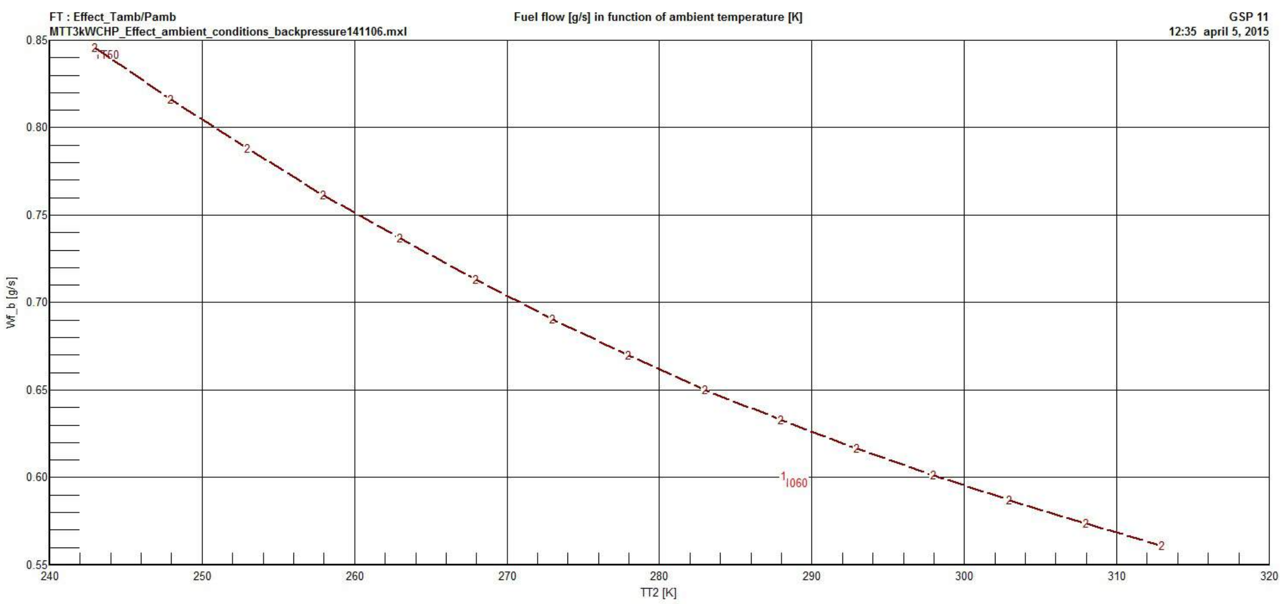

(c) Effect of ambient temperature on fuel flow

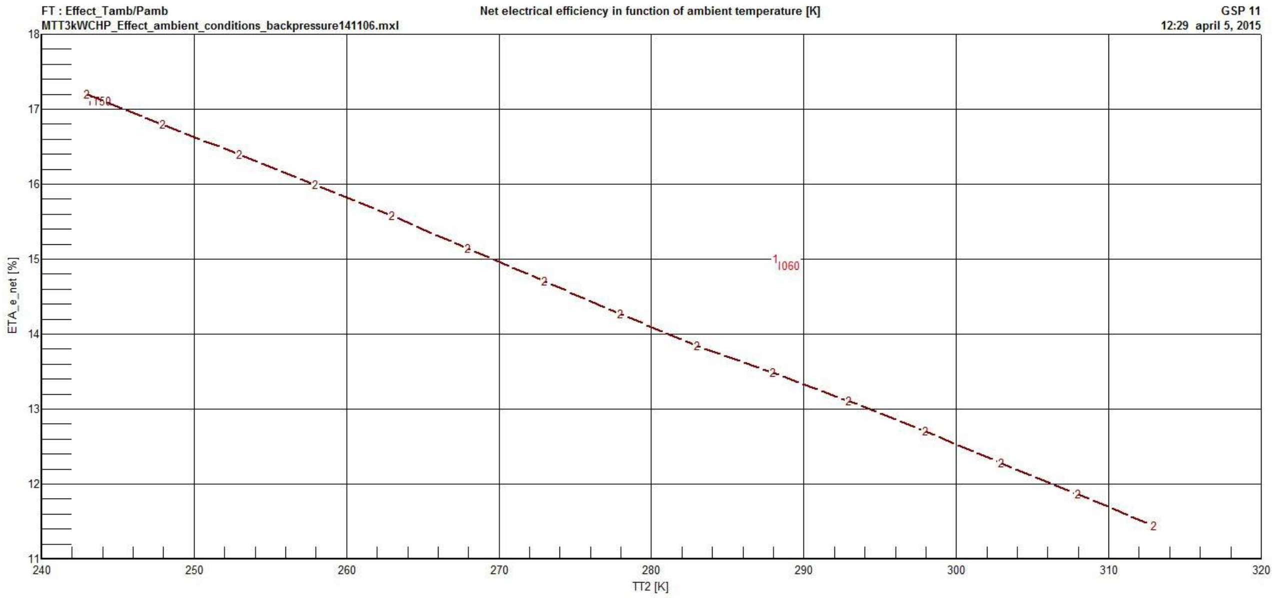

(a) Effect of ambient temperature on net electrical efficiency

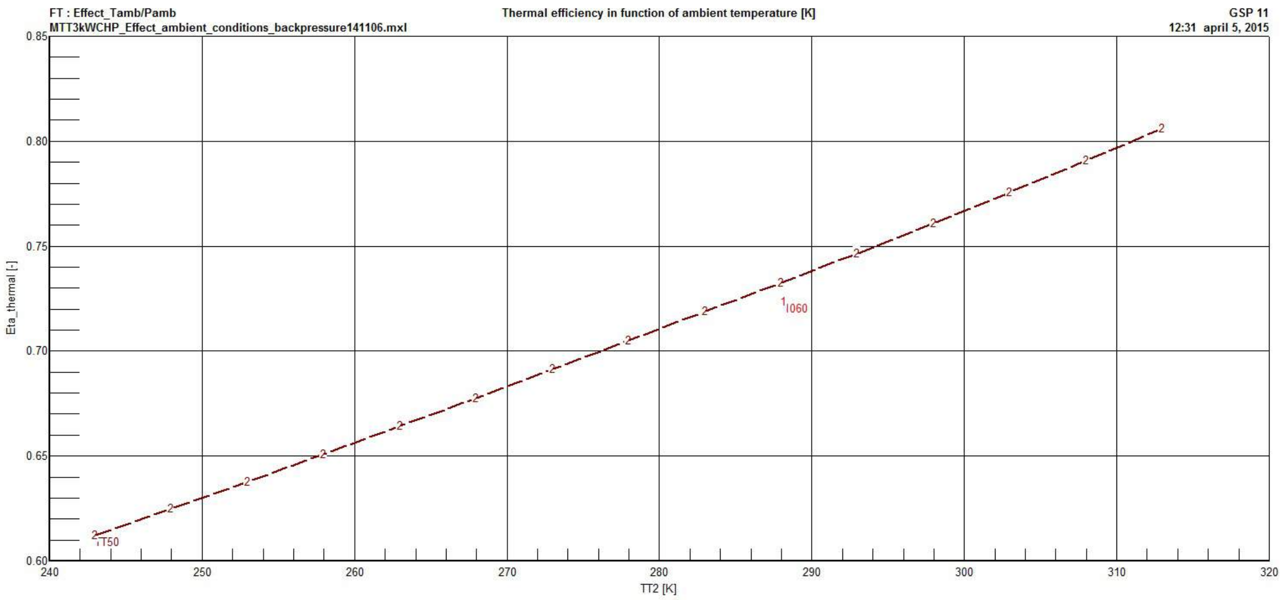

(b) Effect of ambient temperature on thermal efficiency

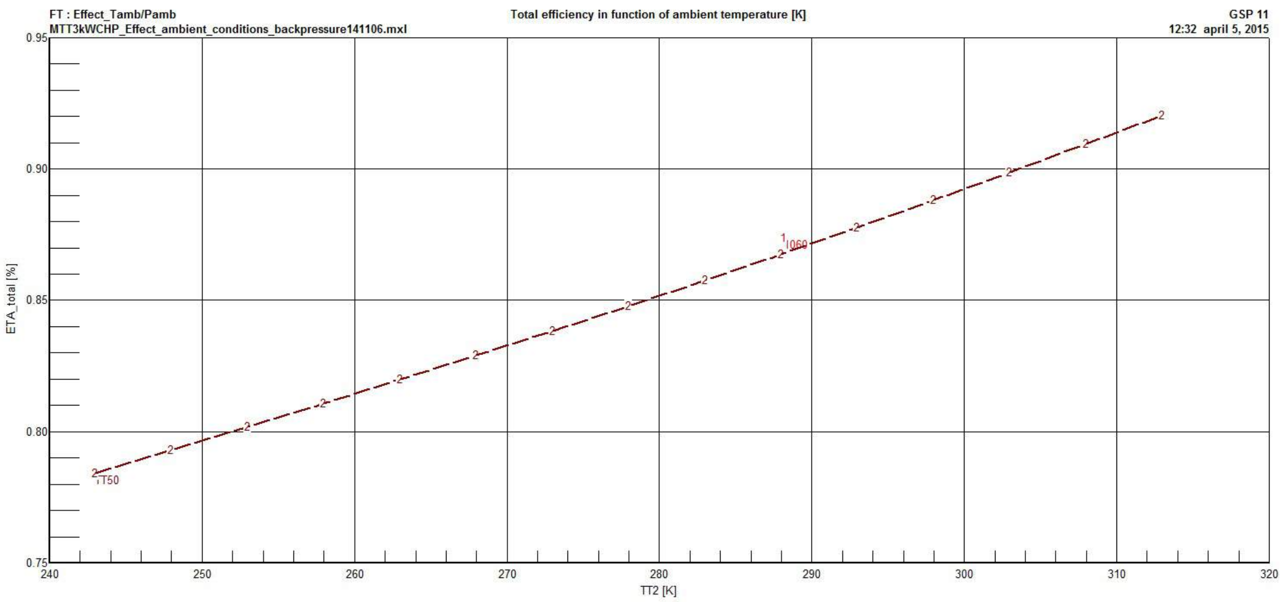

(c) Effect of ambient temperature on overall efficiency

Figure A.2: Effect of ambient temperature on efficiency

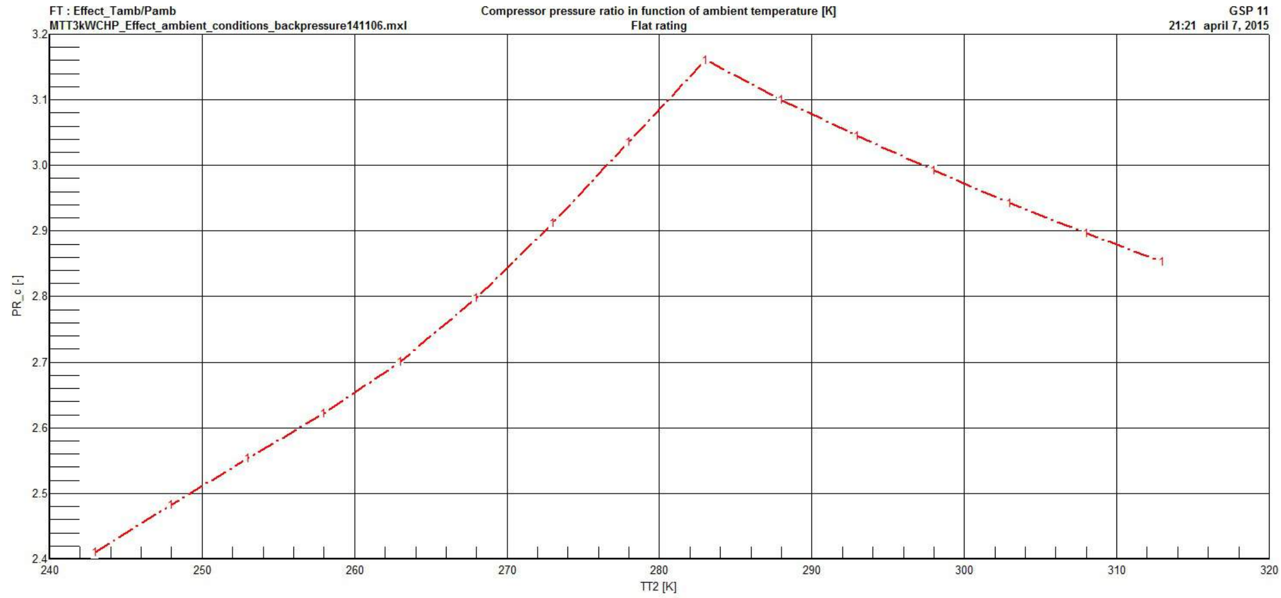

(a) Effect flat rating on compressor pressure ratio

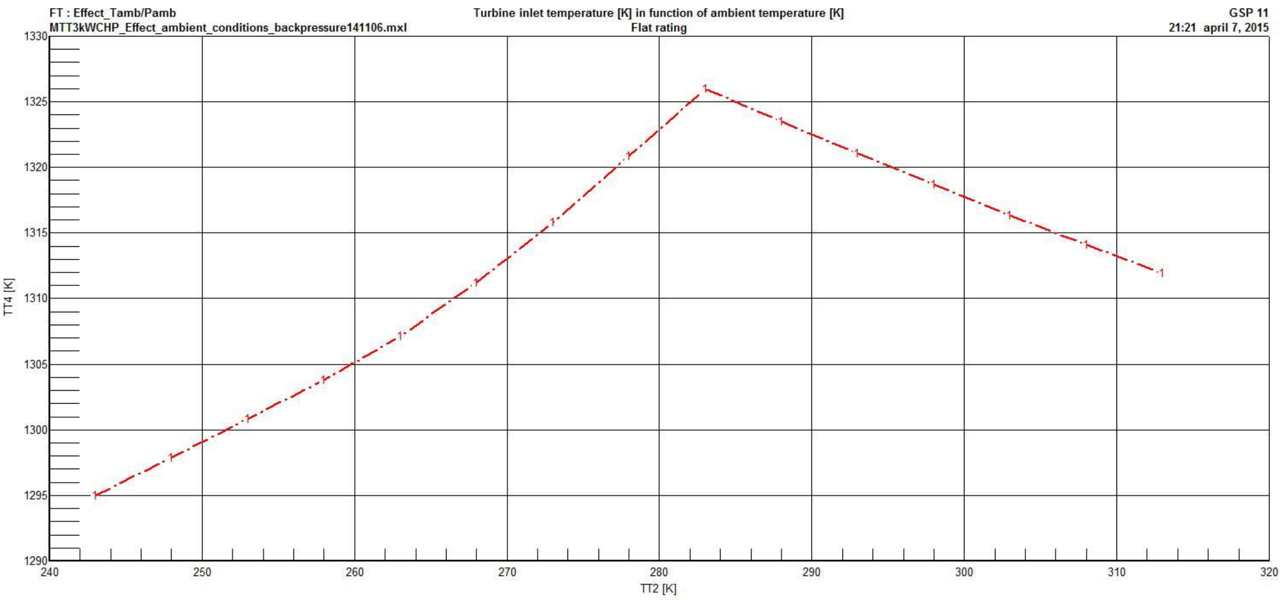

(b) Effect of flat rating on TIT

Figure A.3: Effect of flat rating on performance

A.2. EFFECT OF AMBIENT PRESSURE

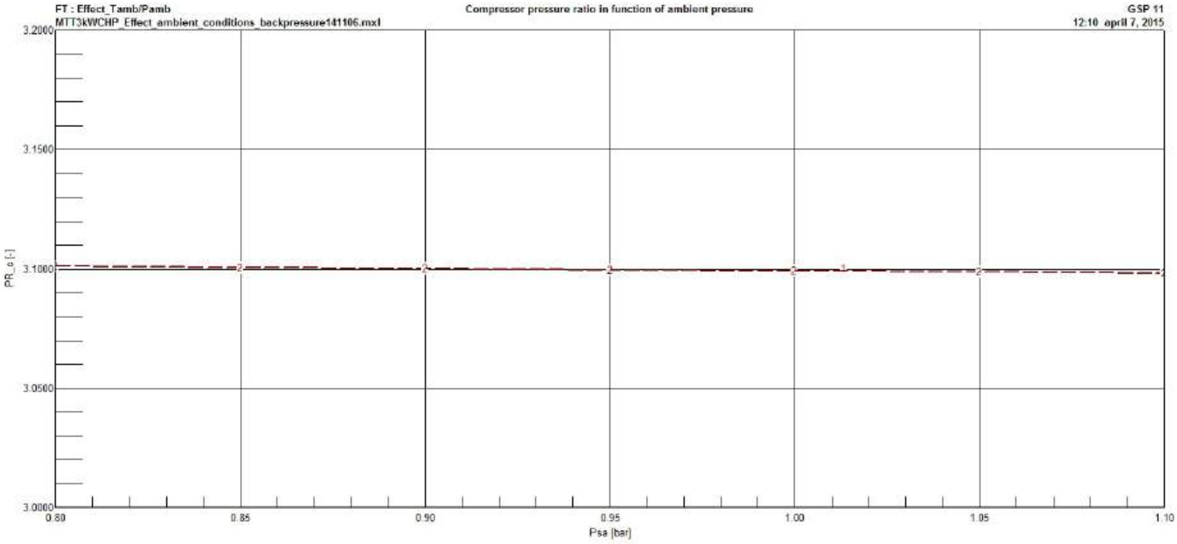

Figure A.4: Pressure ratio in function of ambient pressure [bar]

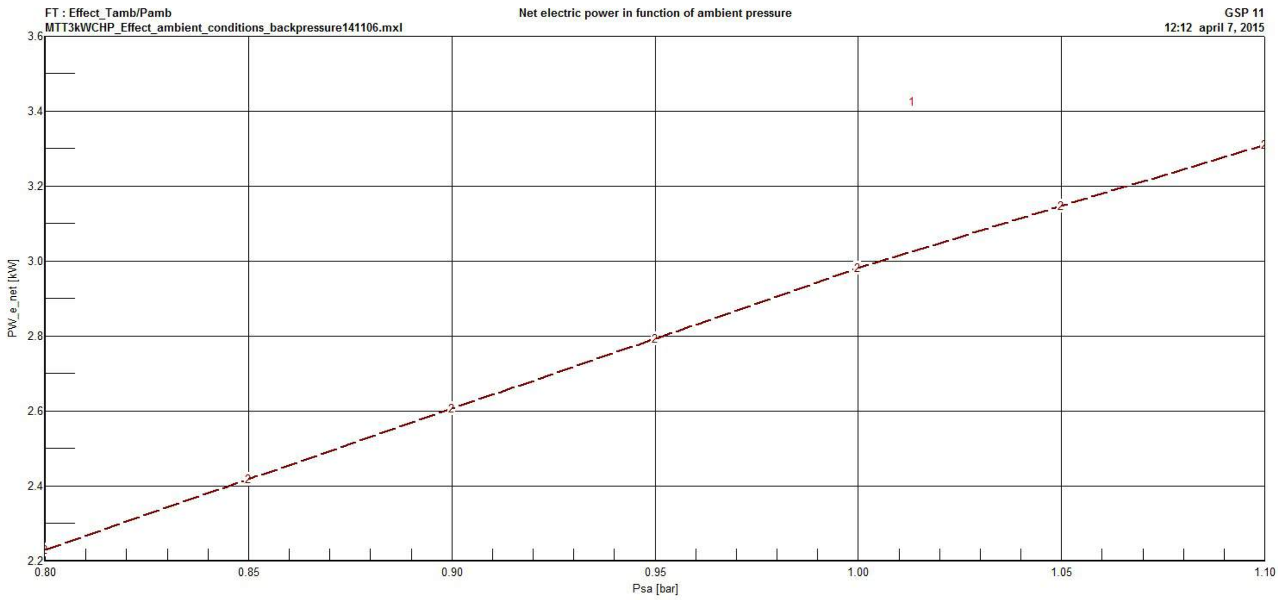

(a) Effect of ambient pressure on net electric power

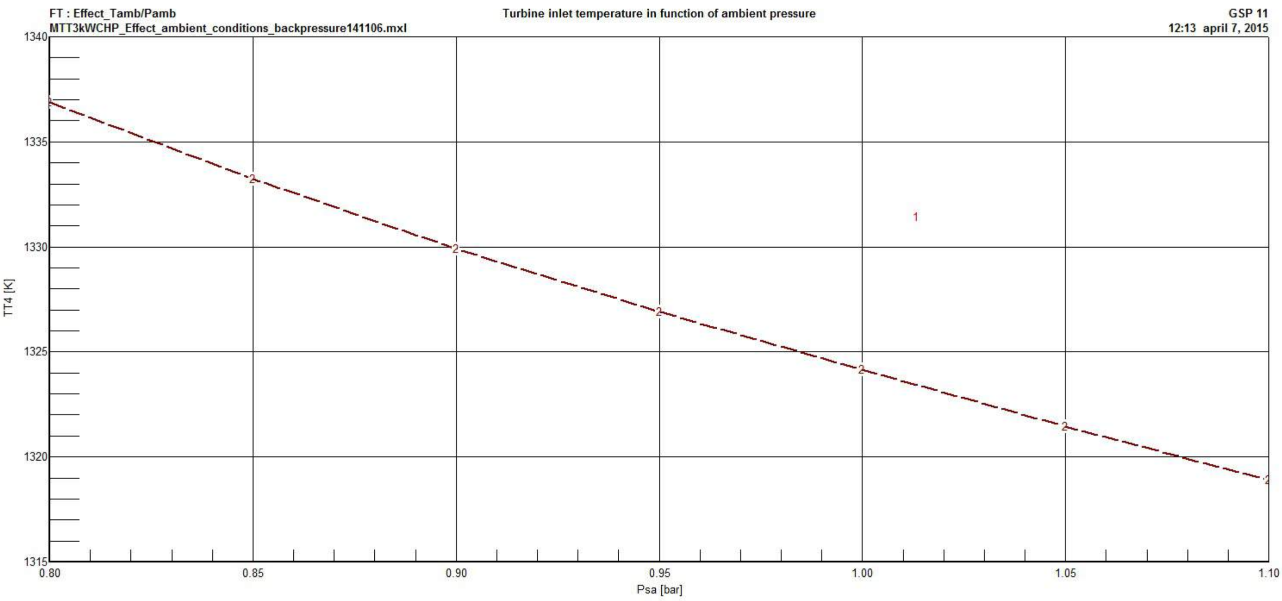

(b) Effect of ambient pressure on turbine inlet temperature

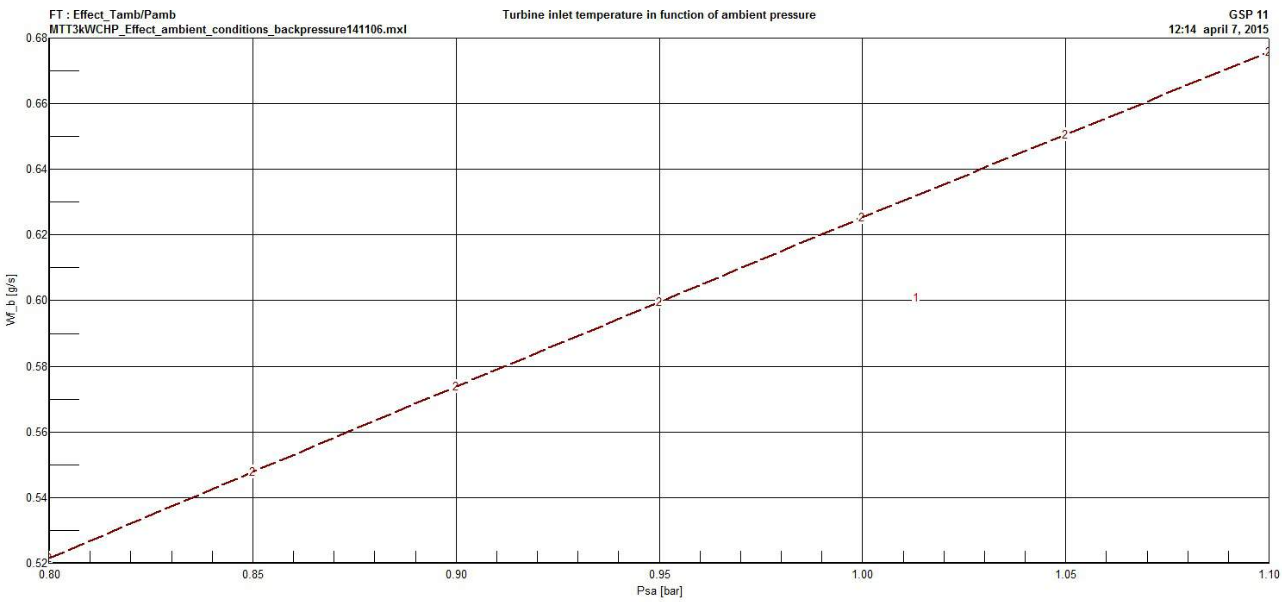

(c) Effect of ambient pressure on fuel flow

Figure A.5: Effect of ambient pressure on global engine performance

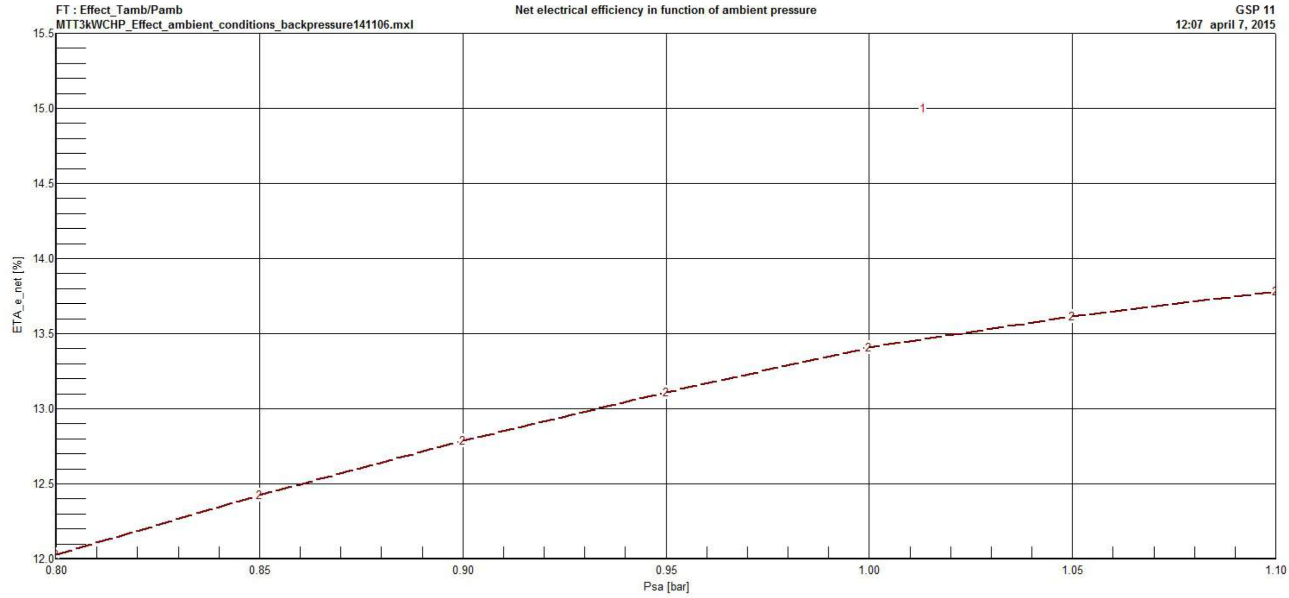

(a) Effect of ambient pressure on net electrical efficiency

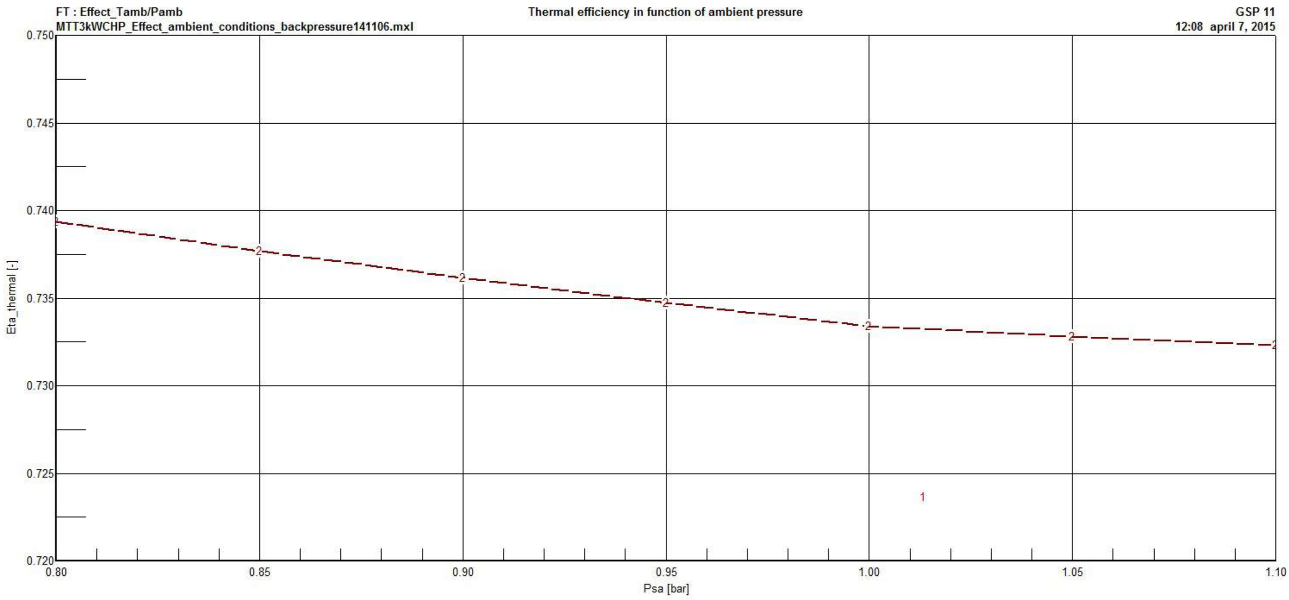

(b) Effect of ambient pressure on thermal efficiency

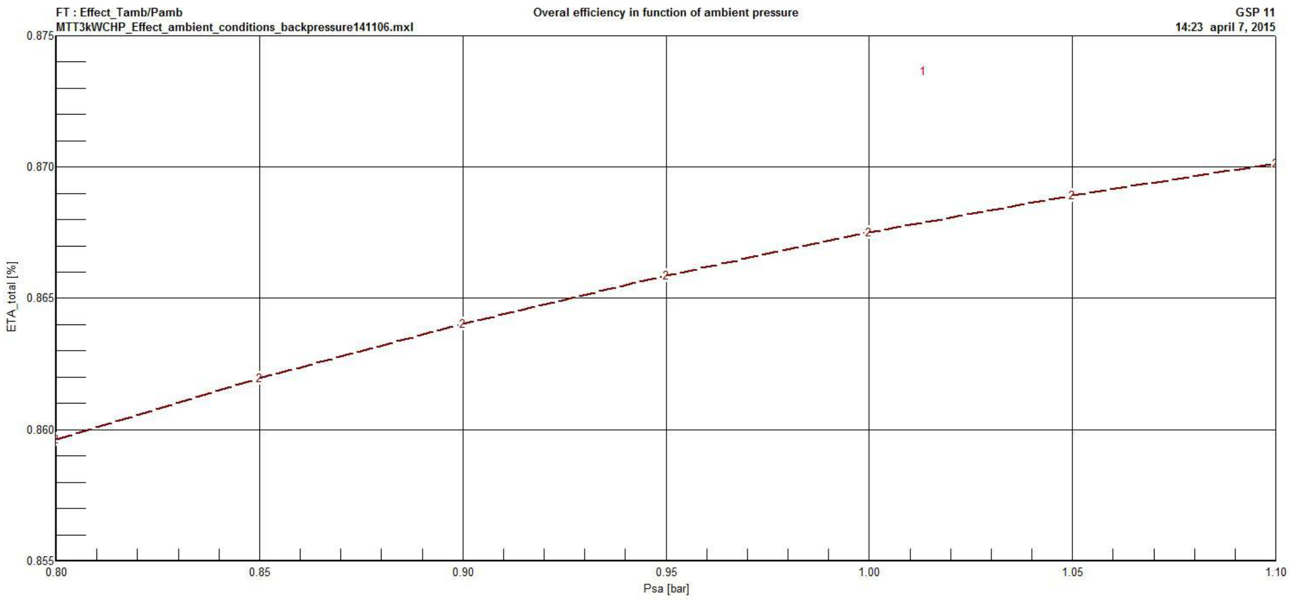

(c) Effect of ambient pressure on overall efficiency

Figure A.6: Effect of ambient pressure on efficiency

B

PERFORMANCE PARAMETER BASELINES FOR THE HEALTHY MTT ENGINE UNDER BASE-LOAD OPERATION

Following figures complete the set of corrected performance parameter baselines of the healthy micro-turbine engine.

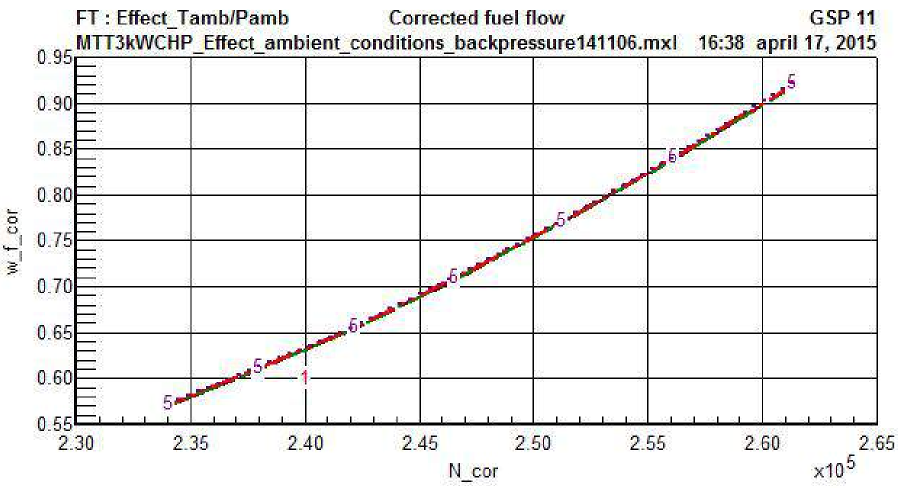

Figure B.1: Corrected fuel flow function of corrected rotational speed

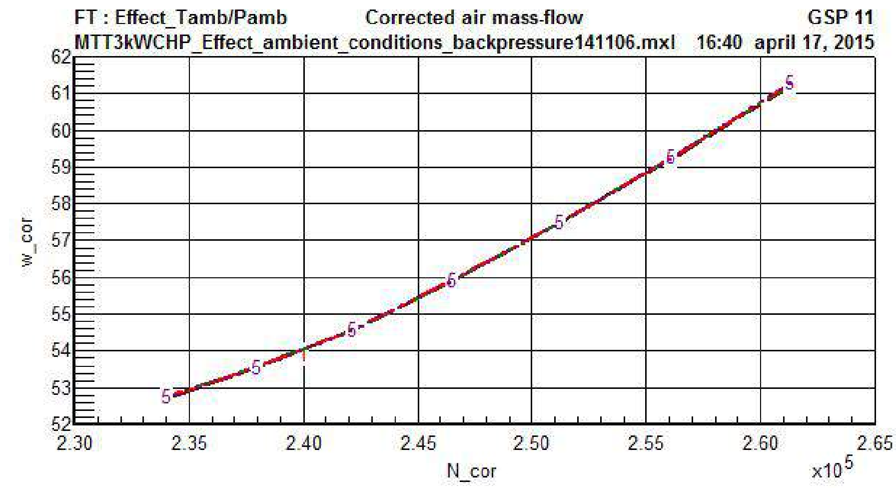

Figure B.2: Corrected mass-flow in function of corrected rotational speed

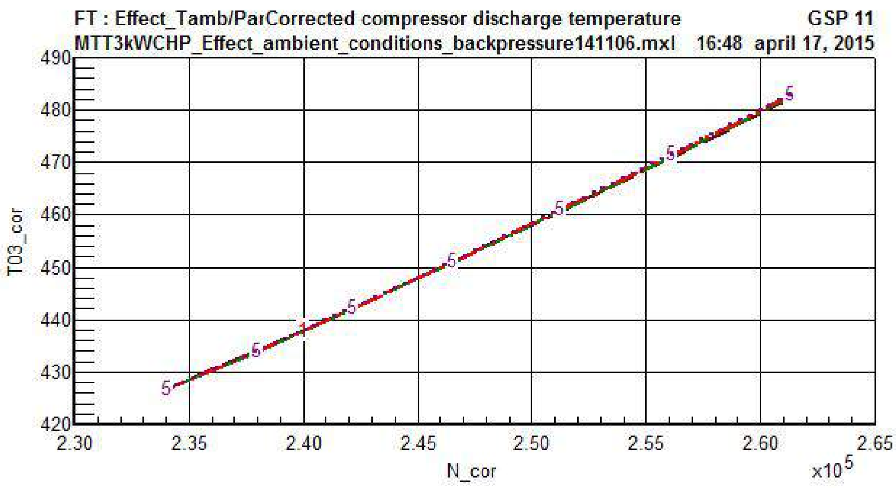

Figure B.3: Corrected compressor discharge temperature in function of corrected rotational speed

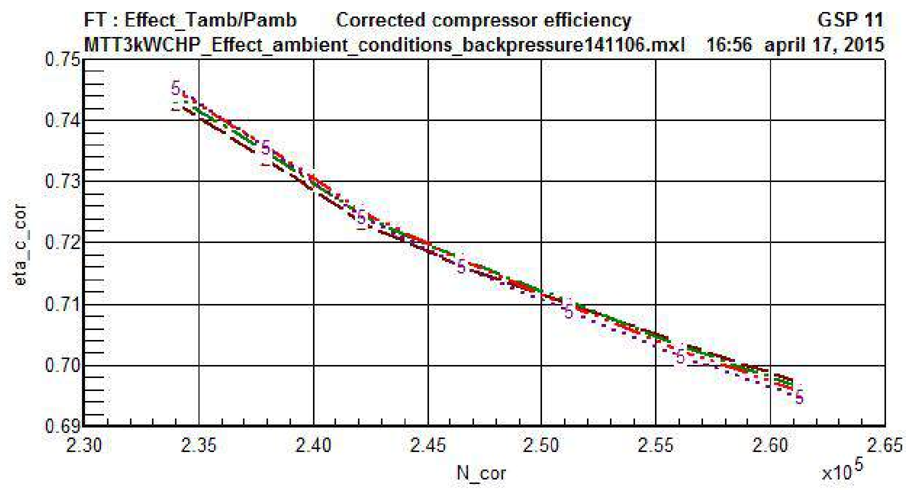

Figure B.4: Corrected isentropic compressor efficiency in function of corrected rotational speed

C

BUCKINGHAM PI THEOREM

The Buckingham PI theorem states that an equation of n physical variables can be rewritten in terms of a set of $p = n - k$ dimensionless parameters where k is the number of physical dimensions. In mathematical terms a physical meaningful equation $f(q_1, q_2, .., q_n) = 0$ where q_i are the n physical variables can be restated as $(F(\Pi_1, \Pi_2, ..., \Pi_p))$ where Π_i are the p dimensional groups or PI-groups. For instance, the performance of a compressor can be expressed as a function of D, N, $\dot{m}$, p_{02}, p_{03}, $R \cdot T_{02}$ and $R \cdot T_{03}$ [33]. The first column in Table C.1 shows each parameter and its dimensions. The three fundamental units of the 7 dimensional variables are are: $[m]$, $[s]$ and $[kg]$. According to the Buckingham PI theorem the set of 8 variables can be reduced to a set of $4 = 7 - 3$ non-dimensional groups.

The steps in obtaining the dimensional-groups are:

- Write the dimensional variables and their dimensions down (column 1)
- Eliminate the dimension $[m]$ from the variables by multiplying the variables by D^a. Where D is the size parameter with dimension $[m]$ (column 2)
- Eliminate the dimension $[s]$ from the variables of column 2 by multiplying the variable by $\left(\frac{R \cdot T_{02}}{D^2}\right)^b$. Where $\left(\frac{R \cdot T_{02}}{D^2}\right)$ has the dimension $[\frac{1}{s^2}]$. (column 3)
- Eliminate the dimension $[kg]$ from the variables by multiplying the variable of column 3 by $\left(\frac{p_{02} \cdot D^3}{R \cdot T_{02}}\right)^c$. Where $\left(\frac{p_{02} \cdot D^3}{R \cdot T_{02}}\right)$ has the dimension $[kg]$. (column 4)

$$f(D, N, \dot{m}_{,02}, p_{03}, R \cdot T_{02}, R \cdot T_{03}) = 0 \quad \text{(C.1)}$$

Dim. variables	Dim.	Eliminate $[m]$	Dim.	Eliminate $[s]$	Dim.	Non-dim. group	-
$R \cdot T_{02}$	$\left[\frac{m^2}{s^2}\right]$	$\frac{R \cdot T_{02}}{D^2}$	$\left[\frac{1}{s^2}\right]$	-	-	-	-
$R \cdot T_{03}$	$\left[\frac{m^2}{s^2}\right]$	$\frac{R \cdot T_{03}}{D^2}$	$\left[\frac{1}{s^2}\right]$	$\frac{T_{03}}{T_{02}}$	-	$\frac{T_{03}}{T_{02}}$	-
p_{02}	$\left[\frac{kg}{s^2 \cdot m}\right]$	$p_{02} \cdot D$	$\left[\frac{kg}{s^2}\right]$	$\frac{p_{02} \cdot D^3}{R \cdot T_{02}}$	$[kg]$	-	-
p_{03}	$\left[\frac{kg}{s^2 \cdot m}\right]$	$p_{03} \cdot D$	$\left[\frac{kg}{s^2}\right]$	$\frac{p_{03} \cdot D^3}{R \cdot T_{03}}$	$[kg]$	$\frac{p_{03}}{p_{02}}$	-
D	$[M]$	-	-	-	-	-	-
N	$\left[\frac{1}{s}\right]$	N	$\left[\frac{1}{s}\right]$	$\frac{N \cdot D}{\sqrt{R \cdot T_{02}}}$	-	$\frac{N \cdot D}{\sqrt{R \cdot T_{02}}}$	-
$\dot{m}$	$\left[\frac{kg}{s}\right]$	$\dot{m}$	$\left[\frac{kg}{s}\right]$	$\frac{\dot{m} \cdot D}{\sqrt{R \cdot T_{02}}}$	$[kg]$	$\frac{\dot{m} \cdot \sqrt{R \cdot T_{02}}}{p_{02} \cdot D^2}$	-

Table C.1: Table showing the steps to make 4 non-dimensional groups from the set of 8 dimensional variables

D

EFFECT OF DETERIORATION ON CORRECTED PERFORMANCE PARAMETERS

D.1. EFFECT OF FOULING

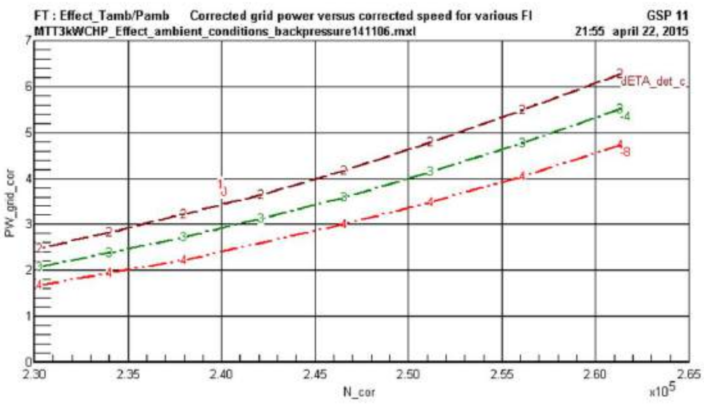

Figure D.1: Effect of fouling on corrected grid power for different fouling indexes (No fouling: brown, FI2: green, FI4: red)

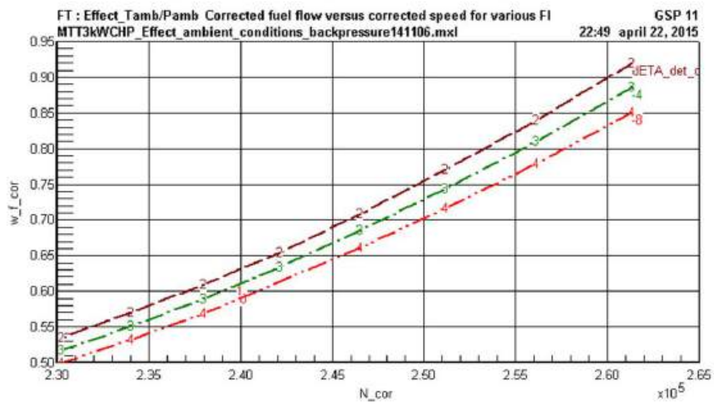

Figure D.2: Effect of fouling on corrected fuel flow (No fouling: brown, FI2: green, FI4: red)

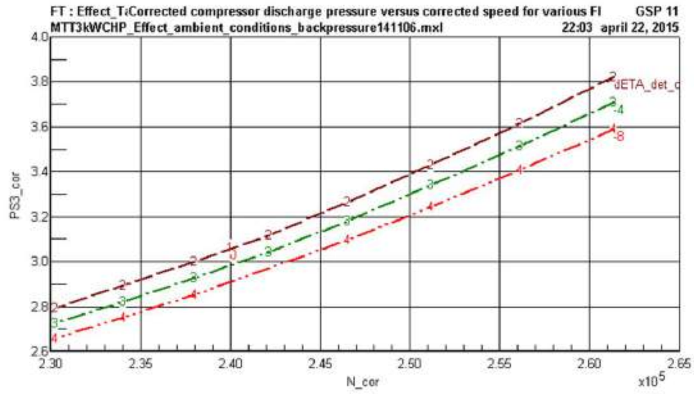

Figure D.3: Effect of fouling on corrected compressor discharge pressure (No fouling: brown, FI2: green, FI4: red)

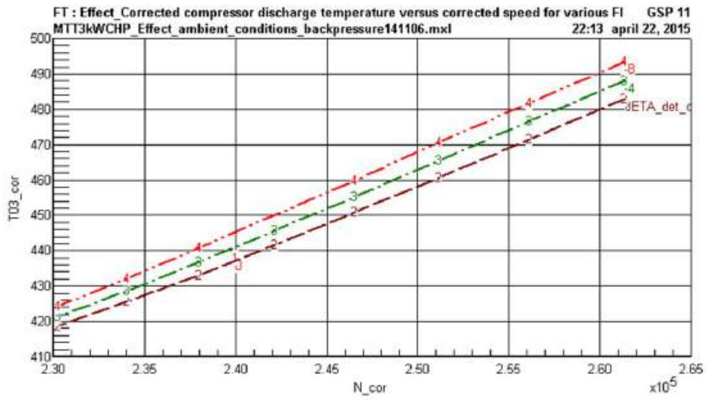

Figure D.4: Effect of fouling on corrected compressor discharge temperature (No fouling: brown, FI2: green, FI4: red)

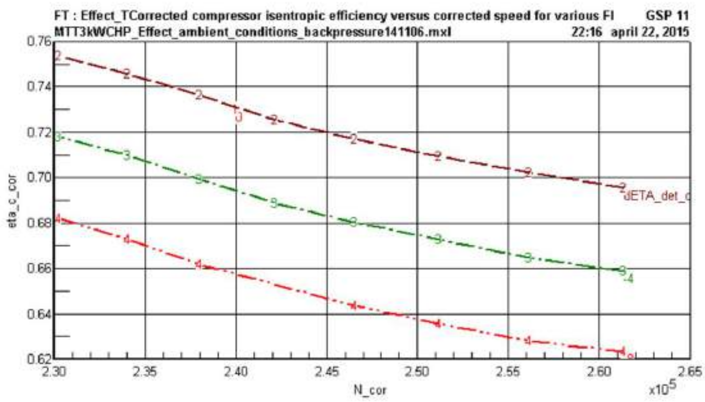

Figure D.5: Effect of fouling on corrected compressor isentropic efficiency (No fouling: brown, FI2: green, FI4: red)

D.2. EFFECT OF TURBINE TIP CLEARANCE

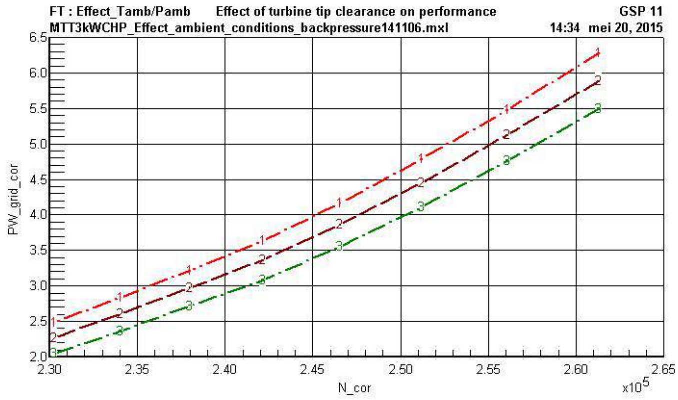

Figure D.6: Effect of turbine tip clearance on corrected grid power (No deterioration: red, $\Delta\eta_t = -2\%$: brown, $\Delta\eta_t = -4\%$: green)

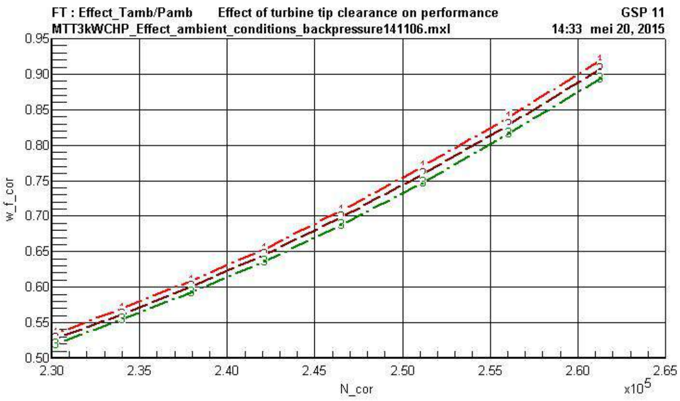

Figure D.7: Effect of turbine tip clearance on corrected fuel flow (No deterioration: red, $\Delta\eta_t = -2\%$: brown, $\Delta\eta_t = -4\%$: green)

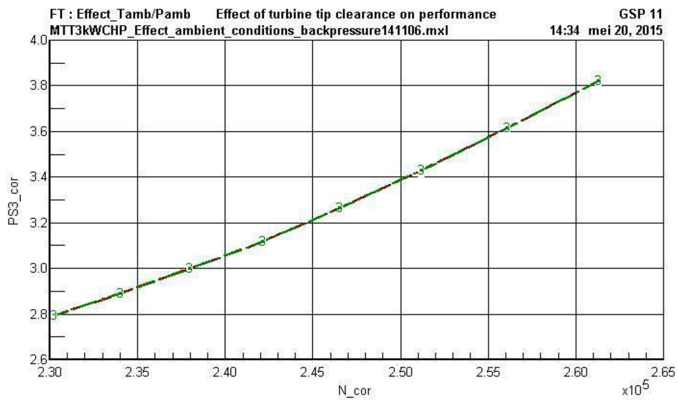

Figure D.8: Effect of turbine tip clearance on compressor discharge pressure (No deterioration:red, $\Delta\eta_t = -2\%$: brown, $\Delta\eta_t = -4\%$: green)

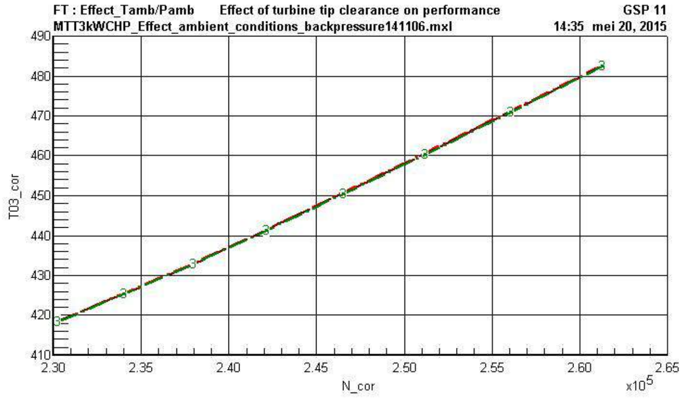

Figure D.9: Effect of turbine tip clearance on compressor discharge temperature (No deterioration: red, $\Delta\eta_t = -2\%$: brown, $\Delta\eta_t = -4\%$:green)

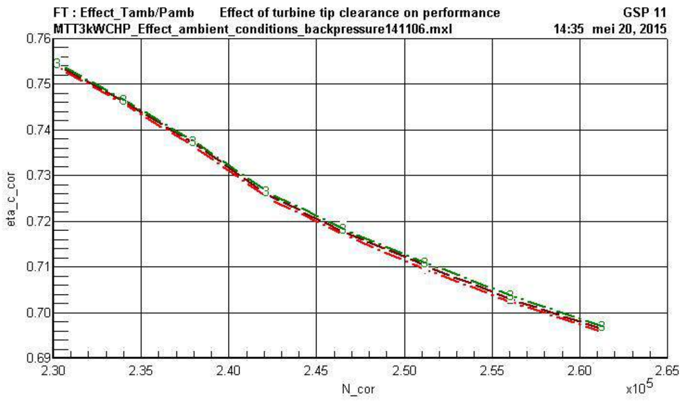

Figure D.10: Effect of turbine tip clearance on corrected isentropic compressor efficiency (No deterioration:red, $\Delta\eta_t = -2\%$: brown, $\Delta\eta_t = -4\%$: green)

D.3. EFFECT OF LEAKAGE ON PERFORMANCE

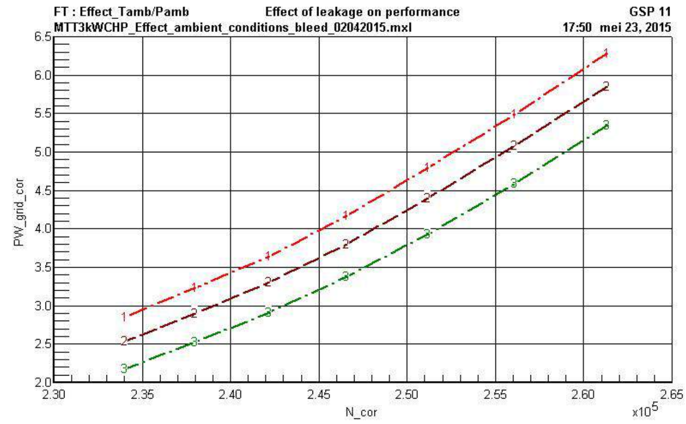

Figure D.11: Effect of flow leakage on corrected grid power for various degrees of leakage (No leakage: red, 5 percent leakage: brown, 10 percent leakage: green)

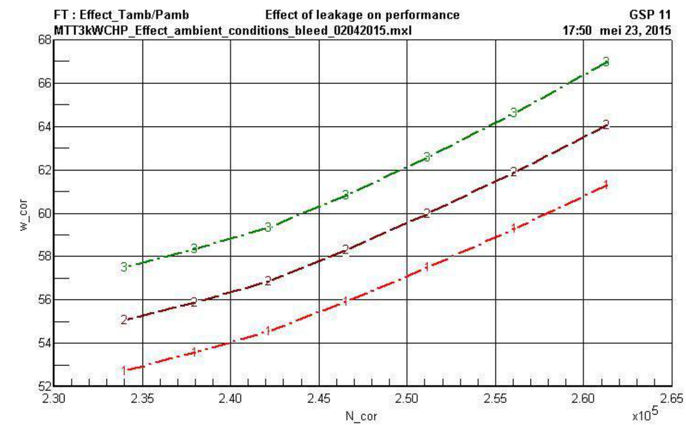

Figure D.12: Effect of flow leakage on corrected air mass flow for various degrees of leakage (No leakage: red, 5 percent leakage: brown, 10 percent leakage: green)

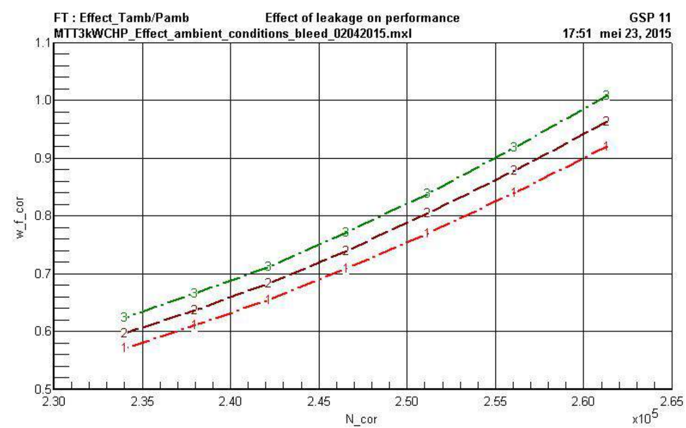

Figure D.13: Effect of flow leakage on corrected fuel flow for various degrees of leakage (No leakage: red, 5 percent leakage: brown, 10 percent leakage: green)

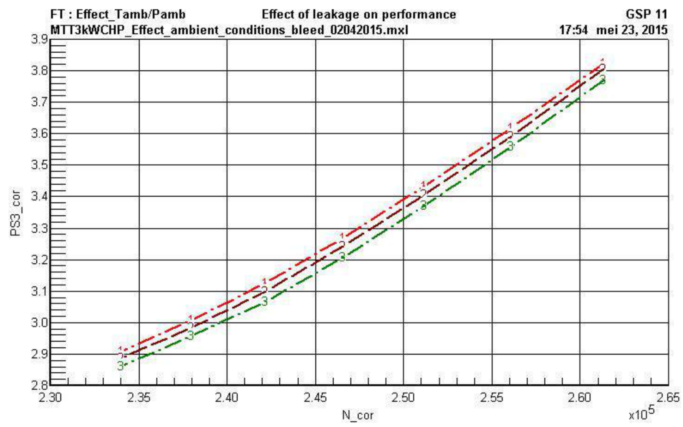

Figure D.14: Effect of flow leakage on corrected corrected discharge pressure for various degrees of leakage (No leakage: red, 5 percent leakage: brown, 10 percent leakage: green)

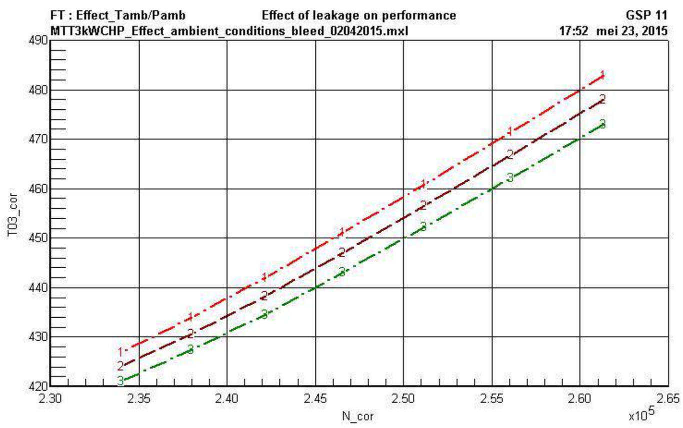

Figure D.15: Effect of flow leakage on corrected compressor discharge temperature for various degrees of leakage (No leakage: red, 5 percent leakage: brown, 10 percent leakage: green)

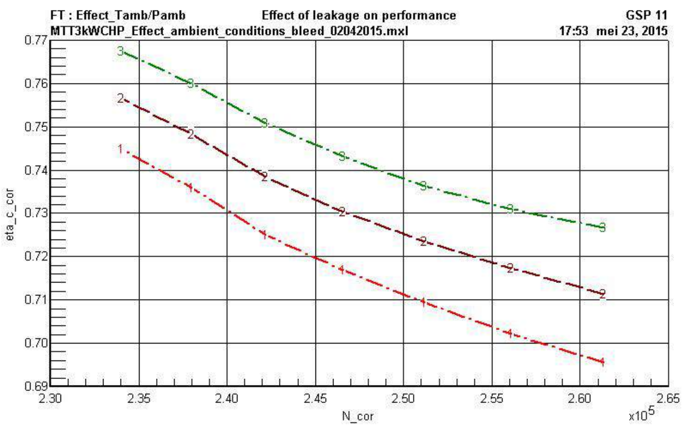

Figure D.16: Effect of flow leakage on corrected grid power for various degrees of leakage (No leakage: red, 5 percent leakage: brown, 10 percent leakage: green)

E

Newton-Raphson method

Newton-Raphson is a numerical solving method used to find a solution for a set of non-linear algebraic equations. In case of non-linear gas path analysis, a set of error equations representing the engine model should be solved for a set of state variables ($\bar{S}$) so that error equations ($\bar{E}(\bar{S})$) become zero. In this appendix, the iterative steps involved in finding a numerical solution based on Newton-Raphson are discussed.

E.1. Geometric representation of Newton-Raphson iteration

Let $f(x)$ be a non-linear, continuous function of which we want to find the roots ($f(x) = 0$). x_0 is the first estimate for the root of the function which is shown in Figure E.1. Equation E.1 is the expression for the tangent line to $y = f(x_0)$ at point (x_0, f(x_0)). The root of the tangent line at $f(x_0)$ is used as a better estimation (x_1) for root of the function. The new and better estimate x_1 is calculated as shown by Equation E.2. Next, the non-linear function will be evaluated for x_1. The root of the tangent line in point (x_1, $f(x_1)$) is calculated in exactly the same way as x_1 was obtained. This new root becomes the next estimate for the root of the non-linear function f(x). In general, the the next estimate x_{i+1} is calculated as shown by equation E.3. This process continuous until the absolute value of the error becomes smaller than a user-defined inaccuracy.

$$y = f(x_0) + (x - x_0) \cdot f'(x_0) \tag{E.1}$$

$$x_1 = x_0 - \frac{f(x_0)}{f'(x_0)} \tag{E.2}$$

$$x_{i+1} = x_i - \frac{f(x_i)}{f'(x_i)} \tag{E.3}$$

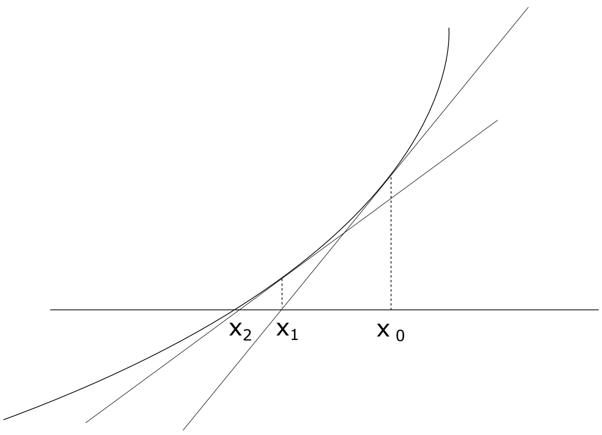

Figure E.1: Newton-Raphson iteration

E.2. NEWTON-RAPHSON IN GSP

Mathematically, the set of error equations to be solved in GSP can be written as:

$$\bar{E}(\bar{S}) = \bar{0} \tag{E.4}$$

Where:
$\bar{E}$ = error variables
$\bar{S}$ = state variables

In GSP, following sequence is followed to solve the set of non-linear differential equations representing the engine's model [45]:

- Normalize states and error variables by dividing these by their corresponding reference (often design-point) values. This is done to avoid numerical instability.
- Linearize equation E.4 in a small region around the initial guess ($\bar{S}$) which yields following set of first order equations: $\Delta\bar{E} = J \cdot \Delta\bar{S}$. Where J is the Jacobian matrix formed by the set of partial derivatives of the error equations to the state variables:

  $$J_{i,j} = \frac{\Delta e_i}{\Delta s_j}(i, j = 1..n) \tag{E.5}$$

  To obtain the Jacobian, the model is calculated n+1 times from front to rear. Once for the reference state variables and n times with a small perturbation Δs_j of each element of the reference state vector. $\Delta\bar{S} = J^{-1} \cdot \Delta\bar{E}$ gives an indication of how much $\bar{S}$ has to change to reduce $\bar{E}$. In GSP, the initial guess for the solution is usually the design operating point or the previously calculated off-design operating point.
- A next estimate for the state variables is obtained based on following equation:

  $$\bar{S}_{i+1} = \bar{S}_i - f \cdot J_i^{-1} \cdot \bar{E}_i \tag{E.6}$$

  This equation has the same form as equation E.3 but is used to solve a set of non-linear differential equations. The variable f is introduced to improve the stability and rate of convergence by limiting the magnitude of the correction steps. In GSP, the Jacobian (J) is not re-calculated for each new estimation of the state variables($\bar{S}$) so that the calculation time can be reduced.

F

OFF-DESIGN GAS TURBINE PERFORMANCE CALCULATIONS

Once the engine design is fixed, the steady state off-design performance of the engine can be calculated. In this appendix, the theory behind off-design gas turbine simulation is discussed briefly. The performance of gas-turbines depends on:

- The operating conditions such as ambient conditions (ambient pressure, temperature and humidity) and installation effects (inlet and exhaust pressure loss).
- The power settings such as turbine exit temperature, fuel flow and shaft rotational speed.
- The condition of the individual components which can be quantified by health parameters such as isentropic efficiencies, pressures ratio's and flow capacities.

Changes in one of the aforementioned items will affect the engine behaviour and hence result in shifts in engine performance. In off-design performance calculations, various component performance levels are matched to each other so that the conservation laws are satisfied. The performance of gas turbine components depends on the geometry of the components and is quantified by dimensionless performance parameter groups. Once the geometry of a component is fixed, relations between performance parameter groups can established experimentally. The established component performance maps such as compressor and turbine maps show the performance for all off-design conditions. Table ... gives an overview of the dimensionless and corrected [1] performance parameter groups that describe the performance of the gas turbine components. Another physical property of the gas that influences the performance is the viscosity. Reynolds Number could be considered as a fifth dimensionless parameter. However, in highly turbulent regions which generally prevail in gas turbines, the influence of Re-number on performance can be neglected. Only for low densities (high altitudes), Reynolds number becomes smaller resulting in a drop in performance of the turbomachinery due to the increased friction losses.

A valid off-design operating point is found by matching the performance parameter groups such that the conservation laws are satisfied while each component is operating in a valid point in its component map. In GSP, the operating points of gas turbine components is represented numerically by the model state vector. The conservation laws on the other hand are expressed by error equations. Equation ... gives an example of an error equation showing the conservation of mass between the inlet and compressor. The process of finding the operating point for specific ambient conditions and power settings is highly iterative and requires successive guesses of the operating points in individual component maps. In practice, the iteration can be achieved either via *serial nested loops* or via a *matrix solution*. The serial nested loop approach is easier to understand physically, but becomes computational inefficient for increasing number of nested loops. On the other hand, the matrix solution used in GSP is more computational efficient because the error equations are solved simultaneously by using numerical methods such as Newton-Raphson which is discussed in Appendix E.

[1] Corrected to standard ambient conditions $T_{amb} = 288.15K$ and $p_{amb} = 1.01325 bar$

F.1. EXAMPLE FOR SERIAL NESTED LOOP ITERATION FOR SINGLE-SHAFT GAS TURBINE [33]

In this section, the iteration process for a single-shaft gas turbine by using serial nested loops is discussed. In the example, inlet and exhaust pressure loss are neglected so that the pressure ratio over the turbine can be calculated from the compressor pressure ratio and pressure loss in the combustion chamber. A stable steady state point is obtained as follows:

1. Select a random point on the referred speed line of the compressor map. Values $\frac{m\cdot\sqrt{T_{01}}}{p_{01}}$, $\frac{p_{02}}{p_{01}}$, η_c and $\frac{N}{\sqrt{T_{01}}}$ are now determined.
2. Determine the corresponding point on the turbine characteristic from the compatibility of rotational speed and flow:
   - Compatibility of rotational speed: $\frac{N}{\sqrt{T_{03}}} = \frac{N}{\sqrt{T_{01}}} \cdot \sqrt{\frac{T_{01}}{T_{03}}}$
   - Compatibility of flow (Assume $m_3 = m_1 = m$): $\frac{m\sqrt{T_{03}}}{p_{03}} = \frac{m\sqrt{T_{01}}}{p_{01}} \cdot \frac{p_{01}}{p_{02}} \cdot \frac{p_{02}}{p_{03}} \cdot \sqrt{\frac{T_{03}}{T_{01}}}$

   Where $\frac{p_{02}}{p_{03}}$ is calculated from the combustion pressure loss: $\frac{p_{03}}{p_{02}} = \frac{p_{02}-\Delta p_b}{p_{02}} = 1 - \frac{\Delta p_b}{p_{02}}$ and $\frac{m\sqrt{T_{03}}}{p_{03}}$ is determined from the turbine map once $\frac{p_{03}}{p_{04}}$ is known. If inlet and exhaust pressure loss are neglected, $\frac{p_{03}}{p_{04}} = \frac{p_{03}}{p_{02}} \cdot \frac{p_{02}}{p_{01}}$. The turbine inlet temperature (T_{03}) can now be determined from the compatibility of flow equation. Once T_{03} is known, the corrected rotational speed of the turbine can be calculated from the compatibility of rotational speed.
3. The next step is to calculate the net power output of engine. From the turbine characteristics, the turbine isentropic efficiency can be determined which is required to calculate the turbine temperature drop: $\Delta T_{034} = \eta_t T_{03}\left[1-\left(\frac{1}{\frac{p_{03}}{p_{04}}}\right)^{\frac{(\gamma-1)}{\gamma}}\right]$. The compressor temperature rise can be calculated as follows: $\Delta T_{012} = \frac{T_{01}}{\eta_c}\left[\left(\frac{p_{02}}{p_{01}}\right)^{\frac{\gamma-1}{\gamma}} - 1\right]$. The net power output can be calculated as shown in Equation F.1

$$PW_{net} = m \cdot C_{pg} \cdot \Delta T_{034} - \frac{1}{\eta_m} \cdot m \cdot C_{pa} \Delta T_{012} \tag{F.1}$$

4. Now, the characteristics of the load for a specific rotational speed should be considered. On should check if the compatibility of power is satisfied for the current operating point. If the net power output does not match the power required by the load, a new point on the speed-line of the compressor map should be chosen. This process should be repeated until all the compatibility requirement are satisfied

BIBLIOGRAPHY

[1] P. P. Walsh and P. Fletcher, *Gas turbine performance* (John Wiley & Sons, 2004).

[2] A. K. Jardine, D. Lin, and D. Banjevic, *A review on machinery diagnostics and prognostics implementing condition-based maintenance,* Mechanical systems and signal processing **20**, 1483 (2006).

[3] Y. Li, *Performance-analysis-based gas turbine diagnostics: A review,* Proceedings of the Institution of Mechanical Engineers, Part A: Journal of Power and Energy **216**, 363 (2002).

[4] M. Provost, *The use of optimal estimation techniques in the analysis of gas turbines (PhD Thesis)* (Cranfield University, 1994).

[5] L. A. Urban, *Gas path analysis applied to turbine engine condition monitoring,* Journal of Aircraft **10**, 400 (1973).

[6] L. A. Urban, *Gas turbine engine parameter interrelationships* (Hamilton Standard Division of United Aircraft Corporation, 1969).

[7] P. Kamboukos and K. Mathioudakis, *Comparison of linear and non-linear gas turbine performance diagnostics,* in *ASME Turbo Expo 2003, collocated with the 2003 International Joint Power Generation Conference* (American Society of Mechanical Engineers, 2003) pp. 451–459.

[8] W. Visser, O. Kogenhop, and M. Oostveen, *A generic approach for gas turbine adaptive modeling,* Journal of engineering for gas turbines and power **128**, 13 (2006).

[9] A. Stamatis, K. Mathioudakis, K. Papailiou, and G. Berios, *Jet engine fault detection with discrete operating points gas path analysis,* Journal of Propulsion and Power **7**, 1043 (1991).

[10] L. M. Schmitt, *Theory of genetic algorithms,* Theoretical Computer Science **259**, 1 (2001).

[11] S. J. Russell, *Rationality and intelligence,* Artificial intelligence **94**, 57 (1997).

[12] M. Zedda, *Gas turbine "engine and sensor fault diagnostics",* Ph. D. Thesis (2000).

[13] R. Dundas, D. Sullivan, and F. Abegg, *Performance monitoring of gas turbines for failure prevention,* ASME paper (1992).

[14] T. J. Ross, *Fuzzy logic with engineering applications* (John Wiley & Sons, 2009).

[15] MathWorks, *Foundations of fuzzy logic,* (2014).

[16] E. Applebaum, *Fuzzy classification for fault isolation in gas turbine engines,* in *IFSA World Congress and 20th NAFIPS International Conference, 2001. Joint 9th*, Vol. 1 (IEEE, 2001) pp. 292–297.

[17] M. Ullmann, *Thermal analysis of heat transfer of the MTT Micro Gas Turbine CHP system for steady state operation (Classified report)* (Micro Turbine Technology, 2013).

[18] I. W. V. Prof. Ir. J.P. van Buijtenen, *Aero engine technology,* (TU Delft, Faculty Aerospace Engineering, 2009).

[19] C. Rodgers, *Some effects of size on the performances of small gas turbines,* in *ASME Turbo Expo 2003, collocated with the 2003 International Joint Power Generation Conference* (American Society of Mechanical Engineers, 2003) pp. 17–26.

[20] Y. Gong, B. Sirakov, A. Epstein, and C. Tan, *Aerothermodynamics of micro-turbomachinery,* in *ASME Turbo Expo 2004: Power for Land, Sea, and Air* (American Society of Mechanical Engineers, 2004) pp. 95–102.

[21] F. P. Incropera, *Introduction to heat transfer* (John Wiley & Sons, 2011).

[22] R. C. Warren, *Design of thermocouple probes for measurement of rocket exhaust plume temperatures,* Tech. Rep. (DTIC Document, 1994).

[23] W. P. Visser and M. J. Broomhead, *Gsp a generic object-oriented gas turbine simulation environment,* (2000).

[24] d. L. Marco, *Performance modeling of the MTT Mk 4 Micro Gas Turbine (Classified Master Thesis)* (Delft University of Technology, 2009).

[25] M. L. Verbist, W. P. Visser, R. Pecnik, and J. P. van Buijtenen, *Component map tuning procedure using adaptive modeling,* in *ASME Turbo Expo 2012: Turbine Technical Conference and Exposition* (American Society of Mechanical Engineers, 2012) pp. 371–379.

[26] N. Petchers, *Combined heating, cooling & power handbook: Technologies & applications: An integrated approach to energy resource optimization* (The Fairmont Press, Inc., 2003).

[27] J. Williams, *Engineering tribology* (Cambridge University Press, 1994).

[28] S. Muyeen, *Wind energy conversion systems* (Springer, 2012).

[29] Berenblut and Masom, *Radiation pyrometry for gas turbine engines- an introduction,* in *The British Journal of Non- Destructive Testing,* Vol. 24, pp. 268–269.

[30] W. Visser, H. Pieters, M. Oostveen, and E. van Dorp, *Experience with gsp as a gas path analysis tool,* in *ASME Turbo Expo 2006: Power for Land, Sea, and Air* (American Society of Mechanical Engineers, 2006) pp. 175–182.

[31] H. Cohen, G. F. C. Rogers, H. I. H. Saravanamuttoo, and H. (r.) Saravanamutto, *Gas turbine theory,* (1987).

[32] J. Kurzke, *Model based gas turbine parameter corrections,* in *ASME Turbo Expo 2003, collocated with the 2003 International Joint Power Generation Conference* (American Society of Mechanical Engineers, 2003) pp. 91–99.

[33] H. I. H. Saravanamuttoo, G. F. C. Rogers, and H. Cohen, *Gas turbine theory* (Pearson Education, 2001).

[34] I. S. Diakunchak, *Performance deterioration in industrial gas turbines,* Journal of Engineering for Gas Turbines and Power **114**, 161 (1992).

[35] R. Kurz and K. Brun, *Degradation in gas turbine systems,* Journal of Engineering for Gas Turbines and Power **123**, 70 (2001).

[36] G. Aker and H. Saravanamuttoo, *Predicting gas turbine performance degradation due to compressor fouling using computer simulation techniques,* Journal of engineering for gas turbines and power **111**, 343 (1989).

[37] A. V. Zaita, G. Buley, and G. Karlsons, *Performance deterioration modeling in aircraft gas turbine engines,* Journal of engineering for gas turbines and power **120**, 344 (1998).

[38] M. Nili-Ahmadabadi, A. Hajilouy-Benisi, M. Durali, and S. M. Motavalli, *Experimental and numerical investigation of a centrifugal compressor and numerical study of the area ratio and tip clearance effects on the performance characteristic,* in *ASME Turbo Expo 2008: Power for Land, Sea, and Air* (American Society of Mechanical Engineers, 2008) pp. 1627–1637.

[39] S. M. Futral Jr and D. E. Holeski, *Experimental results of varying the blade-shroud clearance in a 6.02-inch radial-inflow turbine,* (1970).

[40] R. Dambach, H. Hodson, and I. Huntsman, *1998 turbomachinery committee best paper award: An experimental study of tip clearance flow in a radial inflow turbine,* Journal of turbomachinery **121**, 644 (1999).

[41] A. Lakshminarasimha, M. Boyce, and C. Meher-Homji, *Modeling and analysis of gas turbine performance deterioration,* Journal of engineering for gas turbines and power **116**, 46 (1994).

[42] P. Zhu and Saravanamuttoo, *Simulation of an advanced twin-spool industrial gas turbine,* Journal of Eng. Gas Turbines Power **114**, 185 (2008).

[43] J. MacLeod, V. Taylor, and J. Laflamme, *Implanted component faults and their effects on gas turbine engine performance,* Journal of engineering for gas turbines and power **114**, 174 (1992).

[44] A. A. Alsaeed, *A study of methods for improving the dynamic stability of high-speed turbochargers (PhD Thesis)* (Virginia Tech, 2010).

[45] W. Visser, *Generic analysis methods for gas turbine engine performance (PhD Thesis)* (Delft University of Technology, 2014).